Roles of Multiple Mechanisms in Regulating Auxin Levels during Plant Growth and Development

A DISSERTATION
SUBMITTED TO THE FACULTY OF THE GRADUATE SCHOOL
OF THE UNIVERSITY OF MINNESOTA
BY

Xing Liu

IN PARTIAL FULFILLMENT OF THE REQUIREMENTS
FOR THE DEGREE OF
DOCTOR OF PHILOSOPHY

Advisers: Jerry Cohen, Gary Gardner

April, 2012

Acknowledgements

First and foremost I would like to sincerely thank my advisors Dr. Jerry Cohen and Dr. Gary Gardner, who have guided me throughout my thesis work with their patience, knowledge and experience, while also allowing me the room to develop my own way of thinking and to work independently. I attribute my achievements during my graduate studies to their encouragement, continuous support, and open minds, and without which this dissertation would not be completed. In my scientific career, they have been great models for me, and their mentoring will continue to help me become a respectable investigator and educator.

I would like to express my great appreciation for faculty members of my advisory committee, Dr. Jane Glazebrook, Dr. Neil Olszewski, and Dr. Adrian Hegeman, for their valuable suggestions, critical comments, and helpful guidance on my graduate work and thesis research. I also thank faculty members at the University of Minnesota, Dr. Carolyn Silflow for advice during my first-year graduate studies and recommendations of exceptional courses, Dr. Bill Gray for suggestions on my experimental design, and Dr. John Ward for sharing the Arabidopsis *nakr1* mutant seeds and his comments on my project.

During my thesis research, I received generous and enormous support from Dr. Lana Barkawi and Dr. Wen-Ping Chen, who shared with me their knowledge and techniques with great patience and warm encouragement. Dr. Angela Hendrickson helped me better comprehend the knowledge I received early in my graduate career, and Mr. Doug Brinkman assisted in the preparation of my experimental systems. Further, I want to give credit to all members in the lab groups associated with Dr. Cohen, Dr. Gardner and Dr. Hegeman, who have provided comments on my research and helped improve my presentation and writing skills.

Mentorship from faculty members outside of my university has left a profound impression. Dr. Gloria Muday (Wake Forest University) taught me the method of measuring polar auxin transport used in her lab. Dr. Jennifer Normanly (University of

Massachusetts, Amherst), while on sabbatical in my lab, shared with me her professional life experiences. Dr. Lucia Strader (Washington University in St. Louis) and Dr. Bonnie Bartel (Rice University) provided Arabidopsis *ibr 1 ibr 3 ibr 10* seeds and offered inspiration in my current research and future career. Dr. Cris Kuhlemeier (University of Bern, Switzerland) and Dr. Klaus Palme (University of Freiburg, Germany) hosted my visit in their labs, where I learned techniques in visualizing proteins using florescent tags and experienced European academic culture.

I thank Cold Spring Harbor Laboratory for holding the "Molecular Techniques in Plant Science" workshop and providing me the tuition waiver scholarship when I attended. I also thank Tomato Genetics Resource Center (University of California, Davis) for offering the *cry1*, *phyA*, *phyB1*, and *phyB2* tomato mutant seeds.

My research was funded by the U.S. Department of Agriculture National Research Initiative (USDA-NRI), the National Science Foundation (NSF), Plant Biological Science (PBS) Graduate Program, the Minnesota Agricultural Experiment Station (AES), and the Gordon and Margaret Bailey Endowment for Environmental Horticulture. I have been fortunate to receive a number of grants and awards that have supported my travel to international meetings and the presentation of my research, including funds from the Plant Biological Sciences (PBS) graduate program, the Microbial and Plant Genomics Institute (MPGI), the Council of Graduate Students (COGS), the International Plant Growth Substance Association (IPGSA), and the "US-German Arabidopsis Functional Genomics Exchange Program" from NSF.

Last but not least, I thank my parents, my relatives, and my friends for their encouragement during my graduate studies. And I thank all the people I met worldwide at conferences and during my travels that have had a lasting impact on me by sharing their thoughts and experiences.

Abstract

Auxins, primarily indole-3-acetic acid (IAA), are endogenous plant hormones well known as key regulators of plant growth and development. Both genetic and biochemical studies have demonstrated that plants have developed a complex system to regulate the level of IAA, including biosynthesis of IAA from Trp-dependent and Trp-independent pathways, polar auxin transport, conjugation and hydrolysis of auxin. To accurately measure changes in IAA levels and identify pathways that contribute to the changes, I developed methods for quantitative analyses of auxin levels, auxin biosynthesis, and polar auxin transport. Using radioisotope labeling and stable-isotope dilution, I found that in etiolated tomato seedlings, a brief light exposure increased both IAA biosynthesis in the upper tissue sections and polar IAA transport in hypocotyls in a phytochrome-dependent manner, leading to unchanged free IAA levels in the top section and increased free IAA levels in the lower hypocotyl regions. In addition, using stable-isotope labeling and stable-isotope dilution, I quantified polar auxin transport in Arabidopsis hypocotyls, and I found that the transport of indole-3-butyric acid (IBA), another endogenous auxin, was much lower than IAA and that its transport mechanism was distinct from IAA transport. I also found that a small amount of IBA metabolic products, such as ester-linked IBA and IAA, was transported, while the majority of transported IAA remained as free IAA, suggesting that the polar transport of IAA could directly change the level of IAA while the transport of IBA could be an additional means to regulate IAA. In summary, my studies provide comprehensive views of auxin regulation in plants under different physiological conditions, showing that multiple mechanisms cooperatively regulate local auxin levels.

Table of Contents

List of Figures

Chapter 1

Introduction:
Regulation of Auxin through Multiple Mechanisms

Phytohormones are chemical messengers that are produced in any one part of a plant and modulate physiological processes in another part of the plant by interacting with specific protein receptors (Went and Thimann, 1937; Taiz and Zeiger, 2006). Auxin was the first phytohormone to be discovered, and the major form of natural auxin is indole-3-acetic acid (IAA). As suggested by its name—derived from a Greek word meaning "to grow"—auxin is a key factor that controls the growth of plants and allows them to react to their environment (Vogel, 2006). Perhaps due to auxin's critical role in growth and development, plants have evolved complex systems to regulate the level of free, active IAA (Fig. 1-1).

IAA can be polarly transported in plants to trigger growth responses at sites distant from where it is produced or applied, which was the feature leading to the discovery of auxin (Darwin and Darwin, 1881) and formed the basis for early techniques of auxin measurement (Went and Thimann, 1937). Auxin transport is controlled by a series of influx and efflux proteins (Peer *et al*., 2011) and is considered as a predominant way to generate and maintain differential distribution of auxin required for many plant developmental processes (Petrásek and Friml, 2009).

Although some computational models of auxin-regulated development have been generated exclusively based on auxin transport (Grieneisen *et al*., 2007; Bayer *et al*., 2009), the local biosynthesis of auxin has also been shown to play important roles in plant development (Zhao, 2010). The knowledge of IAA biosynthesis in plants has been significantly advanced in the past two decades by both isotope labeling and molecular genetic studies. IAA can be directly synthesized from indole via Trp-independent

pathways, through intermediates and enzymes that remain to be identified (Wright *et al*., 1991; Normanly *et al*., 1993). Meanwhile, IAA is also produced from indole through the formation of Trp via several different intermediates (Fig. 1-2). Among these Trp-dependent pathways, the indole-3-pyruvic acid (IPyA) pathway may be the most important, because it has been shown to operate in both monocot and dicot plants (Phillips *et al*., 2011; Mashiguchi *et al*., 2011; Won *et al*., 2011; Stepanova *et al*., 2011), and because it is thus far the only pathway with intermediates and enzymes completely known. On the other hand, the indole-3-acetaldoxime (IAOx) pathway may not be a common IAA biosynthetic pathway, because IAOx and its biosynthetic enzymes were not detected in monocot plants or in dicot plants such as tobacco (Sugawara *et al*., 2009). Indole-3-acetamide (IAM) is another potential IAA biosynthetic precursor, but the enzyme converting Trp to IAM remains to be identified in plants. Additionally, indol-3-butyric acid (IBA) has been demonstrated as an important precursor of IAA (Strader *et al*., 2010; Strader *et al*., 2011), but the biosynthetic pathway that utilizes IBA as an intermediate remains to be discovered.

To reduce active IAA in cells, plants have also developed strategies to either remove free IAA from its functional cell compartment or deactivate free IAA by oxidation or conjugation. It was reported that free IAA was compartmented into chloroplasts in tobacco protoplasts (Sitbon *et al*., 1993), and the endoplasmic reticulum (ER)-localized Arabidopsis PIN5 protein was involved in regulating auxin flow between the cytosol and the ER lumen (Mravec *et al*., 2009). As summarized in Figure 1-3, IAA can be catabolized by ring oxidation to OxIAA, which can be further conjugated to hexose or glucose (Ostin *et al*., 1998; Kai *et al*., 2007). In addition, IAA can be conjugated to other small molecules, peptides, or proteins via ester or amide bonds, and some conjugates can also be oxidized and catabolized (Fig. 1-3; Kai *et al*., 2007). Conjugated IAA also forms a large IAA reservoir, which can release free IAA by hydrolase enzymes (summarized by Woodward and Bartel, 2005), and conjugation of IBA may also provide a means to regulate the level of free IAA (Fig. 1-3).

Although multiple mechanisms are involved in the regulation of free IAA, they do not work independently. During early seedling development, the hydrolysis of IAA conjugates serves as an important source for free IAA when there is little or no *de novo* biosynthesis (Nowacki and Bandurski, 1980; Bialek and Cohen, 1992; Ljung *et al*., 2001). The transport of IAA can be increased by elevated amount of free IAA (Paciorek *et al*., 2005), and disruption in either biosynthesis or transport of IAA abolished the shade avoidance response in Arabidopsis seedlings (Tao *et al*., 2008; Keuskamp *et al*., 2010). Overexpression of IAA biosynthetic genes led to increased levels of not only free IAA, but also OxIAA and conjugated IAA (Mashiguchi *et al*., 2011; Stepanova *et al*., 2011). When the expression of the ER-localized IAA transport protein PIN5 was induced in tobacco cells, the level of free IAA was decreased and levels of IAA conjugates were increased (Mravec *et al*., 2009). Taken together, these reports suggest that the IAA regulatory pathways interact with each other, constructing a network that precisely regulates free IAA levels at targeted locations in plants.

My thesis research studies the roles of these IAA regulatory pathways and how they interact to regulate physiological processes. Chapter 2 provides protocols for precise, sensitive and quantitative determination of auxin levels and auxin biosynthesis, which forms a solid foundation for the work that follows. Chapter 3 describes how etiolated plants regulate auxin levels in a tissue-specific manner, after their exposure to a small amount of light. Chapter 4 illustrates that the substrate in the auxin transport stream is free IAA, but not its precursor IBA or its conjugates. The addenda at the end contain work I contributed to collaborative projects, which are all aimed at understanding the regulation of IAA though different pathways under varies environmental and physiological conditions.

Figures

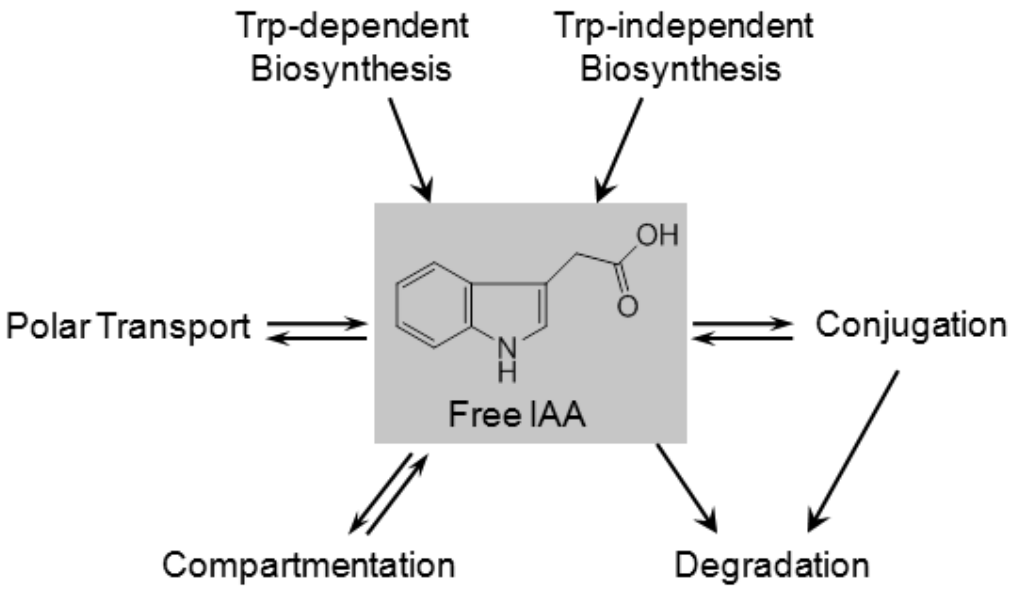

Figure 1-1. A summary of mechanisms regulating the level of free IAA. Arrows pointing to free IAA represent positive regulation pathways, and arrows pointing away from free IAA represent negative regulation pathways.

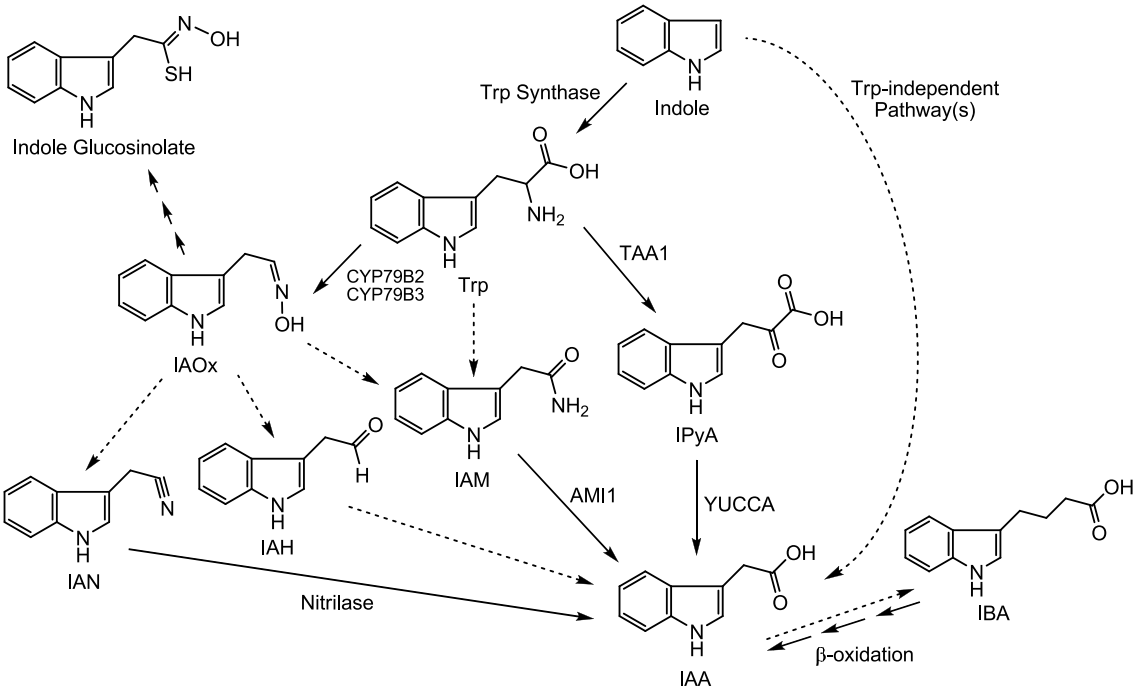

Figure 1-2. Proposed IAA biosynthetic pathways in plants. Solid arrows: steps with catalytic enzymes identified in plants. Dashed arrows: enzymes and/or intermediates remain to be identified. Three continuous solid arrows: multiple steps abbreviated.

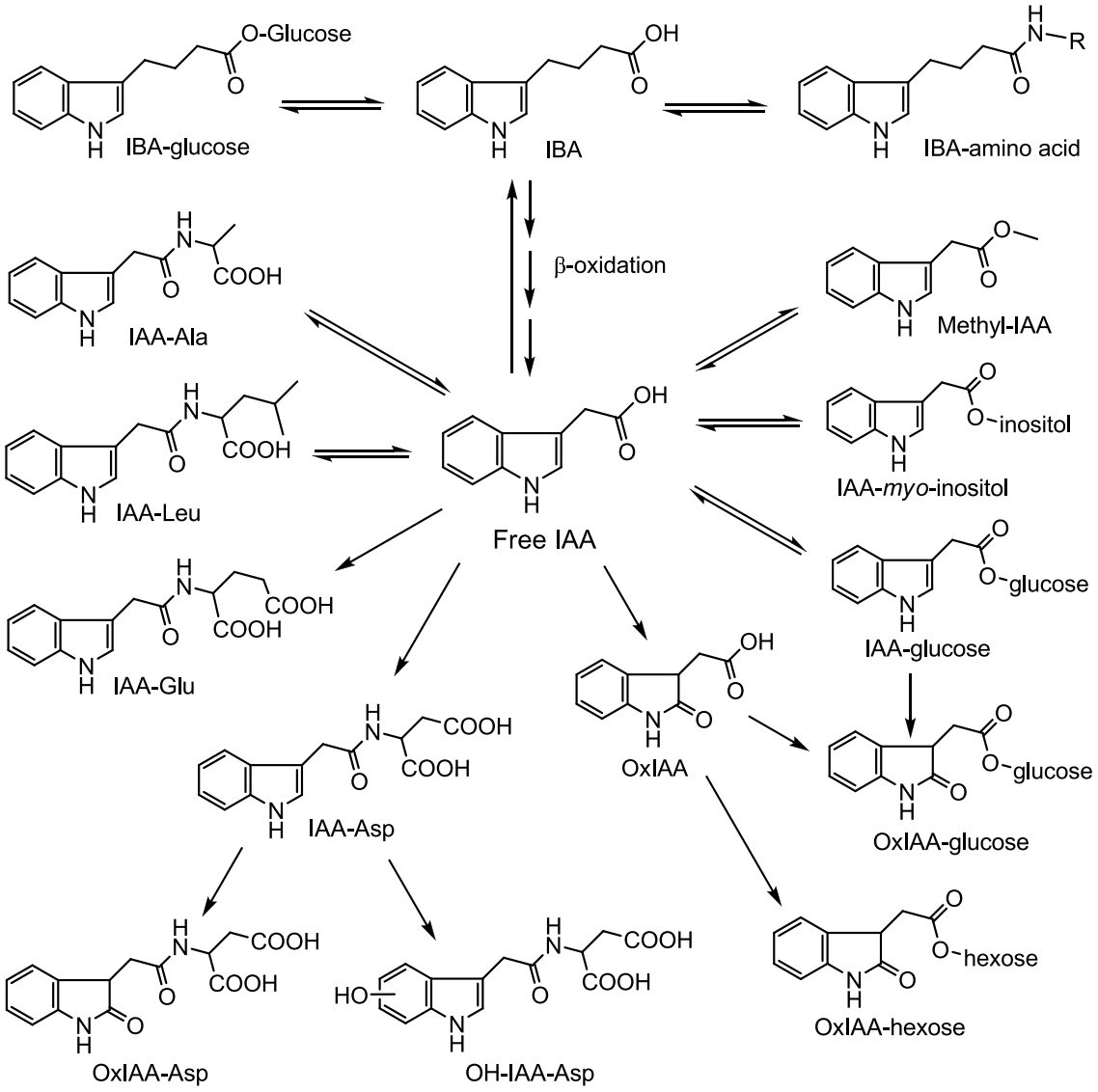

Figure 1-3. Potential products of IAA conjugation and oxidation identified in plants. Arrowhead suggests the proposed direction of the reaction. Three continuous arrows indicate multiple steps abbreviated.

Chapter 2

High-throughput and Quantitative Assays of Auxin and Auxin Precursors from Minute Tissue Samples

Introduction

Auxin, the first discovered plant hormone, plays critical roles in plant growth, organ formation, and plant responses to environmental stimuli. As the major form of natural auxin, indole-3-acetic acid (IAA) has been extensively studied, and mechanisms of its function and regulation are being revealed. To trigger downstream signaling responses, IAA functions like molecular glue, which ties its receptor TIR1, an F-box protein, with Aux/IAA transcriptional repressors, leading to degradation of Aux/IAA and thus releasing the transcriptional suppression of auxin responsive genes (Tan *et al.*, 2007). Based on this functional mechanism, auxin responses in cells can be partially controlled by the cellular concentration of IAA. Because IAA is a mobile signaling molecule that can be transported among cells to form auxin gradients and auxin maxima that are essential for plant development (reviewed by Petrásek and Friml, 2009), a method that allows quick and precise measurement of IAA in specific plant tissues will greatly facilitate understandings of auxin regulated plant growth and development.

Among the different pathways of IAA regulation (reviewed by Woodward and Bartel, 2005), the biosynthesis of IAA is a central way to regulate cellular IAA levels and has been actively studied for the past six decades (reviewed by Zhao, 2010). In general, two types of pathways exist in plants to synthesize IAA, Trp-dependent and Trp-independent (Fig. 2-1). The Trp-independent biosynthesis of IAA was implied by a study showing low incorporation of ^{15}N from [^{15}N-indole]Trp into IAA (Baldi *et al.*, 1991) and was confirmed by studies showing the production of labeled IAA from its labeled

precursors in Trp auxotrophic mutant plants (Wright *et al.*, 1991; Normanly *et al.*, 1993). Because no genes involved in Trp-independent pathways have been identified, analyzing the incorporation of labeled atoms into IAA and Trp from their common labeled precursors has been shown to be a useful tool to study the activity of Trp-independent IAA biosynthesis (Wright *et al.*, 1991; Normanly *et al.*, 1993; Sztein *et al.*, 2002; Epstein *et al.*, 2002; Liu *et al.*, 2011, see also Chapter 3). On the other hand, IAA can also be synthesized from multiple Trp-dependent pathways (Mashiguchi *et al.*, 2011), and importantly, several recent studies illustrated that in both Arabidopsis (*Arabidopsis thaliana*) and maize (*Zea mays* L.), IAA can be synthesized from Trp via the formation of indole-3-pyruvic acid (IPyA) (Fig. 2-1; Phillips *et al.* 2011; Mashiguchi *et al.*, 2011; Won *et al.*, 2011; Stepanova *et al.*, 2011). Thus, IPyA has been demonstrated as an important intermediate of Trp-dependent IAA biosynthesis, and quantification of IPyA provides great potential to reveal mechanisms regulating this IAA biosynthetic pathway.

Indole-3-butyric acid (IBA) is another small molecule that displays auxin activity and has been identified as an endogenous plant compound (reviewed by Ludwig-Müller, 2000). Recent studies have confirmed that IAA can be produced from IBA via β-oxidation (Strader *et al.*, 2010), and have shown that the IBA-derived IAA is important for plant development (Strader *et al.*, 2011). Additionally, the regulation of IBA metabolism also affects plant development and stress tolerance (Tognetti *et al.*, 2010). Therefore, analysis of IBA levels and its conversion to IAA also provides insights into the understanding of IAA regulation.

A method was previously reported for quantitative analyses of IAA and IBA, using solid phase extraction (SPE) columns and gas chromatography (GC) coupled with selected ion monitoring (SIM) on a single quadrupole mass spectrometer (MS) (Barkawi *et al.*, 2008; Barkawi *et al.*, 2010). Here I am describing an improved method that allows simpler equipment setup for sample preparation and smaller amounts of plant tissues collected for analysis, using selected reaction monitoring (SRM) on a GC triple-quadrupole MS (GC-MS/MS). In addition, this protocol describes methods for analyses of IAA precursors including indole, Trp and IPyA, and methods for rapid synthesis of

stable-labeled internal standards. Thus, this protocol can be used to either measure levels of IAA and its precursors or to analyze IAA biosynthesis in plants.

Development and principles of the protocol

The protocol of high-throughput SPE purification and GC-MS analysis has been validated as a good approach to quantify auxin levels and auxin biosynthesis (Tam and Normanly, 1998; Barkawi *et al.*, 2008; Liu *et al.*, 2011, see also Chapter 3). Major procedures of the protocol are summarized in Fig. 2-2. Briefly, indole, Trp, IAA, and IBA can be extracted from the same aliquot of plant homogenate and analyzed by GC-MS/MS separately, except that IAA and IBA are contained in the same sample and are analyzed in one GC-MS/MS run; using another aliquot of plant homogenate, IPyA can be extracted, derivatized, and analyzed by GC-MS/MS.

To quantify the level of endogenous compounds using isotope dilution, proper stable isotope labeled internal standards are required. An ideal internal standard should contain stable isotopes at non-exchangeable positions on compounds identical to the analytes, with mass increments of three or more (Cohen *et al.*, 1986). When exchange of stable isotopes occurs during sample preparation and analysis, the amount of internal standard would decrease, leading to overestimation of the endogenous compound. When an internal standard with a small mass increment is used, the interference by natural abundance would greatly complicate the calculation (for example, [$^{13}C_1$]indole-3-acetonitrile, Ilic *et al.*, 1996). However, such stable-labeled internal standards are not always readily available, especially for IPyA which degrades rapidly in solution (Tam and Normanly, 1998). Therefore, I developed and describe herein protocols to rapidly synthesize [$^{13}C_8$,$^{15}N_1$]IBA from [$^{13}C_8$,$^{15}N_1$]indole (**Supplemental Method 1**) and [$^{13}C_{11}$,$^{15}N_1$]IPyA from [$^{13}C_{11}$,$^{15}N_2$] Trp (**Supplemental Method 2**). Considering the high cost of [$^{13}C_{11}$,$^{15}N_2$] Trp, [2,4,5,6,7-$^{2}H_5$-indole]Trp can be a good alternative when GC-MS is used for the analysis (Tam and Normanly, 1998). However, when liquid chromatography-mass spectrometry (LC-MS) is used, the deuterium atoms on the indole ring may be lost during the ionization process (Davies *et al.*, 2010), and thus deuterium-

labeled indolic compounds should generally not be used as internal standards with LC-MS. After proper stable-labeled internal standards are available, they should be introduced into plant samples at the earliest possible step, and as I described in the protocol, they are added together with the homogenization buffer right before tissue homogenization.

The SPE purification of IAA and IBA is derived from a protocol previously published (Barkawi *et al.*, 2010), and the most significant improvement is the use of TopTips (Fig. 2-3), which can retain SPE resin while letting liquid pass through the 1-2 µl slit at the bottom (http://www.glysci.com/products/TopTip.html). In addition to commercial TopTips, SPE tips can also be made by inserting small pieces of glass wool into regular pipette tips (Ribnicky *et al.*, 1998). The first SPE tip used for IAA and IBA extraction contains amino (NH_2) resin, which retains the ionized organic acids at neutral pH but not Trp, so Trp can be collected in the flow-through and extracted separately (Fig. 2-2). The second SPE tip contains polymethylmethacrylate epoxide (PMME) resin, which binds protonated IAA and IBA when the pH is around 3.0 and releases them when methanol is added for elution. Finally, IAA and IBA are methylated by diazomethane in the presence of methanol (Fig. 2-4), and the methylated IAA and IBA are analyzed by monitoring the quinolinium ion produced from the molecular ion (SRM; Fig. 2-5) after GC separation.

The flow-through from the NH_2 tip is collected to extract the IAA precursor Trp, using DOWEX50 resin (Chen *et al.*, 2010). If only amino acids are of interest, they can be extracted by loading diluted plant homogenate onto DOWEX50 tips, skipping the NH_2 tip. DOWEX50 resin retains cations, such as the protonated amino group on Trp at neutral pH, and releases Trp when the pH is increased by ammonium hydroxide (NH_4OH). Both the amino and carboxyl groups are then derivatized by methyl chloroformate (MCF) in the presence of methanol and pyridine at basic pH, based on a mechanism described previously (Chen *et al.*, 2010; Fig. 2-4), and the derivatized Trp is analyzed by GC-MS using the SIM acquisition mode (Fig. 2-5).

Chapter 1

Introduction:
Regulation of Auxin through Multiple Mechanisms

Phytohormones are chemical messengers that are produced in any one part of a plant and modulate physiological processes in another part of the plant by interacting with specific protein receptors (Went and Thimann, 1937; Taiz and Zeiger, 2006). Auxin was the first phytohormone to be discovered, and the major form of natural auxin is indole-3-acetic acid (IAA). As suggested by its name—derived from a Greek word meaning "to grow"—auxin is a key factor that controls the growth of plants and allows them to react to their environment (Vogel, 2006). Perhaps due to auxin's critical role in growth and development, plants have evolved complex systems to regulate the level of free, active IAA (Fig. 1-1).

IAA can be polarly transported in plants to trigger growth responses at sites distant from where it is produced or applied, which was the feature leading to the discovery of auxin (Darwin and Darwin, 1881) and formed the basis for early techniques of auxin measurement (Went and Thimann, 1937). Auxin transport is controlled by a series of influx and efflux proteins (Peer *et al*., 2011) and is considered as a predominant way to generate and maintain differential distribution of auxin required for many plant developmental processes (Petrásek and Friml, 2009).

Although some computational models of auxin-regulated development have been generated exclusively based on auxin transport (Grieneisen *et al*., 2007; Bayer *et al*., 2009), the local biosynthesis of auxin has also been shown to play important roles in plant development (Zhao, 2010). The knowledge of IAA biosynthesis in plants has been significantly advanced in the past two decades by both isotope labeling and molecular genetic studies. IAA can be directly synthesized from indole via Trp-independent

pathways, through intermediates and enzymes that remain to be identified (Wright *et al*., 1991; Normanly *et al*., 1993). Meanwhile, IAA is also produced from indole through the formation of Trp via several different intermediates (Fig. 1-2). Among these Trp-dependent pathways, the indole-3-pyruvic acid (IPyA) pathway may be the most important, because it has been shown to operate in both monocot and dicot plants (Phillips *et al*., 2011; Mashiguchi *et al*., 2011; Won *et al*., 2011; Stepanova *et al*., 2011), and because it is thus far the only pathway with intermediates and enzymes completely known. On the other hand, the indole-3-acetaldoxime (IAOx) pathway may not be a common IAA biosynthetic pathway, because IAOx and its biosynthetic enzymes were not detected in monocot plants or in dicot plants such as tobacco (Sugawara *et al*., 2009). Indole-3-acetamide (IAM) is another potential IAA biosynthetic precursor, but the enzyme converting Trp to IAM remains to be identified in plants. Additionally, indol-3-butyric acid (IBA) has been demonstrated as an important precursor of IAA (Strader *et al*., 2010; Strader *et al*., 2011), but the biosynthetic pathway that utilizes IBA as an intermediate remains to be discovered.

To reduce active IAA in cells, plants have also developed strategies to either remove free IAA from its functional cell compartment or deactivate free IAA by oxidation or conjugation. It was reported that free IAA was compartmented into chloroplasts in tobacco protoplasts (Sitbon *et al*., 1993), and the endoplasmic reticulum (ER)-localized Arabidopsis PIN5 protein was involved in regulating auxin flow between the cytosol and the ER lumen (Mravec *et al*., 2009). As summarized in Figure 1-3, IAA can be catabolized by ring oxidation to OxIAA, which can be further conjugated to hexose or glucose (Ostin *et al*., 1998; Kai *et al*., 2007). In addition, IAA can be conjugated to other small molecules, peptides, or proteins via ester or amide bonds, and some conjugates can also be oxidized and catabolized (Fig. 1-3; Kai *et al*., 2007). Conjugated IAA also forms a large IAA reservoir, which can release free IAA by hydrolase enzymes (summarized by Woodward and Bartel, 2005), and conjugation of IBA may also provide a means to regulate the level of free IAA (Fig. 1-3).

Although multiple mechanisms are involved in the regulation of free IAA, they do not work independently. During early seedling development, the hydrolysis of IAA conjugates serves as an important source for free IAA when there is little or no *de novo* biosynthesis (Nowacki and Bandurski, 1980; Bialek and Cohen, 1992; Ljung *et al*., 2001). The transport of IAA can be increased by elevated amount of free IAA (Paciorek *et al*., 2005), and disruption in either biosynthesis or transport of IAA abolished the shade avoidance response in Arabidopsis seedlings (Tao *et al*., 2008; Keuskamp *et al*., 2010). Overexpression of IAA biosynthetic genes led to increased levels of not only free IAA, but also OxIAA and conjugated IAA (Mashiguchi *et al*., 2011; Stepanova *et al*., 2011). When the expression of the ER-localized IAA transport protein PIN5 was induced in tobacco cells, the level of free IAA was decreased and levels of IAA conjugates were increased (Mravec *et al*., 2009). Taken together, these reports suggest that the IAA regulatory pathways interact with each other, constructing a network that precisely regulates free IAA levels at targeted locations in plants.

My thesis research studies the roles of these IAA regulatory pathways and how they interact to regulate physiological processes. Chapter 2 provides protocols for precise, sensitive and quantitative determination of auxin levels and auxin biosynthesis, which forms a solid foundation for the work that follows. Chapter 3 describes how etiolated plants regulate auxin levels in a tissue-specific manner, after their exposure to a small amount of light. Chapter 4 illustrates that the substrate in the auxin transport stream is free IAA, but not its precursor IBA or its conjugates. The addenda at the end contain work I contributed to collaborative projects, which are all aimed at understanding the regulation of IAA though different pathways under varies environmental and physiological conditions.

Figures

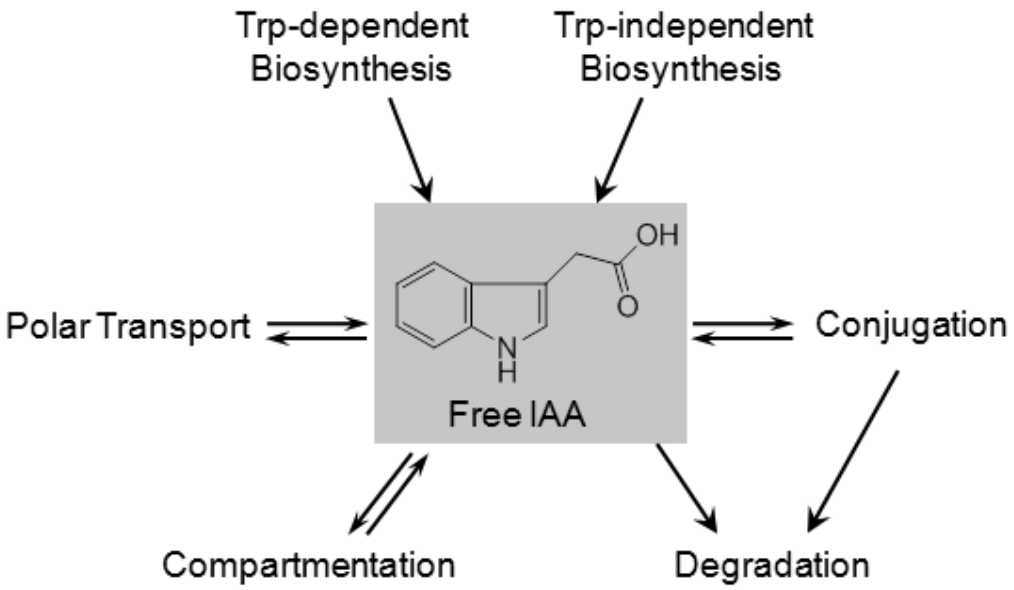

Figure 1-1. A summary of mechanisms regulating the level of free IAA. Arrows pointing to free IAA represent positive regulation pathways, and arrows pointing away from free IAA represent negative regulation pathways.

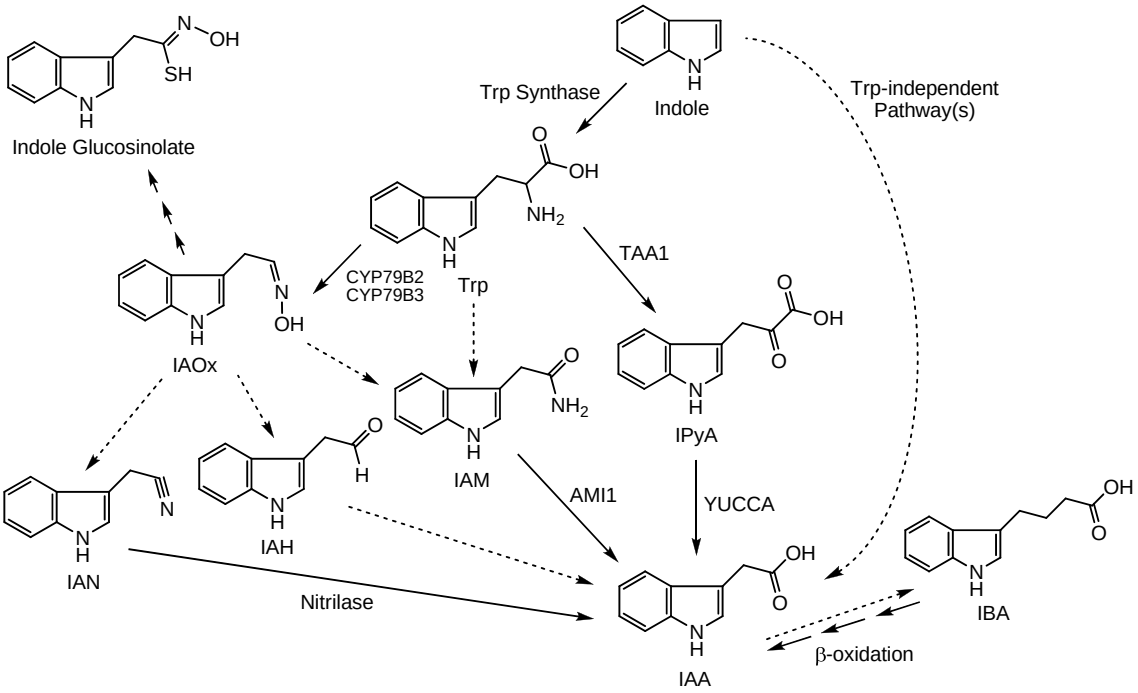

Figure 1-2. Proposed IAA biosynthetic pathways in plants. Solid arrows: steps with catalytic enzymes identified in plants. Dashed arrows: enzymes and/or intermediates remain to be identified. Three continuous solid arrows: multiple steps abbreviated.

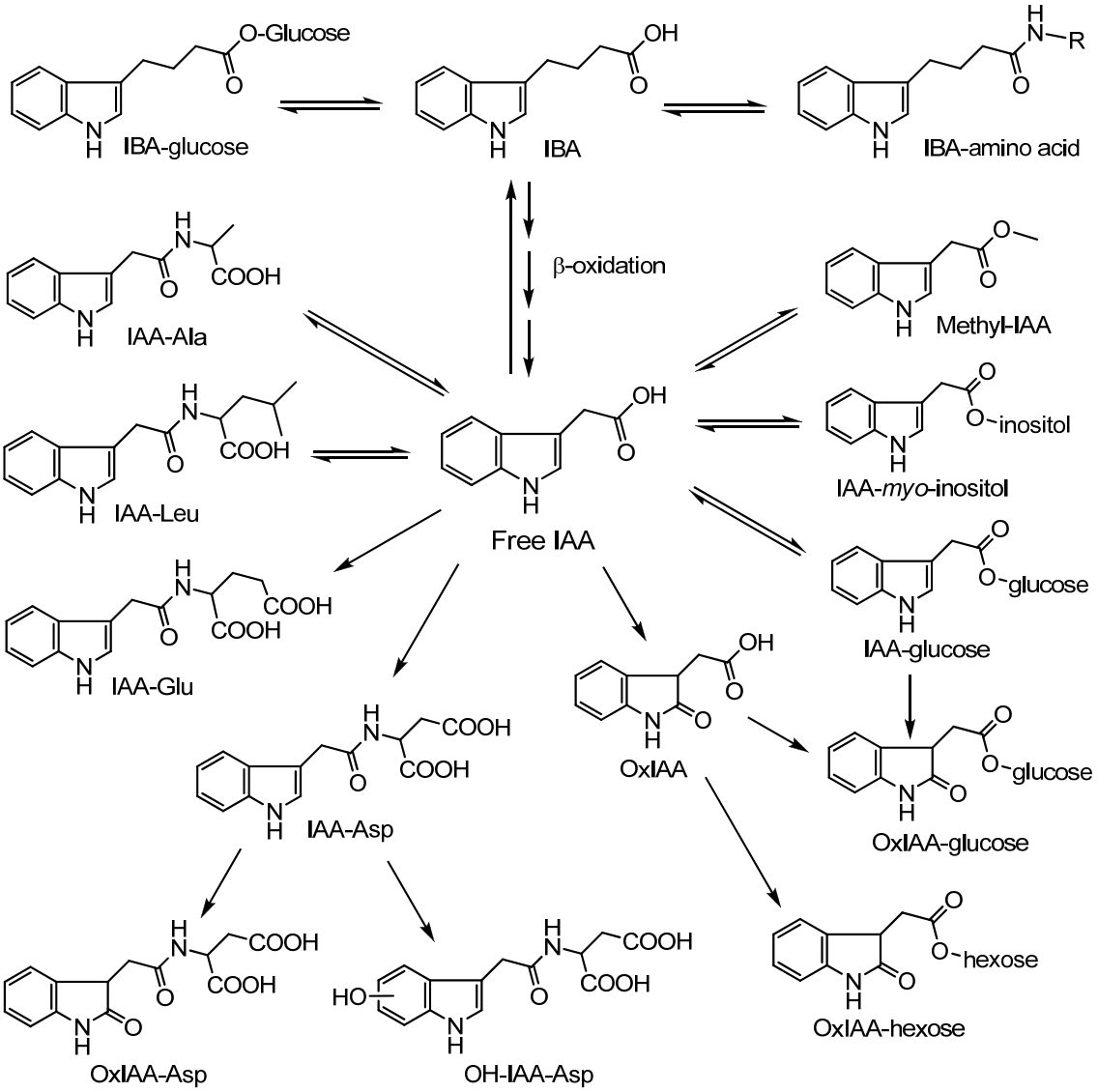

Figure 1-3. Potential products of IAA conjugation and oxidation identified in plants. Arrowhead suggests the proposed direction of the reaction. Three continuous arrows indicate multiple steps abbreviated.

Chapter 2

High-throughput and Quantitative Assays of Auxin and Auxin Precursors from Minute Tissue Samples

Introduction

Auxin, the first discovered plant hormone, plays critical roles in plant growth, organ formation, and plant responses to environmental stimuli. As the major form of natural auxin, indole-3-acetic acid (IAA) has been extensively studied, and mechanisms of its function and regulation are being revealed. To trigger downstream signaling responses, IAA functions like molecular glue, which ties its receptor TIR1, an F-box protein, with Aux/IAA transcriptional repressors, leading to degradation of Aux/IAA and thus releasing the transcriptional suppression of auxin responsive genes (Tan *et al.*, 2007). Based on this functional mechanism, auxin responses in cells can be partially controlled by the cellular concentration of IAA. Because IAA is a mobile signaling molecule that can be transported among cells to form auxin gradients and auxin maxima that are essential for plant development (reviewed by Petrásek and Friml, 2009), a method that allows quick and precise measurement of IAA in specific plant tissues will greatly facilitate understandings of auxin regulated plant growth and development.

Among the different pathways of IAA regulation (reviewed by Woodward and Bartel, 2005), the biosynthesis of IAA is a central way to regulate cellular IAA levels and has been actively studied for the past six decades (reviewed by Zhao, 2010). In general, two types of pathways exist in plants to synthesize IAA, Trp-dependent and Trp-independent (Fig. 2-1). The Trp-independent biosynthesis of IAA was implied by a study showing low incorporation of ^{15}N from [^{15}N-indole]Trp into IAA (Baldi *et al.*, 1991) and was confirmed by studies showing the production of labeled IAA from its labeled

precursors in Trp auxotrophic mutant plants (Wright *et al.*, 1991; Normanly *et al.*, 1993). Because no genes involved in Trp-independent pathways have been identified, analyzing the incorporation of labeled atoms into IAA and Trp from their common labeled precursors has been shown to be a useful tool to study the activity of Trp-independent IAA biosynthesis (Wright *et al.*, 1991; Normanly *et al.*, 1993; Sztein *et al.*, 2002; Epstein *et al.*, 2002; Liu *et al.*, 2011, see also Chapter 3). On the other hand, IAA can also be synthesized from multiple Trp-dependent pathways (Mashiguchi *et al.*, 2011), and importantly, several recent studies illustrated that in both Arabidopsis (*Arabidopsis thaliana*) and maize (*Zea mays* L.), IAA can be synthesized from Trp via the formation of indole-3-pyruvic acid (IPyA) (Fig. 2-1; Phillips *et al.* 2011; Mashiguchi *et al.*, 2011; Won *et al.*, 2011; Stepanova *et al.*, 2011). Thus, IPyA has been demonstrated as an important intermediate of Trp-dependent IAA biosynthesis, and quantification of IPyA provides great potential to reveal mechanisms regulating this IAA biosynthetic pathway.

Indole-3-butyric acid (IBA) is another small molecule that displays auxin activity and has been identified as an endogenous plant compound (reviewed by Ludwig-Müller, 2000). Recent studies have confirmed that IAA can be produced from IBA via β-oxidation (Strader *et al.*, 2010), and have shown that the IBA-derived IAA is important for plant development (Strader *et al.*, 2011). Additionally, the regulation of IBA metabolism also affects plant development and stress tolerance (Tognetti *et al.*, 2010). Therefore, analysis of IBA levels and its conversion to IAA also provides insights into the understanding of IAA regulation.

A method was previously reported for quantitative analyses of IAA and IBA, using solid phase extraction (SPE) columns and gas chromatography (GC) coupled with selected ion monitoring (SIM) on a single quadrupole mass spectrometer (MS) (Barkawi *et al.*, 2008; Barkawi *et al.*, 2010). Here I am describing an improved method that allows simpler equipment setup for sample preparation and smaller amounts of plant tissues collected for analysis, using selected reaction monitoring (SRM) on a GC triple-quadrupole MS (GC-MS/MS). In addition, this protocol describes methods for analyses of IAA precursors including indole, Trp and IPyA, and methods for rapid synthesis of

stable-labeled internal standards. Thus, this protocol can be used to either measure levels of IAA and its precursors or to analyze IAA biosynthesis in plants.

Development and principles of the protocol

The protocol of high-throughput SPE purification and GC-MS analysis has been validated as a good approach to quantify auxin levels and auxin biosynthesis (Tam and Normanly, 1998; Barkawi *et al.*, 2008; Liu *et al.*, 2011, see also Chapter 3). Major procedures of the protocol are summarized in Fig. 2-2. Briefly, indole, Trp, IAA, and IBA can be extracted from the same aliquot of plant homogenate and analyzed by GC-MS/MS separately, except that IAA and IBA are contained in the same sample and are analyzed in one GC-MS/MS run; using another aliquot of plant homogenate, IPyA can be extracted, derivatized, and analyzed by GC-MS/MS.

To quantify the level of endogenous compounds using isotope dilution, proper stable isotope labeled internal standards are required. An ideal internal standard should contain stable isotopes at non-exchangeable positions on compounds identical to the analytes, with mass increments of three or more (Cohen *et al.*, 1986). When exchange of stable isotopes occurs during sample preparation and analysis, the amount of internal standard would decrease, leading to overestimation of the endogenous compound. When an internal standard with a small mass increment is used, the interference by natural abundance would greatly complicate the calculation (for example, [$^{13}C_1$]indole-3-acetonitrile, Ilic *et al.*, 1996). However, such stable-labeled internal standards are not always readily available, especially for IPyA which degrades rapidly in solution (Tam and Normanly, 1998). Therefore, I developed and describe herein protocols to rapidly synthesize [$^{13}C_8$,$^{15}N_1$]IBA from [$^{13}C_8$,$^{15}N_1$]indole (**Supplemental Method 1**) and [$^{13}C_{11}$,$^{15}N_1$]IPyA from [$^{13}C_{11}$,$^{15}N_2$] Trp (**Supplemental Method 2**). Considering the high cost of [$^{13}C_{11}$,$^{15}N_2$] Trp, [2,4,5,6,7-$^{2}H_5$-indole]Trp can be a good alternative when GC-MS is used for the analysis (Tam and Normanly, 1998). However, when liquid chromatography-mass spectrometry (LC-MS) is used, the deuterium atoms on the indole ring may be lost during the ionization process (Davies *et al.*, 2010), and thus deuterium-

labeled indolic compounds should generally not be used as internal standards with LC-MS. After proper stable-labeled internal standards are available, they should be introduced into plant samples at the earliest possible step, and as I described in the protocol, they are added together with the homogenization buffer right before tissue homogenization.

The SPE purification of IAA and IBA is derived from a protocol previously published (Barkawi *et al.*, 2010), and the most significant improvement is the use of TopTips (Fig. 2-3), which can retain SPE resin while letting liquid pass through the 1-2 µl slit at the bottom (http://www.glysci.com/products/TopTip.html). In addition to commercial TopTips, SPE tips can also be made by inserting small pieces of glass wool into regular pipette tips (Ribnicky *et al.*, 1998). The first SPE tip used for IAA and IBA extraction contains amino (NH_2) resin, which retains the ionized organic acids at neutral pH but not Trp, so Trp can be collected in the flow-through and extracted separately (Fig. 2-2). The second SPE tip contains polymethylmethacrylate epoxide (PMME) resin, which binds protonated IAA and IBA when the pH is around 3.0 and releases them when methanol is added for elution. Finally, IAA and IBA are methylated by diazomethane in the presence of methanol (Fig. 2-4), and the methylated IAA and IBA are analyzed by monitoring the quinolinium ion produced from the molecular ion (SRM; Fig. 2-5) after GC separation.

The flow-through from the NH_2 tip is collected to extract the IAA precursor Trp, using DOWEX50 resin (Chen *et al.*, 2010). If only amino acids are of interest, they can be extracted by loading diluted plant homogenate onto DOWEX50 tips, skipping the NH_2 tip. DOWEX50 resin retains cations, such as the protonated amino group on Trp at neutral pH, and releases Trp when the pH is increased by ammonium hydroxide (NH_4OH). Both the amino and carboxyl groups are then derivatized by methyl chloroformate (MCF) in the presence of methanol and pyridine at basic pH, based on a mechanism described previously (Chen *et al.*, 2010; Fig. 2-4), and the derivatized Trp is analyzed by GC-MS using the SIM acquisition mode (Fig. 2-5).

The derivatization and extraction of IPyA is derived from a method previously described (Tam and Normanly, 1998), with modifications that confer more rapid sample preparation. Because IPyA has a short half-life in solution, the [$^{13}C_{11}$,$^{15}N_1$]IPyA internal standard should be made just prior to use (**Supplemental Method 2**). After tissue homogenization, IPyA is quickly derivatized by sodium borodeuteride (NaB^2H_4) to produce [$^2H_1$]indole-3-lactic acid ([$^2H_1$]ILA, Fig. 2-4), which degrades much more slowly and thus allows reliable quantification (Tam and Normanly, 1998). Because low levels of ILA exists in plants (Gibson *et al*., 1972; Hoenicke *et al*., 2001), it is necessary to use NaB^2H_4 (instead of $NaBH_4$) to produce [$^2H_1$]ILA that can be distinguished from endogenous ILA by MS. After converting IPyA to [$^2H_1$]ILA, the [$^2H_1$]ILA is protonated by acidifying the homogenate, and extracted by Oasis® HLB resin, a hydrophilic-lipophilic-balanced reversed-phase sorbent (http://www.waters.com/waters/nav.htm?cid=513209). The carboxyl group of [$^2H_1$]ILA is also methylated by diazomethane (Fig. 2-4), and the methylated product is analyzed by GC-MS using SRM (Fig. 2-5).

Application of the method and experimental design

Firstly, this protocol can be used for absolute quantification of IAA and IAA precursors. Because the extraction and GC-MS analysis of IPyA is essentially extraction and analysis of its reduced product ILA, the method can also be used to quantify endogenous ILA using [$^{13}C_{11}$,$^{15}N_1$]ILA as the internal standard, which can be made by reducing synthesized [$^{13}C_{11}$,$^{15}N_1$]IPyA using $NaBH_4$ (similar to Steps 17-22 in **Supplemental Method 2**). The IAA content in plants can vary significantly depending on growth conditions and developmental stages (Miller *et al*., 1987; Michalczuk *et al*., 1992; Gray *et al*., 1998; Rapparini *et al*., 2002; Tao *et al*., 2008), thus plants should be grown under controlled environmental conditions and the tissues collected for analysis should be at similar developmental stages. Because the levels of IAA or its precursors are usually expressed as ng g^{-1} fresh weight of plant tissue, the tissue weight should be precisely determined before freezing, and water or soil attached to the plant surface

should be removed before tissue collection. To minimize the effects of wounding, samples should be frozen in liquid N_2 quickly after weighing, and stored continuously at -80 ºC until tissue homogenization to avoid changes in IAA content. After homogenization, internal standards are added and plant metabolic enzymes are denatured by isopropanol in the homogenization buffer, so the plant homogenate can then be manipulated or stored at a higher temperature with no alterations to the quantification results.

Additionally, the protocol can be used to quantify the enrichment of stable-labeled IAA synthesized from stable-labeled IAA precursors or putative precursors. For this type of analysis, plants should be incubated with stable-labeled compounds such as [$^{13}C_1$]indole or [$^{13}C_8$,$^{15}N_1$]IBA for a certain period of time before tissue collection, and the abundance of both endogenous IAA and putative stable-labeled IAA should be monitored by GC-MS/MS. Because the enrichment is determined by the abundance of labeled IAA divided by abundance of endogenous IAA (see "anticipated result"), it is often not necessary to record the fresh weight of plant tissue or add internal standards prior to homogenization, unless the yield of labeled IAA is to be quantified. To quantify the amount of labeled IAA, the internal standard should contain a mass significantly different from the mass of labeled tracer IAA. For example, to quantify the amount of [$^{13}C_8$,$^{15}N_1$]IAA synthesized from [$^{13}C_8$,$^{15}N_1$]IBA, [$^{13}C_6$]IAA was used as the internal standard (Strader *et al.*, 2010); and to quantify the amount of transported [$^{13}C_6$]IAA in Arabidopsis hypocotyls, [4,5,6,7-$^{2}H_4$-indole]IAA was added as the internal standard (Liu *et al*., 2012, see also Chapter 4).

Using this protocol, the activity of IAA biosynthetic pathways can also be analyzed. By comparing the incorporation of ^{13}C from [$^{13}C_1$]indole into Trp and IAA pools (Fig. 2-6, D and E), it is possible to identify biotic and abiotic factors that change the activity of Trp-independent and/or Trp-dependent IAA biosynthesis (Epstein *et al.*, 2002; Rapparini *et al.*, 2002; Liu *et al.*, 2011, see also Chapter 3). Similarly, by quantifying the enrichment of labeled IAA and IPyA, the significance of IPyA-dependent

IAA biosynthesis under various biological conditions can be analyzed (Cooney and Nonhebel, 1991).

Advantage of the method

A major advantage of this method is the improved detectability of analytes. The SRM acquisition mode confers an order of magnitude higher sensitivity compared with the SIM acquisition mode, so the amount of plant tissue required in this protocol is at least ten times less than in the previous method (Barkawi *et al.*, 2010). Considering the accuracy of weighing, a minimal amount of 2 mg tissue is recommended for quantification of IAA and IBA (Fig. 2-6A). The lower requirement for plant tissue allows faster tissue collection and tissue-specific analysis, which enables detection of localized changes in IAA content and IAA biosynthesis (Ljung *et al*., 2005; Ikeda et al., 2009; Liu *et al.*, 2011, see also Chapter 3) and thus provides better understanding of IAA-regulated biological processes. In addition, with the more sensitive assay, plants can be incubated with IAA precursors for shorter periods of time and still yield sufficient amounts of labeled IAA for detection while reducing artifacts generated by exogenous compounds (Ribnicky *et al*., 1996; Liu *et al*., 2011, see also Chapter 3). Therefore, this more sensitive method can also provide more accurate assessments of IAA regulatory mechanisms.

To better quantify the trace amount of plant endogenous compounds in a high-throughput manner, I modified the inlet port of the GC (see "GC-MS/MS system setup"). I replaced the standard septum with a Merlin Microseal™ high pressure seal to reduce injection of the septum material into the GC column and permit less frequent change of the septum. I used a custom Teflon washer to provide a better seal between the Merlin seal adaptor and the GC inlet and to avoid interaction between the seal material and injected analytes. I also replaced the inlet liner with a custom quartz liner to minimize the effect of residual analytes from earlier injections carried-over to later injections and thus increased the accuracy of the assay.

Another highlight of the protocol is the use of SPE tips. Compared with SPE columns which usually require a manifold connected with a vacuum pump for liquid

manipulation, SPE tips can be manipulated by a standard microcentrifuge, allowing simpler instrumental setup, less solvent consumption/waste, and preparation of more samples at one time. Because the SPE resin can be packed into tips simply by adding the resin suspension, SPE tips can be easily customized, which significantly reduces the cost and greatly facilitates development of new methods. Based on my experimental design, I decided to use 200-µl TopTips, but other tip sizes such as 10-µl or 1000-µl tips can also be used when different sample sizes are to be applied.

Materials

REAGENTS

- Nitrogen gas [ultra high purity (UHP)]
- Helium gas (UHP)
- Argon gas (UHP)
- Hexane (HPLC grade; Fisher, cat. no. H302) ►*CAUTION*: flammable
- Ethyl acetate (HPLC grade; Fisher, cat. no. E195) ►*CAUTION*: flammable
- Acetonitrile (HPLC grade; Fisher, cat. no. A998) ►*CAUTION*: flammable
- Methanol (HPLC grade; Fisher, cat. no. A452) ►*CAUTION*: flammable
- Dichloromethane (Sigma-Aldrich, cat. no. 154792) ►*CAUTION*: harmful
- Pyridine (ACS grade; EMC Chemicals, cat. no. PX2020) ►*CAUTION*: flammable
- Diethyl ether (HPLC grade; Sigma-Aldrich, cat. no. 309966) ►*CAUTION*: flammable; forms peroxides
- [$^{13}C_6$]IAA (Cambridge Isotope Laboratories, cat. no. CLM-1896)
  ► *CRITICAL*: keep container tightly closed and store in a dry place at -20 ºC.
- [$^{13}C_8$,$^{15}N_1$]Indole (Cambridge Isotope Laboratories, cat. no. CNLM-4786)
  ► *CRITICAL*: keep container tightly closed and store in a dry place at -20 ºC.
- [$^{13}C_{11}$,$^{15}N_2$]L- Trp (Cambridge Isotope Laboratories, cat. no. CNLM-2475)
  ► *CRITICAL*: keep container tightly closed and store in a dry place at -20 ºC.
- [$^{13}C_8$,$^{15}N_1$]IBA [synthesized from [$^{13}C_8$,^{15}N]indole as described in **Supplemental Method 1** (Cohen and Schulze, 1981; Barkawi *et al.* 2008)]

- [$^{13}C_{11}$,$^{15}N_1$]IPyA (synthesized from [$^{13}C_{11}$,$^{15}N_2$] Trp as described in **Supplemental Method 2**)
- Sodium sulfate (Na_2SO_4, anhydrous; Sigma-Aldrich, cat. no. 239313)
- Sodium borodeuteride (NaB^2H_4; Sigma-Aldrich, cat. no. 205591)
- Methanol : water (8:1, v:v)
- Methanol : 8 M ammonium hydroxide (NH_4OH; Fisher, cat. no. A669) (1:1, v:v)
- 0.3 N Sodium hydroxide (NaOH; Sigma-Aldrich, cat. no. S8045)
- 0.1 M Sodium bicarbonate, pH 7.0 ($NaHCO_3$; Mallinckrodt, cat. no. 7412)
- 50 mM $NaHCO_3$
- 0.2 M Imidazole, pH 7.0 (Sigma-Aldrich, cat. no. 56750) ►*CAUTION*: corrosive

  • NOTE: yellows with storage and yellowed material is not suitable for use. It may be recrystallized; otherwise should be discarded
- 50% (v/v) Isopropanol (HPLC grade; Fisher, cat. no. A451)
- Homogenization buffer: 65% isopropanol and 35% 0.2 M imidazole (pH 7.0)
- 0.25% Phosphoric acid (PA) (ACS grade; Fisher, cat. no. A242)
- 0.1 M Succinic acid, pH 6.0 (SA) (Sigma-Aldrich, cat. no. 224731)

  ► *CRITICAL*: store in refrigerator or prepare freshly, because bacteria grow well on succinic acid solutions.
- PA:SA (5:1, v:v), pH 3.0

  ► *CRITICAL*: store in refrigerator or prepare freshly, because bacteria grow well on succinic acid solutions.
- 25% (w/v) Polymethylmethacrylate epoxide resin (PMME, Macro-Prep; Bio-Rad, cat. no. 156-0000) suspension in 0.1 M $NaHCO_3$ (pH 7.0)
- 25% (w/v) NH_2 resin (Agilent, cat. no. 12213020) suspension in distilled water
- 25% (w/v) DOWEX® 50X2-400 ion-exchange resin (Sigma-Aldrich, cat. no. 217476), H^+ form, suspension in distilled water
- 25% (w/v) Oasis® HLB resin (collected from HLB cartridges; Waters, cat. no. WAT106202) suspension in methanol

- Ethereal diazomethane [prepared as previously described (Cohen, 1984; Barkawi and Cohen, 2010)]
- Methyl chloroformate (MCF; Sigma-Aldrich, cat. no. M35304) ►*CAUTION*: flammable, highly toxic by inhalation, toxic by ingestion, corrosive.

EQUIPMENT

- MICROMAN positive-displacement pipettes (Gilson, cat. no. F148501, F148502, F148503, F148504, F148505, F148506)
- MICROMAN positive-displacement pipette tips (Gilson, cat. no. F148412, F148112, F148113, F148414, F148114, F148560)
- 10-200 µl Empty TopTip for solid phase extraction (SPE) and adaptors for centrifugation (Glygen, cat. no. TT2EMT)
- Repeater® plus positive displacement pipette (Eppendorf, cat. no. 022260201)
- Eppendorf Combitips plus (1.0 ml, 5.0 ml; Eppendorf, cat. no. 022266209, 022266403)
- Tungsten-carbide beads (2.38 mm; Craig Ball Sales, cat. no. CATU.002380.000.0010)
- SealRite® microcentrifuge tubes (0.5 ml, 2.0 ml; USA Scientific, cat. no. 1605-0000, 1620-2700)
- Teflon Mixer-Mill adapter for 1.5- to 2-ml microcentrifuge tubes (Qiagen, cat. no. 69984)
- Vibration Mill (Mixer-Mill; Qiagen, cat. no. MM300)
- Microcentrifuge (Eppendorf, cat. no. 5417R)
- 2-ml Screw capped micro tubes (Sarstedt, cat. no. 72.694)
- 2-ml Clear glass vials with polytetrafluoroethylene (PTFE)-lined caps (Fisher Scientific, cat. no. 03-391-7A)
- 2-ml Amber glass vials with PTFE-lined caps (Fisher Scientific, cat. no. 03-391-8A)
- 8-ml Clear glass vials with PTFE-lined caps (Fisher Scientific, cat. no. 03-391-7C)
- 4-ml Amber glass vials with PTFE-lined caps (Fisher Scientific, cat. no. 03-391-8B)

- Color pHast Strips (Fisher Scientific, cat. no. S60170)
- Wide-mouth crimp vials (Chrom Tech, cat. no. CTV-1104)
- 250 µl Glass inserts with bottom spring (Chrom Tech, cat. no. CTI-9425)
- Crimp cap with silicone rubber septum, PTFE coated (Chrom Tech, cat. no. 515011)
- Crimper for 11-mm crimp caps (Sigma-Aldrich, cat. no. 33195)
- Decapping pliers (Chrom Tech, cat. no. 904371)
- Micro-dissecting forceps (Sigma-Aldrich, cat. no. F4017)
- Gas chromatograph (GC)-mass spectrometer (MS): Trace GC Ultra with TriPlus autosampler, TSQ Quantum triple quadrupole MS (Thermo Scientific®)
- GC capillary column 1: HP-5ms, 30 m, 0.25 mm diameter, 0.25 µm film thickness (Agilent Technologies, cat. no. 19091S-433UI)
- GC capillary column 2 (for analysis of indole-3-pyruvic acid only): DB-17ms, 30 m, 0.25 mm diameter, 0.25 µm film thickness (Agilent Technologies, cat. no. 122-4732)

EQUIPMENT SETUP

Diazomethane derivatization equipment

The following items are needed:

- Glass diazomethane generator with clear-seal joints as described in Cohen (1984)
- Teflon tubing (3 mm, Cole-Parmer, cat. no. C-06407-10)
- 8-ml Clear glass vials with PTFE-lined caps (Fisher Scientific, cat. no. 03-391-7C
- Stainless steel evaporator (six-position evaporator, Barvap 6, Zanntek, cat. no. 11-06000)
- Sand bath heated to 55 ºC

The stainless steel evaporator is connected with N_2 gas tank by Teflon tubing, and the probes of the evaporator are positioned above the sand bath so that samples can be heated while being evaporated by flowing N_2 gas. The Teflon tubing can be connected with the diazomethane generator during the diazomethane generation process (Cohen, 1984; Barkawi and Cohen, 2010).

SPE TopTips

Insert empty TopTips into adaptors that are placed on top of 2-ml screw capped micro tubes (Fig. 2-3A). Load SPE resin suspension into each tip from the top of the tip. For NH_2 resin, DOWEX® 50X2-400 ion-exchange resin, or Oasis® HLB resin, load 20 µl suspensions; for PMME resin, load 80 µl suspension. Then, spin the micro tubes together with the tips at 3,000 g for a few seconds (use "short" button on centrifuge). Repeat with higher centrifugal force and/or longer time if liquid does not pass though the tips.

GC-MS/MS system setup

The following items are used to set up the GC:

- Merlin Microseal™ high pressure kit (Thermo Scientific®, part no. 19050205, or contact Thermo Scientific® for the current part number)
- Merlin Microseal high pressure replacement septum (Merlin, part no. 410)
- Customized Teflon washer (made by Metro Industries, Inc. to the exact dimensions of the vespel/graphite washer supplied by Thermo Scientific®; a number of extras are available directly from our laboratory)
- 10 µl Syringe with an 80-mm needle (SGE Analytical Science, cat. no. 002989)
- Custom liners: Quartz glass tubes (outside diameter: 8 mm, inside diameter: 4 mm; part no. 4x8, Technical Glass Products, Inc.) cut to a length of 105 mm, lightly fire-polished and treated by Sylon CT™ (Sigma-Aldrich, cat. no. 33065-U) to deactivate the surface.
- Silanized quartz wool (Alltech, cat. no. 4233)

The GC was equipped with a split/splitless capillary inlet, and the standard septum was replaced by an adapter to accept the Merlin Microseal™ high pressure seal. To provide a better seal of the inlet and avoid adsorption of indolic compounds, the original vespel/graphite seal from the Thermo Scientific adapter kit was replaced by the custom Teflon washer, which was placed under the hexagonal adapter. A 10-µl syringe with an 80-mm needle was installed in the injector of the autosampler, and the injector position was adjusted to match the position and height of the Merlin Microseal™ valve. The

original straight inlet liner (Restek, cat. no. 20939) was replaced by a custom quartz liner with a cluster of quartz wool inserted at the center. The MS was equipped with an electron impact (EI) source with an electron emission of 70 eV.

GC-MS/MS program

Software Xcalibur™ 2.1 (Thermo Scientific®, part. no. XCALI-64155) and TSQ Series 2.0.6 (Thermo Scientific®, part. no. XCALI-64251) were installed to operate the GC-MS/MS.

- TriPlus Autosampler: Sample volume was 1.0 µl; injection depth was standard; pre- and post-injection dwell time was 0 s; sampling depth mode was custom and sampling vial depth was 88%; sample type was "non viscous".
- TRACE GC Ultra: in the "Oven" tab, under "Ramps", the initial oven temperature was 70 ºC and the hold time was 2 minutes; the Ramp 1 rate was 20 ºC/min until temperature reached 280 ºC, and the hold time was 5 minutes. In the "Right SSL" tab, the inlet mode was splitless; the inlet temperature was 240 ºC; the split flow was 10 ml/min, and the splitless time was 1 min; the "constant septum purge" was checked. In the "Right Carrier" tab, the carrier gas was run under "constant flow" mode, and the flow rate was 1.0 ml/min; the "vacuum compensation" was checked. In the "Aux Zones" tab, the MS transfer line temperature was set to 280 ºC.
- TSQ Quantum (Condition 1): in the "EI/CI" tab, the number of states was 2; the state at start of run was "off", and the state duration was 4 min; the emission current was 100 µA. The calibration gas setting was "off" and the CI method was unchecked. In the "scan editor" tab, the calibration correction method was unchecked; the MS acquire time was 17.50 min; scan type can be either SRM (selected reaction monitoring) or SIM (selected ion monitoring), and scan time was 0.025 s; the polarity was positive and the data type was centroid. When SRM mode was used, the argon collision gas pressure was 1.5 mTorr, and the collision energy was 10 V. The masses of ions to be monitored depended on the metabolites analyzed and will be described in the "procedure" section.

- TSQ Quantum (Condition 2, for analysis of indole-3-pyruvic acid only): similar to Condition 1, but the emission current in the "EI/CI" tab was 120 μA, the scan type in the "scan editor" tab was SRM, and the collision energy was 25 V.

Procedures

Plant sample preparation and homogenization

1. Collect plant material in 0.5-ml microcentrifuge tubes, and quickly freeze the tubes in liquid N_2. If performing absolute quantification of endogenous metabolites, determine the exact fresh weight (FW) of plant material quickly and accurately before freezing the tubes. Keep tubes on dry ice or store them at -80 ºC.

- ➢ CRITICAL STEP: Sufficient plant material is necessary for the yield of satisfactory GC-MS/MS signals. Usually, 2-10 mg plant tissue is enough for the analysis of IAA/IBA, indole, and Trp; about 10 mg plant tissue is needed for the analysis of IPyA alone. Because IAA, IBA, indole, and Trp are extracted from the same aliquot of plant homogenate while IPyA is extracted from a separate aliquot of plant homogenate, this protocol assumes that ~20 mg plant tissue is collected as one sample.
- ❖ PAUSE POINT: Frozen samples can be stored at -80 ºC or shipped in a dry ice package.

2. Add 40 μl homogenization buffer and a tungsten carbide bead to each tube. If performing absolute quantification of endogenous compounds, add known amounts of internal standards together with homogenization buffer. Samples need to be kept on dry ice before next step.

- ➢ CRITICAL STEP: Add 20 μl homogenization buffer for a sample containing no more than 10 mg plant tissue. For every increment of 10 mg plant tissue, add an additional 20 μl homogenization buffer.
- ➢ CRITICAL STEP: For absolute quantification, in 40 μl homogenization buffer, 0.4-1 ng of [$^{13}C_6$]IAA, [$^{13}C_8$,^{15}N]IBA, [$^{13}C_8$,$^{15}N_1$]indole, [$^{13}C_{11}$,^{15}N]IPyA are added, and (or) 100 ng of [$^{13}C_{11}$,$^{15}N_2$]Trp is added.

3. Place the sample tubes into a vibration mill (with the Teflon adaptor and de-capped 2.0-ml microcentrifuge tubes placed in the adaptor), and homogenize for 4 min at 20-25 Hz. Repeat this step if tissues are not fully homogenized. If tissues are difficult to homogenize, add more tungsten carbide beads and increase the vibration frequency.

Extraction and derivatization of IPyA

4. Transfer 20 µl plant homogenate into a new tube. Leave the rest of plant homogenate on ice (see Step 24).

5. Add 8 µl 20 mg/ml NaB^2H_4 into each tube, and mix well.

► *CRITICAL*: The 20 mg/ml NaB^2H_4 needs to be freshly prepared in 0.3 N NaOH, because NaB^2H_4 decomposes over time in aqueous solutions (Andrieux *et al*., 2011). Perform this step soon after homogenization to avoid significant degradation of IPyA.

6. Incubate samples at 35ºC for 1 h.

❖ PAUSE POINT: IPyA is reduced to [$^2H_1$]indole-3-lactic acid ([$^2H_1$]ILA), which is much more stable than IPyA, so samples can be stored at -20 ºC for a few days.

7. Add 5 µl 25% PA to acidify the sample and consume the residual NaB^2H_4.

8. Dilute the sample 10 fold by adding 200 µl distilled water and mixing well.

9. Check the pH of the diluted sample using a pH strip. The pH should be 2.5-3.0.

10. Wash the TopTips containing Oasis® HLB resin two times with 80 µl methanol and two times with 80 µl PA:SA (pH 3.0). Use repeater pipette to dispense the liquid into multiple TopTips. Liquid is forced to pass through TopTips by centrifugation at 3,000-6,000 g for a few seconds (Fig. 2-3B).

► *CRITICAL*: The 2-ml screw capped micro tubes can hold up to 500 µl liquid before the liquid reaches the bottom of the TopTips. Therefore, discard the liquid waste when ~400 µl liquid is passed through TopTips. If 2-ml microcentrifuge tubes are used instead of screw capped tubes, less liquid can be held and the liquid waste needs to be discarded more frequently.

11. Spin the diluted samples at 12,000 g for 10 min.

12. Load the supernatant of each sample into individual TopTip.

13. Spin TopTips at 2,000 g to allow samples to pass through slowly and completely.
14. Wash the TopTips two times with 60 µl PA:SA (pH 3.0).
15. Wash the TopTips with 10 µl methanol. Spin the TopTips at 10,000 g for 1-2 min.

➢ CRITICAL STEP: The methanol wash and long period of centrifugation are designed to remove the water residue in the resin. If a significant amount of water is retained in the resin, the efficiency of methylation (by ethereal diazomethane) will be reduced, and the drying process will be elongated.

16. Transfer the TopTips to new 2-ml tubes to collect the eluate.
17. Elute TopTips three times with 70 µl methanol.
18. Discard the TopTips.
19. Transfer the methanol eluate into a 2-ml clear glass vial.

❖ PAUSE POINT: Samples can be stored in capped vials at -20 ºC for a few days.

20. Fill each glass vial with ethereal diazomethane, and incubate for ~5 minutes.
21. Evaporate the solvents to complete dryness using a gentle N_2 gas stream in a sand bath heated to 55 ºC.

► *Caution*: Diazomethane is a toxic and explosive gaseous compound, and it is potentially explosive on contact with sharp edges such as scratched or broken glass. It should be prepared and used only in a fume hood and handled by hands protected with gloves. Read precautions in Cohen (1984) and Barkawi *et al.* (2010) before use.

22. Use 15 µl of ethyl acetate to re-suspend the sample, and transfer the ethyl acetate solution into a glass insert.
23. Place the glass insert into a crimp vial, and cap the vial.

❖ PAUSE POINT: Methylated samples can be stored at -20 ºC for a few days before GC-MS/MS analysis.

Extraction of Indole, IAA, and IBA

24. Leave the rest of plant homogenate on ice for at least 1 h for isotopic equilibration.

▪ NOTE: This step follows Step 4.

❖ PAUSE POINT: Homogenized samples can be stored at -20 ºC overnight.

25. Spin samples shortly to pellet plant homogenate debris to the bottom of the tubes.

26. Dilute the sample 10 fold by adding 180 µl distilled water and mix thoroughly.

27. Add 80 µl hexane and mix thoroughly.

28. Spin samples shortly to allow the organic and aqueous phases to separate clearly.

29. Transfer ~60 µl of the organic layer (upper layer) to a glass insert. Place the glass insert into a crimp vial, and cap the vial. This sample contains indole and can be analyzed by GC-MS/MS without derivatization.

- NOTE: Step 27-29 are designed to extract indole. These steps can be skipped if indole is not a targeted analyte. The samples of indole can be stored in sealed vials at 4 ºC in the dark for one week, but because indole is volatile do not let the sample dry.

30. Wash the TopTips containing NH_2 resin sequentially with 60 µl of hexane, acetonitrile, ethyl acetate, 0.2 M imidazole, followed by three times with 100 µl of distilled water.

31. Transfer the TopTips to new 2-ml tubes to collect the flow-through from NH_2 TopTips.

32. Spin the diluted samples at 12,000 g for 10 min.

33. Load the supernatant of each sample into individual TopTip.

34. Spin TopTips at 2,000 g to allow samples to pass through slowly and completely.

35. Transfer the TopTips to new 2-ml tubes. Cap the tubes containing the flow-through from the NH_2 tips and store in a refrigerator. The flow-through contains Trp.

- NOTE: the flow-through is collected to extract Trp (See Step 53). It can be discarded if only IAA and IBA are of interest. The flow-through can be stored at 4 ºC for one month.

36. Wash the TopTips with 60 µl each of hexane and methanol.

37. Transfer the TopTips to new 2-ml tubes, each of which contains 25 µl of SA.

38. Elute IAA and IBA from the TopTips using 50 µl, 100 µl, and 50 µl PA, separately.

39. Discard the NH_2 TopTips, and collect 2-ml tubes containing the acidic eluate.

40. Prewash the TopTips containing PMME resin two times with 100 µl methanol, followed by two times with 100 µl PA:SA.

41. Load the acidic eluate into the PMME TopTips.

42. Spin TopTips at 2,000 g to allow liquid to pass through slowly and completely.

43. Wash the TopTips three times with 60 µl PA:SA.

44. Wash the TopTips with 10 µl methanol. Spin the TopTips at 10,000 g for 1-2 min.

- CRITICAL STEP: Remove the water residue in the PMME resin to gain good methylation efficiency (similar to Step 15).

45. Remove the plastic spring from the bottom of the 250-µl glass inserts, and put the glass inserts into 2-ml screw capped micro tubes (Fig. 2-3C).

46. Transfer the PMME TopTips to the micro tubes containing glass inserts. Make sure that the TopTips insert into the glass inserts (Fig. 2-3C).

47. Elute IAA and IBA two times with 50 µl methanol. The eluate contains both IAA and IBA and is collected in the glass inserts in the micro tubes.

48. Discard the PMME TopTips.

49. Use the micro-dissecting forceps to take the glass inserts out of the micro tubes. Re-install the plastic spring at the bottom of the glass inserts, and put the glass inserts into crimp vials (Fig. 2-3D).

❖ PAUSE POINT: Vials can be capped and stored at -20 ºC overnight.

Derivatization of IAA and IBA

50. Add ethereal diazomethane into each glass insert until the insert is full, and incubate for ~5 minutes (Fig. 2-3D).

51. Evaporate the solvents until complete dryness using a gentle N_2 gas stream in a sand bath heated to 55 ºC in a solvent hood.

► *Caution*: Diazomethane is toxic and potentially explosive (see Step 21).

52. Add 15 µl of ethyl acetate into each glass insert to re-suspend the methylated IAA and IBA. Cap the vials.

❖ PAUSE POINT: Methylated samples can be stored at -20 ºC for a few months or at -80 ºC for up to one year.

Extraction and derivatization of Trp

53. Wash the TopTips containing DOWEX® 50X2-400 resins two times with 100 µl methanol and two times with 100 µl distilled water.

54. Load the TopTips with the flow-through from NH_2 TopTips collected in Step 35.

55. Spin TopTips at 2,000 g to allow liquid to pass through slowly and completely.

56. Wash the TopTips with methanol : water (8:1, v:v).

57. Transfer the TopTips onto new 2-ml tubes.

58. Elute Trp two times with 100 µl methanol : 8 M NH_4OH (1:1, v:v).

❖ PAUSE POINT: Trp eluate can be stored at 4 ºC for a few days.

59. Transfer 100 µl of the eluate containing Trp into a 2-ml clear glass vial.

60. In a fume hood, add 20 µl pyridine to each glass vial, and gently shake the vial to make sure the solvents mix.

61. Continuing in the fume hood, add 20 µl MCF into each vial. Wait for a minute to allow the reaction to complete.

62. Sequentially add 300 µl each of 50 mM $NaHCO_3$ and then dichloromethane into the vial. Cap the vial and mix thoroughly. Keep the vials still until two layers form clearly.

63. In a new 2-ml clear glass vial, add 10-20 mg anhydrous Na_2SO_4 (add enough to cover the bottom of the vial).

64. Transfer the dichloromethane layer (bottom layer) into the glass vial containing Na_2SO_4. Cap the vial. The dichloromethane contains derivatized Trp.

65. Wait for 30-60 min to allow Na_2SO_4 to absorb water from the dichloromethane solution.

❖ PAUSE POINT: Derivatized Trp is less stable than Trp, and it can be stored at -20 ºC for a few days. The actual time length for storage depends on the abundance of the compound in each sample. It is recommended to analyze the samples soon after derivatization.

66. Transfer 50 µl of the dichloromethane sample solution into a glass insert. Place the glass insert into a crimp vial, and cap the vial.

GC-SRM-MS/MS analysis of derivatized IPyA

67. SRM is used as the acquisition mode, and the quinolinium ions produced from the molecular ions (Fig. 2-5A) are monitored. For unlabeled methyl-[$^{2}H_{1}$]ILA, the parent mass is 220 and the product mass is 130; for the methyl-[$^{13}C_{11}$,^{15}N, $^{2}H_{1}$]ILA internal standard, the parent mass is 232 and the product mass is 140.

► *CRITICAL*: Because only the product (quinolinium) ions are monitored in the SRM mode, it is important to know what atoms are included in the quinolinium ions (Fig. 2-5A) when stable-labeled IPyA is analyzed. Some stable-labeled atoms are missing from the quinolinium ions after fragmentation.

GC-SIM-MS/MS analysis of Indole

68. SIM is used as the acquisition mode and the molecular ions are monitored. The MS mode under "Scan Modes" is set to "Q1MS". For the unlabeled indole, ion m/z 117 is monitored; for the [$^{13}C_{8}$,^{15}N]indole, ion m/z 126 is monitored; for other types of labeled indole, the m/z of the monitored ion equals the nominal molecular mass.

GC-SRM-MS/MS analysis of derivatized IAA and IBA

69. SRM is used as the acquisition mode and the quinolinium ions produced from the molecular ions (Fig. 2-5, B and C) are monitored. Under the "Run Settings" in the "Scan Editor" tab (of TSQ Quantum), the "Segments" are set to 2; "Segment Time" is 10.5 min for Segment 1 and 7.0 min for Segment 2. In Segment 1, methyl-IAA is monitored. For unlabeled methyl-IAA, the parent mass is 189 and the product mass is 130; for the methyl-[$^{13}C_{6}$]IAA internal standard, the parent mass is 195 and the product mass is 136. In Segment 2, methyl-IBA is monitored. For unlabeled methyl-IBA, the parent mass is 217 and the product mass is 130; for the methyl-[$^{13}C_{8}$,^{15}N]IBA internal standard, the parent mass is 226 and the product mass is 139.

- CRITICAL STEP: methyl-IAA and methyl-IBA are analyzed in one GC-MS/MS run, and the GC retention time of Me-IBA is about 1 min longer than Me-IAA under the conditions described in the "Materials" section. Under these conditions, the retention

time is about 10 min for Me-IAA and about 11 min for Me-IBA, so the division of the two segments in the run is set at 10.5 min. However, if different conditions are used (*e.g.*, different GC column type or length, different oven temperatures), this setting needs to be adjusted based on the actual retention time of Me-IAA and Me-IBA.

► *CRITICAL*: Because only the product (quinolinium) ions are monitored in the SRM mode, it is important to know what atoms are included in the quinolinium ions (Fig. 2-5. B and C) when stable-labeled IAA and IBA are analyzed. Some stable-labeled atoms are missing from the quinolinium ions after the fragmentation.

GC-SIM-MS/MS analysis of derivatized Trp

70. SIM is used as the acquisition mode, and both the molecular ions and the quinolinium product ions are monitored. For unlabeled Trp, the molecular ion m/z 276 and quinolinium ion m/z 130 (Fig. 2-5D) are monitored; for the [$^{13}C_{11}$,$^{15}N_2$]Trp, the molecular ion m/z 289 and quinolinium ion m/z 140 are monitored. The quinolinium ions are much more abundant than the molecular ions, so the abundance of the quinolinium ions is used for quantification.

Timing

Step 1: Variable

Step 2: 15 min per 16 samples

Step 3: 5-10 min

Step 4-5: 10 min per 16 samples

Step 7-19: 30 min per 16 samples

Step 20-23: 30 min per 16 samples

Step 25-29: 30 min per 16 samples

Step 30-49: 50 min per 16 samples

Step 50-52: 30 min per 16 samples

Step 53-58: 20 min per 16 samples

Step 59-64: 30 min per 16 samples

Step 66: 10 min per 16 samples

Step 67-70: 17.5 min per sample

Troubleshooting

Problems	Possible Reasons	Possible Solutions
Liquid does not pass through TopTips before loading plant samples	The slit on TopTips is too narrow	Increase the centrifugal force to make liquid pass through. Or, switch to a new TopTip.
Liquid does not pass through TopTips after loading plant samples	Plant debris blocks the TopTip	Always try to avoid transferring plant debris into TopTips. Increase the centrifugal force to make liquid pass through. Use a dissecting probe to remove visible plant debris.
Drift of GC retention time	Deuterium labeled compounds are analyzed	It is normal for deuterium labeled compounds to have slightly shorter retention times.
	Carrier gas leaks significantly	Use a leak detector to find out where the leak is. Often, a worn Merlin Microseal septum is the source of the leak.
	Change of carrier gas	If the drift of GC retention time occurs after the change of carrier gas cylinders, check if correct gas cylinders are used.

Low yield of both endogenous IAA/IBA and IAA/IBA internal standards	Water in the methanol eluate reduces the methylation efficiency	If it takes a long time to evaporate the solvents to dryness, the samples are likely to contain residual water. Re-methylate samples by adding ethereal diazomethane and 10% methanol, and run samples again after drying and re-suspension.
	Wrong NH_2 resin	Make sure that correct NH_2 resin is used to extract IAA/IBA. Some brands of NH_2 resin do not bind IAA/IBA sufficiently.
	The pH of solutions loaded onto PMME TopTips is too high	The pH has to be between 3 and 3.5. Cut a pH strip into narrower strips, and dip a strip in the solution to check the pH. Make sure that correct concentration of PA is made (pH ≤ 1.8), and avoid adding too much SA which increases the pH.
Low yield of endogenous IAA/IBA, but normal yield of IAA/IBA internal standard	Insufficient tissue homogenization and/or equilibration	Make sure that plant tissues are well homogenized. Allow longer time period for equilibration, e.g., overnight in the dark at 4 ºC.
	Low endogenous IAA/IBA content in plant tissues	Collect more plant material for extraction. Usually, more plant material is required for IBA analysis as compared with IAA analyses.

Broad/tailed peaks	The GC liner is dirty	Change the liner, and cut ~30 cm from GC column from the injector end.
	The GC column is dirty	Turn off the MS, and change the GC column.
Overlapping peaks	The GC may need maintenance	See above.
	The plant sample may contain other metabolites that elute at similar GC retention time and produce ions with m/z values the same as the analytes	Run samples again using a different GC temperature gradient program. The temperature gradient commonly used is 20 ºC/minute, and a slower or faster gradient can be used. Note that the retention time will be different when a different gradient is used. Run a standard to obtain the new retention time.
Reduced MS sensitivity	The tune file is out of date	Auto-tune the MS system.
	The EI source is dirty	Turn off the MS, and remove the parts of EI source. Reassemble the EI source after cleaning the parts.

Anticipated Results

A group of results generated from extractions of IAA and IAA precursors is shown in Figure 6. The results were displayed by Qual Browser in Xcalibur™ 2.1 software, and the chromatogram of each ion (SIM) or reaction product ion (SRM) selected to be monitored is shown in each panel. Peaks were detected automatically by the software, and peak areas were also determined by the software. When necessary, peaks can also be determined manually by defining the start and end points of the peak.

All the chromatograms should be evaluated before calculations are applied. Each peak should be completely separated from its surrounding peaks, if any, and should be well resolved from the background, with a signal-to-noise ratio of greater than three. In general, it is more likely to have a second peak overlapping with the peak of analyte when the SIM acquisition mode is used, but this may also occur in the SRM acquisition mode. If peak overlapping forms a problem, samples can be analyzed again by GC-MS/MS using a different GC temperature gradient program (see Troubleshooting).

For absolute quantification, the amount of plant endogenous compounds can be calculated from peak areas of the endogenous compound and the labeled internal standard. For example, in Figure 6A, IAA and IBA from 2 mg Arabidopsis root tissue were extracted together with 0.2 ng each of [$^{13}C_6$]IAA and [$^{13}C_8$,$^{15}N_1$]IBA. Using the isotope dilution equation that was fully discussed previously (Barkawi *et al.*, 2010), the masses of endogenous IAA and IBA can be calculated (R-value: 1.13 for IAA; 1.33 for IBA), which are then divided by the fresh weight (FW) of the plant sample in order to calculate concentrations of IAA and IBA. Therefore, the sample shown in Figure 6A contains 4.25 ng g^{-1} FW of IAA and 1.18 ng g^{-1} FW of IBA. Similarly, in Figure 6B, IPyA from 9.5 mg Arabidopsis seedlings was extracted with 0.5 ng [$^{13}C_{11}$,$^{15}N_1$]IPyA. Because the amount of [$^{13}C_{11}$,$^{15}N_1$]IPyA was determined based on unlabeled IPyA using reverse isotope dilution (**Supplemental Method 2**), the R-value is not necessary for the calculation, and the sample shown in Figure 6B contains 15.02 ng g^{-1} FW of IPyA.

To study the activity of auxin biosynthesis, isotopic enrichment of stable-labeled auxin and auxin precursors can be analyzed. Figure 6C, 6D, and 6E show the enrichment

of ^{13}C in tomato seedlings after incubation with 0.1 mM [$^{13}C_1$]indole for four hours. Figure 6C shows that [$^{13}C_1$]indole is greatly enriched in the plant indole pool, suggesting that [$^{13}C_1$]indole was taken up into plants effectively. Figure 6D shows the enrichment of [$^{13}C_1$]Trp in the plant Trp pool (3,355,515 divided by 8,196,046), and, after subtraction of the natural abundance of [$^{13}C_1$]Trp (10%, a constant determined from unlabeled Trp), the enrichment of [$^{13}C_1$]Trp synthesized from [$^{13}C_1$]indole was determined to be 30.9%. Similarly, Figure 6E shows the enrichment of [$^{13}C_1$]IAA in the plant IAA pool (23,394 divided by 48,276), and, after subtraction of the natural abundance of [$^{13}C_1$]IAA (10%, a constant determined from unlabeled IAA), the enrichment of [$^{13}C_1$]IAA synthesized from [$^{13}C_1$]indole was determined to be 38.5%. Because the enrichment of [$^{13}C_1$]IAA synthesized from [$^{13}C_1$]indole exceeded the enrichment of [$^{13}C_1$]Trp synthesized from [$^{13}C_1$]indole, it can be concluded that a portion of [$^{13}C_1$]IAA was synthesized in the tomato plants via the Trp-independent biosynthetic pathway.

Supplemental Method 1: Preparation of [$^{13}C_8$,$^{15}N_1$]indole-3-butyric acid

Materials:

- [$^{13}C_8$,$^{15}N_1$]Indole
- Solid NaOH
- Ethyl acetate
- 50% Isopropanol
- γ-Butyrolactone (Sigma-Aldrich, cat. no. B103608) ►*CAUTION*: harmful
- Chloroform (HPLC grade; Sigma-Aldrich, cat. no. 650498) ►*CAUTION*: toxic
- 6 N Hydrogen chloride (HCl; Fisher Scientific, cat. no. A144-212) ►*CAUTION*: open in fume hood; protect eyes, hands and clothing

Equipment:

- Teflon cup with cover, 23 ml (Parr Instruments, cat. no. A280-AC)
- Screw-top reaction bomb (Parr Instruments, cat. no. 276AC-T304-012304)
- Aluminum housed heating mantle (Glas-Col®, cat. no. 102B 5101977001)
- PowrTrol temperature control (Glas-Col®, cat. no. 104A PL912)
- Separatory funnels (250 ml, 500 ml; Fisher Scientific, cat. no. 10-436-1B, 10-436-1C)
- Rotary evaporator (Buchi, Rotavapor®, R-110)
- UV-visible spectrophotometer (Agilent 8453, cat. no. G1812AA)
- Quartz cuvette (LabShopOnline.com, cat. no. TCQ24)

Protocol:

1. In a Teflon cup, add 0.05 g of [$^{13}C_8$,$^{15}N_1$]indole, 3.2 g of NaOH, and 6.09 ml of γ-butyrolactone. It is common that the solid does not dissolve in the liquid.

2. Cover the Teflon insert and fit it into the screw-top reaction bomb. Close reaction bomb securely.

3. Heat the reaction bomb to 220 ºC at a rate of 2 ºC/minute in the heating mantle with the temperature control, and incubate at 220 ºC for a total time of 24 hours.

4. Turn off the temperature control and let the system cool to room temperature.

5. Dissolve the reaction mixture in the Teflon insert completely in ~50 ml distilled water.

6. Transfer the 50 ml reaction mixture solution into a 500-ml separatory funnel.

7. Add 120 ml chloroform in a separatory funnel to partition unreacted [$^{13}C_8$,$^{15}N_1$]indole.

8. Remove the chloroform phase (bottom phase).

9. Repeat Step 7-8 twice.

10. Transfer the aqueous layer to a beaker and adjust the pH to 2.5 by adding 6 N HCl.

11. Transfer the acidified solution into a 250-ml separatory funnel.

12. Add 50 ml ethyl acetate to partition the synthesis product.

13. Remove the aqueous layer (bottom layer) and collect the ethyl acetate layer.

14. Repeat Step 11-13 three times and combine the ethyl acetate extracts.

15. Evaporate the ethyl acetate using a rotary evaporator.

16. Re-dissolve the product in a minimal amout of 50% isopropanol. This concentrated [$^{13}C_8$,$^{15}N_1$]IBA solution can be stored at -20 ºC for a few years.

17. Verify the product by GC-MS/MS after diazomethane methylation (see the procedure in the main text). The product can be further purified by reverse phase liquid chromatography. Similar to IAA (Barkawi *et al*., 2010), the concentration of IBA can be determined by spectrophotometry, with λ_{max} at 282 nm and an absorption coefficient of 6,060 M^{-1} cm^{-1}.

Supplemental Method 2: Preparation of [$^{13}C_{11}$,$^{15}N_1$]indole-3-pyruvic acid

► *CRITICAL*: For absolute quantification of IPyA in biological samples, a known amount of [$^{13}C_{11}$,^{15}N]IPyA is added into each sample as the internal standard, and [$^{13}C_{11}$,^{15}N]IPyA has to be synthesized just prior to or no more than 2 days before use.

Materials:

- 50 mM Phosphate buffer (pH 8.0), made from sodium phosphate monobasic (NaH_2PO_4, Sigma-Aldrich, cat. no. S8282) and sodium phosphate dibasic (Na_2HPO_4; Sigma-Aldrich, cat. no. S7907)
- 0.2 mg/ml Transaminase (Sigma-Aldrich, cat. no. T7684) in 50 mM phosphate buffer
  ► *CRITICAL*: store as 100 µl aliquots at -20 ºC. Use one aliquot for each reaction.
- [$^{13}C_{11}$,$^{15}N_2$]L-Trp (Cambridge Isotope Laboratories, cat. no. CNLM-2475)
- α-Ketoglutarate (Sigma-Aldrich, cat. no. K-1750)
- 5 mM Pyridoxal 5′-phosphate (PLP; Sigma-Aldrich, cat. no. 82870)
- 10 mM Ascorbic acid (Sigma-Aldrich, cat. no. A4544)
- 25% Phosphoric acid (PA) (ACS grade; Fisher, cat. no. A242)
- Indole-3-pyruvic acid (Sigma-Aldrich, cat. no. I7017)
  ► *CRITICAL*: the compound is sensitive to oxygen. Keep container tightly closed and store in a dry place at -20 ºC.
- Ethyl acetate
- 50% Isopropanol

Synthesis of [$^{13}C_{11}$,^{15}N]IPyA using an enzyme-catalyzed transamination reaction

1. Let one aliquot of transaminase solution thaw on ice.
2. In 1 ml of 50 mM phosphate buffer (pH 8.0), add 1 mg [$^{13}C_{11}$,$^{15}N_2$]Trp and 1 mg α-ketoglutarate.
3. Add 20 µl 5 mM PLP and one aliquot of transaminase solution.
4. Mix the solution gently by inverting the tube several times.
5. Incubate the reaction mixture at 37 ºC in the dark for 3 h.

6. Add 1 ml 10 mM ascorbic acid and 50 µl 25% PA to bring the pH to 2.5.

7. Add 600 µl ethyl acetate to partition the synthesized [$^{13}C_{11}$,^{15}N]IPyA.

8. Collect ethyl acetate (upper layer) into a 2-ml amber glass vial.

9. Add another 600 µl ethyl acetate to partition, and collect the ethyl acetate into the same amber glass vial.

10. Evaporate ethyl acetate to complete dryness using a gentle N_2 gas stream in a sand bath heated to 55 ºC.

11. Re-suspend [$^{13}C_{11}$,^{15}N]IPyA in 1 ml 50% isopropanol.

12. Cap the vial and store the solution at -20 ºC.

13. The yield of [$^{13}C_{11}$,^{15}N]IPyA is about 0.1 mg.

► *CRITICAL*: The concentration of the [$^{13}C_{11}$,^{15}N]IPyA solution has to be determined immediately before use (Step 2 in "Procedure").

Determine the concentration of [$^{13}C_{11}$,^{15}N]IPyA solution by reverse isotope dilution

14. Freshly prepare 0.1 mg/ml unlabeled IPyA in 50% isopropanol.

15. Freshly prepare 20 mg/ml NaB^2H_4 in 0.3 N NaOH.

16. In a 0.5-ml microcentrifuge tube, accurately add 5 µl each of unlabeled IPyA and synthesized [$^{13}C_{11}$,^{15}N]IPyA solution.

- CRITICAL STEP: for the ease of calculation in Step 15, it is recommended to add equal volumes of IPyA and [$^{13}C_{11}$,^{15}N]IPyA solutions.

17. Add 8 µl NaB^2H_4 solution and mix well.

18. Incubate the tube at 37 ºC for 30 min.

19. Add 5 µl 25% PA to acidify the mixture and consume the residual NaB^2H_4.

20. Add 200 µl water and mix well.

21. Extract the reduced IPyA (now ILA) by adding 100 µl ethyl acetate to partition.

22. Collect the ethyl acetate extract in a 2-ml clear glass vial.

23. Add 100 µl methanol into the vial.

24. Methylate the sample by filling the vial with ethereal diazomethane.

25. Evaporate the solvents until complete dryness using a N_2 gas stream.

26. Re-suspend the compounds in 1 ml of ethyl acetate.

27. Analyze the sample using GC-MS/MS under SRM mode. For unlabeled methyl-ILA, the transition of parent ion m/z 220 to the product ion m/z 130 is monitored; for methyl-[$^{13}C_{11}$,^{15}N]ILA, the transition of parent ion m/z 232 to the product ion m/z 140 is monitored.

28. The ion abundance ratio of m/z 130 over m/z 140 equals the ratio of IPyA concentration over [$^{13}C_{11}$,^{15}N]IPyA concentration in the initial sample.

Figures

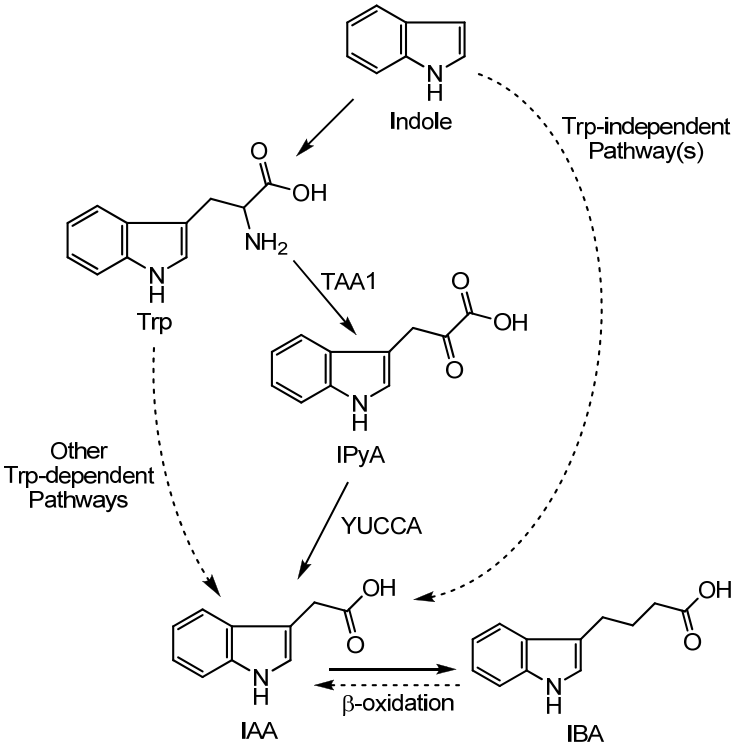

Figure 2-1. A simplified summary of IAA biosynthetic pathways. A solid line represents an enzymatic step. Dashed lines suggest multiple steps or pathways abbreviated. TAA1: Trp aminotransferase of Arabidopsis. YUCCA: an Arabidopsis flavin monooxygenase (Mashiguchi *et al.*, 2011, Woodward and Bartel, 2005).

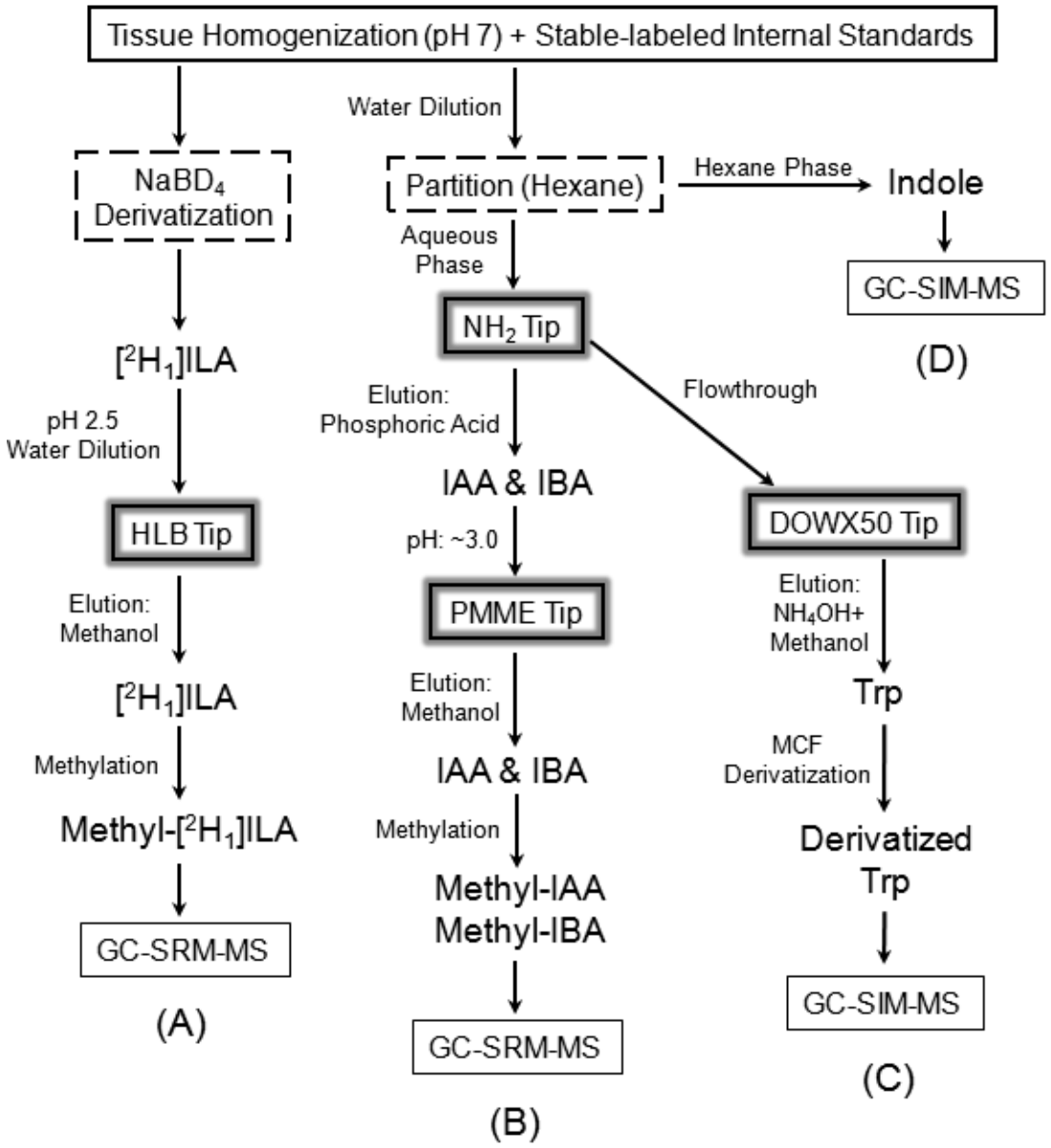

Figure 2-2. Experimental procedures for extraction and derivatization of auxin and auxin precursors. Tissue homogenization and addition of internal standards corresponds to Steps 2-3. Each homogenized sample is spitted to two aliquots. **(A)** Extraction and derivatization of indole-3-pyruvic acid (IPyA). Corresponds to Steps 4-23, and Step 67. **(B)** Extraction and derivatization of indole-3-acetic acid (IAA) and indole-3-butyric acid (IBA). Corresponds to Steps 24-26, 30-52, and Step 69. **(C)** Extraction and derivatization of tryptophan. Corresponds to Steps 53-66, and Step 70. **(D)** Extraction of indole. Corresponds to Steps 24-29, and Step 68.

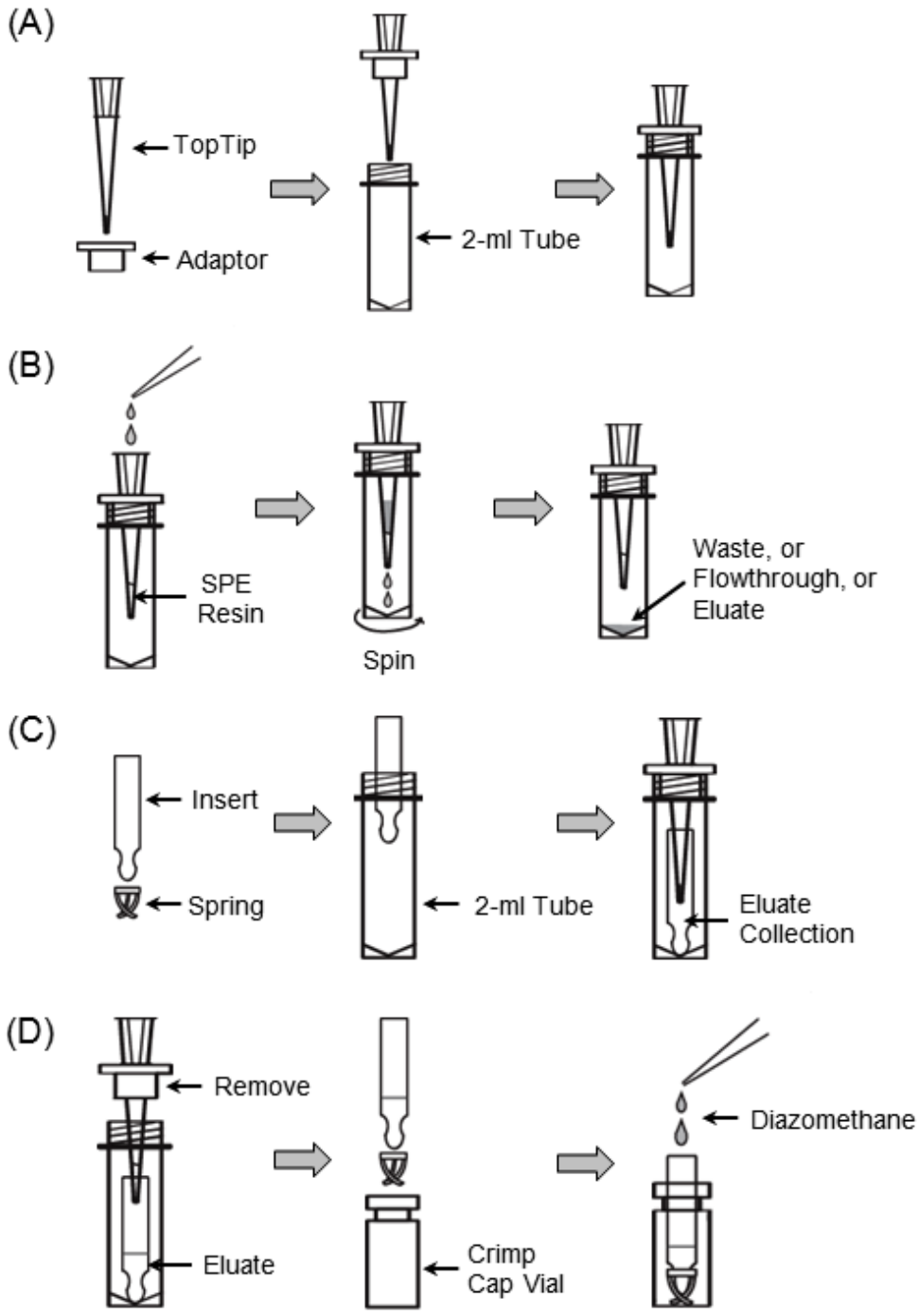

Figure 2-3. Setup and utilization of TopTips for SPE extractions. (A) Setup of a TopTip on a 2-ml centrifuge tube with an adaptor for centrifugation. **(B)** Process of liquid handling on a SPE TopTip. **(C)** Setup of a glass insert in a centrifuge tube for eluate collection. Corresponds to Step 45-46. **(D)** Process of methylating eluate in a glass insert. Corresponds to Steps 48-50.

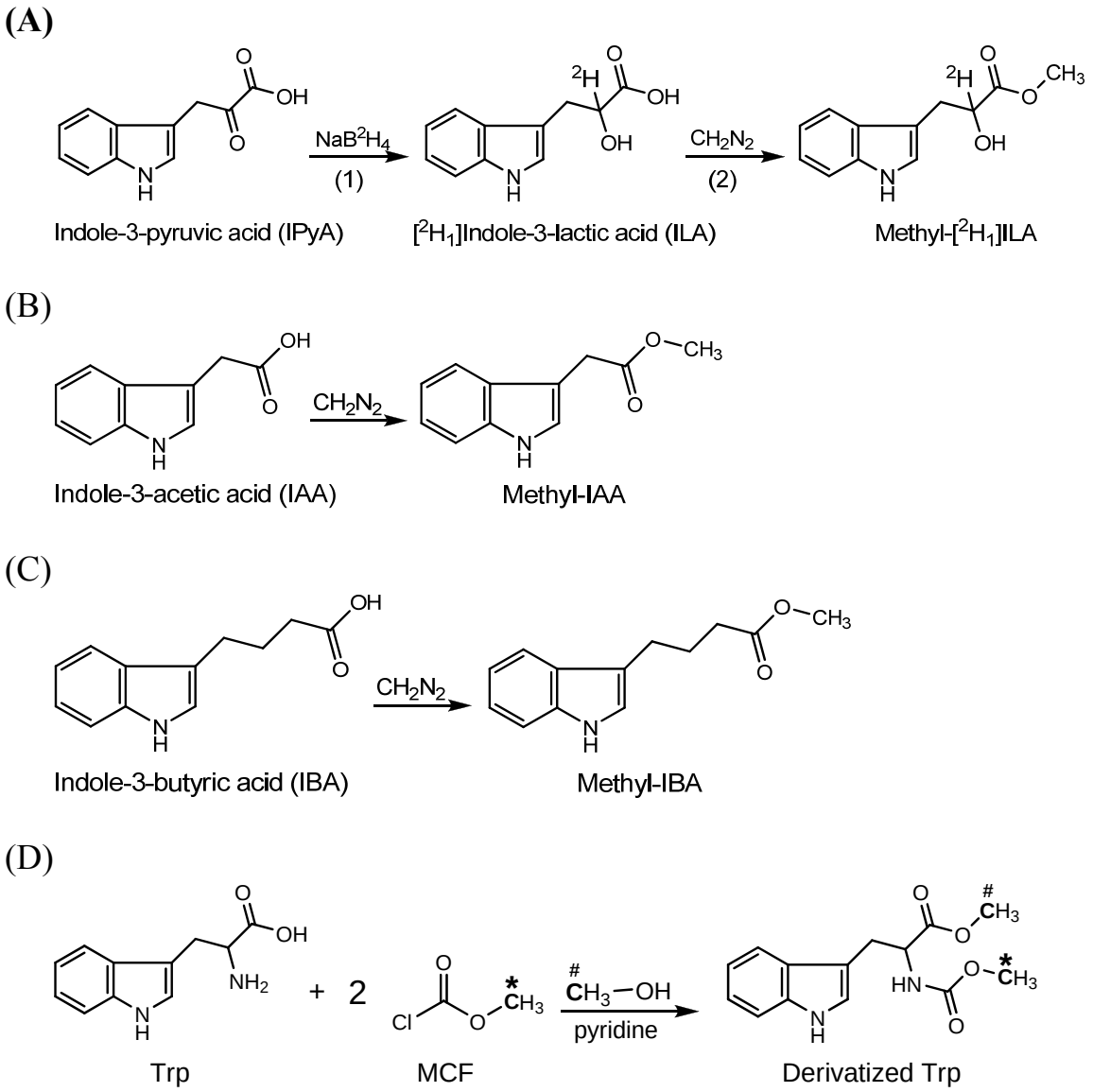

Figure 2-4. Derivatizations of analytes prior to GC-MS analysis. (A) IPA is first reduced by NaB^2H_4 to yield $[^2H_1]$ILA (Steps 5-6). $[^2H_1]$ILA is then methylated by diazomethane to form methyl-$[^2H_1]$ILA (Step 20). **(B)** IAA and **(C)** IBA are methylated by diazomethane, and yield methyl-IAA and methyl-IBA (Step 50). **(D)** Trp is derivatized by methyl chloroformate (MCF) in the presence of methanol and pyridine (Steps 60-61). Carbon atoms from both MCF and methanol are incorporated into the final product. The "*" and "#" labels mark the flow of these carbons (Chen *et al.*, 2010).

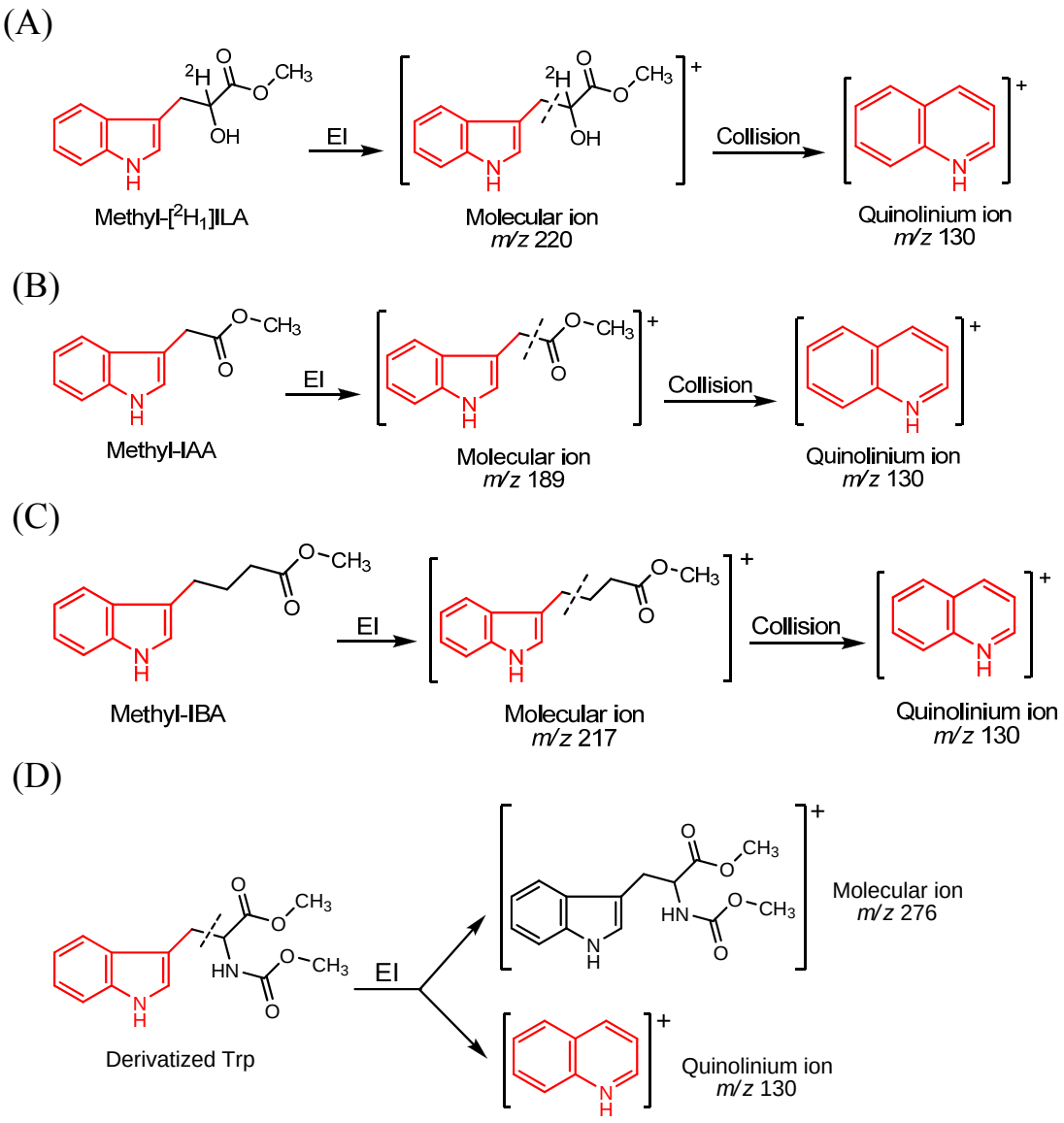

Figure 2-5. Ionization and fragmentation of derivatized analytes during MS analyses. EI: electron impact ionization source. **(A)** Methyl-[$^2H_1$]ILA is first ionized and fragmented by EI. The molecular ion m/z 220 is selected and further fragmented to produce the quinolinium ion. Atoms in the molecular ion to the right of the dashed line are lost in the quinolinium ion. **(B)** Methyl-IAA and **(C)** methyl-IBA are first ionized by EI. The molecular ions m/z 189 and m/z 217 are selected and further fragmented to produce the quinolinium ions. Atoms in the molecular ions to the right of the dashed line are lost in the quinolinium ions. **(D)** Derivatized Trp is ionized and fragmented by EI. The molecular ion m/z 276 and quinolinium ion m/z 130 are the major products and are monitored by MS. Atoms in the original molecule to the right of the dashed line are lost in the quinolinium ion.

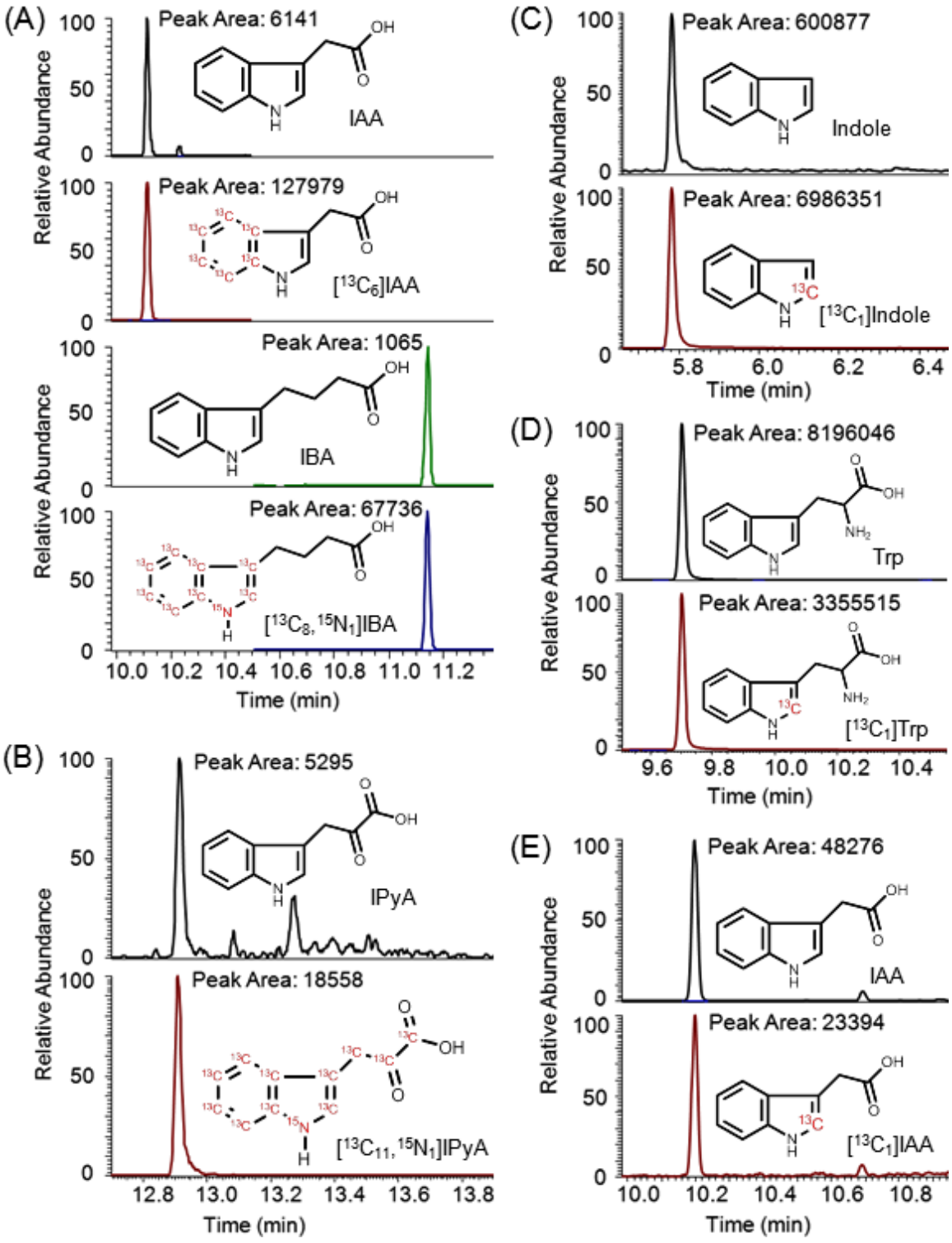
(A)
Peak Area: 6141
IAA
Peak Area: 127979
[13C6]IAA
Peak Area: 1065
IBA
Peak Area: 67736
[13C8,15N1]IBA
Relative Abundance
Time (min)
(B)
Peak Area: 5295
IPyA
Peak Area: 18558
[13C11,15N1]IPyA
(C)
Peak Area: 600877
Indole
Peak Area: 6986351
[13C1]Indole
(D)
Peak Area: 8196046
Trp
Peak Area: 3355515
[13C1]Trp
(E)
Peak Area: 48276
IAA
Peak Area: 23394
[13C1]IAA

Figure 2-6. Examples of GC-MS results from typical plant extracts. Structures of starting compounds analyzed and their peak areas are shown. **(A)** Quantification of IAA and IBA from 2 mg Arabidopsis root tissue using GC-SRM-MS. **(B)** Quantification of IPyA in 9.5 mg Arabidopsis seedlings using GC-SRM-MS. **(C)** Enrichment of [$^{13}C_1$]indole using GC-SIM-MS. **(D)** Enrichment of [$^{13}C_1$]Trp synthesized from [$^{13}C_1$]indole using GC-SIM-MS. **(E)** Enrichment of [$^{13}C_1$]IAA synthesized from [$^{13}C_1$]indole using GC-SRM-MS.

Chapter 3

Low-Fluence Red Light Increases the Transport and Biosynthesis of Auxin[1]

Introduction

Indole-3-acetic acid (IAA), the major form of auxin in plants, is involved in a number of developmental processes and allows plants to react to their environment. Consistent with its importance, plants have evolved a complex system to regulate the level of free, active IAA (Normanly *et al*., 2005). IAA can be actively transported in a polar fashion, maintaining concentration gradients among plant tissues and cells. Biochemical and genetic studies have shown that higher plants synthesize IAA directly from indole by a Trp-independent (TI) pathway, while at least four Trp-dependent (TD) pathways are also potentially operative. IAA can be conjugated to other molecules via covalent bonds, forming an IAA reservoir that can release free IAA via hydrolysis (reviewed by Woodward and Bartel, 2005; Seidel *et al*., 2006). Clearly, multiple IAA regulatory pathways exist in plants, and they function cooperatively to precisely control the level of free IAA, especially when plants perceive environmental changes, such as high temperature (Gray *et al*., 1998), wounding (Sztein *et al*., 2002), and cold stress (Shibasaki *et al*., 2009).

Light also acts as a critical environmental signal that controls plant growth and development. Upon transition from dark growth to light growth, hypocotyl elongation rate decreases, hooks unfold, cotyledons open, and the photosynthetic machinery develops. Such changes are rapid and complex, and a series of photoreceptors are

[1] This chapter has been published in Plant Physiology, 2011, Vol. 157, pp. 891-904. All the work presented here was done by me.

involved in sensing the quantity and quality of light, including phytochromes (red [R] light and far-red [FR] light receptors), cryptochromes (blue [B] and UV-A light receptors), phototropins (B light receptors), and UV-B photoreceptors (Casal *et al*., 1998; Briggs and Olney, 2001). Once the photoreceptors are activated, the light signals are then transferred to the downstream molecular networks that trigger growth and developmental responses, including networks that involve phytohormones (Kraepiel and Miginiac, 1997). Interactions between light and auxin have been reported at multiple levels. In dark-grown corn (*Zea mays*) seedlings, both a single flash and hours of light exposure were found to induce a decrease in free IAA and an increase in conjugated IAA (Bandurski *et al*., 1977; Jones *et al*., 1991; Barker-Bridges *et al*., 1998; Zelená, 2000a), and the effects varied in different tissue types (Zelená, 2000b). After a short period of R light exposure, IAA synthesized from Trp in corn coleoptiles was decreased, and free IAA that diffused out of excised coleoptile tips was greatly reduced (Iino, 1982a; Koshiba *et al*., 1995; Nishimura *et al*., 2006), which could result in a reduction of IAA supply to mesocotyl tissues below the coleoptiles (Iino, 1982b). Light effects on auxin levels and metabolism were also found in dicotyledonous plants. Behringer and Davies (1992) reported that after etiolated pea (*Pisum sativum*) seedlings were exposed to R light for 3 h, the free IAA level stayed constant in upper stem sections but decreased in epidermal peels. When etiolated pea seedlings were exposed to a long period of continuous white light, Symons and Reid (2003) found a transient increase of IAA that started at 24 h, peaked at 48 h, and disappeared at 96 h. In response to decreased R/FR light ratios that mimic a shade condition, IAA biosynthesis and the free IAA level were increased in Arabidopsis (*Arabidopsis thaliana*) seedlings during the shade avoidance response (Tao *et al*., 2008). The shade avoidance response also required polar auxin transport (PAT), and the auxin transport facilitator protein PIN-FORMED3 (PIN3) was recently found to play a critical role in this process (Steindler *et al*., 1999; Keuskamp *et al*., 2010).

Close interaction between light and auxin transport was inferred from the work of Jensen et al. (1998). The elongation of 7-d light-grown Arabidopsis hypocotyls was

greatly inhibited by the PAT inhibitor N-1-naphthylphthalamic acid (NPA), but 7-d dark-grown plants lacked this inhibitory response. Their studies using different light quality and photoreceptor mutants suggested that both phytochrome and cryptochrome were involved in the light-dependent NPA effects on hypocotyl elongation. A later report further supported this finding: when the transport of [^{3}H]IAA was quantified in dark- and light-grown Arabidopsis hypocotyls, auxin transport in dark-grown seedlings was lower than in low-light-grown seedlings, and NPA reduced [^{3}H]IAA transport in light-grown seedlings but not in dark-grown seedlings (Rashotte *et al*., 2003). Partially consistent with their report, Shinkle *et al*. (1998) found that 30 or 50 h of continuous dim R light increased the transport of [^{3}H]IAA in etiolated cucumber (*Cucumis sativus*) hypocotyl segments. However, the transport of [^{3}H]IAA in dark-grown cucumber hypocotyls was greatly inhibited by NPA, suggesting that the lack of NPA inhibition on auxin transport in etiolated Arabidopsis hypocotyls was either species specific or non-detectable by the assay applied. Although these studies established a link between light and auxin transport, they did not address the questions of whether auxin transport affected the level of free IAA or if light changed auxin metabolism in addition to changing auxin transport.

To better understand light effects on PAT in etiolated seedlings, I established a sensitive [^{3}H]IAA transport assay with low background noise and found that PAT in etiolated Arabidopsis and tomato (*Solanum lycopersicum*) hypocotyls was detectable and inhibited by NPA. Light increased PAT in both Arabidopsis and tomato hypocotyl sections, but only in tomato could the increase be induced by low fluences of R or B light followed by a dark period. I also found that this low-fluence response in tomato involved phytochromes but not cryptochrome. In addition to the increase in transport, IAA biosynthesis and free IAA levels were changed by low-fluence R light in a tissue dependent manner, and the level of free IAA was a consequence of both the biosynthesis and transport of IAA.

Materials and Methods

Plant Materials and Growth Conditions

Tomato (*Solanum lycopersicum* 'Ailsa Craig') seeds were purchased from Thompson and Morgan Wholesale and were grown to increase seed quantity in an isolated field in Hugo, Minnesota, during the summer of 2007. Seeds of cv MoneyMaker were purchased from Gourmet Seed International. Mono genic mutants (in a background of cv MoneyMaker) *phyA*, *phyB1*, *phyB2*, and *cry1* were from the Tomato Genetics Resource Center at the University of California and were grown for seed increase in a greenhouse at 27 °C with 16 h of light per day. Individual plants were grown in 5-gallon pots, watered daily, and fertilized with slow-release fertilizer (Osmocote Plus; Scotts-Sierra Horticultural Products). All seeds were imbibed under running tap water overnight, surface sterilized by incubation in 0.1% Micro 90 (International Products) and 10% commercial bleach (0.6% sodium hypochlorite) for 10 min with constant slow shaking, and then washed 10 times with sterile water. Seeds were sown onto Murashige and Skoog medium (4.33 g L^{-1} Murashige and Skoog salts [MSP01-50LT; Caisson Laboratories]) in 0.8% (w/v) Phytoblend agar (PTP01-500GM; Caisson Laboratories), pH 5.7, in Magenta GA-7 Plant Culture Boxes (765200; bio-WORLD [http://www.bio-world.com/index.php]) that were capped by Magenta G-7 boxes with couplers (765201; bio-WORLD). Boxes were placed in a physiological dark room at 24 °C, with only brief exposure to a dim green safelight as needed for manipulations. Seeds germinated on day 3 after sowing were allowed to grow in the dark for 3 d before being used for light treatments or other experiments.

Arabidopsis (*Arabidopsis thaliana* ecotype Colombia) seeds were surface sterilized in 2.0-mL microcentrifuge tubes with 1 mL of 70% ethanol for 2 min, followed by 1 mL of 30% commercial bleach (to yield 1.8% sodium hypochlorite) for 5 min, and washed with sterile water five times. Seeds were sown on Murashige and Skoog medium, 0.8% (w/v) Phytoblend agar, 1.0% (w/v) sucrose (Sigma-Aldrich), pH 5.7, and agar plates were wrapped with Parafilm (Pechiney Plastic Packaging) and kept in a dark room at 24 °C for 4 d before seedlings were used for light treatments.

Light Sources and Light Treatments

All the light treatments were done in a physiological dark room at 24 °C. R light was provided by two R fluorescent lamps (Sylvania F48T12/2364/HO) filtered through an Encapsulite R tube guard (Lighting Plastics of Minnesota) and a single layer of Roscolux 66 cool blue filter; and FR light was provided by two FR fluorescent lamps (Sylvania F48T12/232/HO) filtered through an Encapsulite FR tube guard (Lighting Plastics of Minnesota) and a single layer of Lee 85 deeper blue filter (Howe *et al*., 1996). B light was provided by two B fluorescent lamps (Science-Lite Blue-64805), and W light was provided by two or four W fluorescent tubes (Philips F34T12/CW/RS/EW and Philips F48T12/CW/HO). The radiometric spectra of the R, FR, and B light sources are shown in Figure 3-17. Photosynthetically active radiation (total irradiance between 400 and 700 nm) was measured with a LI-250A Light Meter (LI-COR Biosciences). R and FR light fluences were measured with an SKR 110, 660/730-nm sensor (Skye Instruments). Spectral quality was measured with a model SPEC-UV/PAR Spectroradiometer (Apogee Instruments). Specific light intensity was obtained by adjusting the distance between the plants and the light sources or by covering the plants with neutral density plastic filters. When 10 μmol m^{-2} or lower R light fluence was applied, plants were kept in a steel canister (diameter = 11.5 cm, height = 23.5 cm), and light was allowed to reach the plants only through a neutral density filter on top of the canister. Different light fluences were achieved by adjusting light intensity and the duration of light exposure. Fluence rates varied from 0.07 to 5 μmol m^{-2} s^{-1} for R and 2 to 5 μmol m^{-2} s^{-1} for B, and durations varied from 2 s to 100 min.

Quantification of PAT in Hypocotyls

The hypocotyl basipetal IAA transport assay was modified from that described previously (Gardner and Sanborn, 1989; Lewis and Muday, 2009). Six millimeters of an etiolated tomato hypocotyl section 2 mm below the hook tip, or 6 mm of an etiolated Arabidopsis hypocotyl section directly below the shoot apex, was placed on an agar plate after excision, and an auxin donor agar block of 1.5% agar (Sigma-Aldrich) containing

0.2 M MES (Sigma-Aldrich) and 10^{-7} M [^{3}H]IAA (Amersham, GE Healthcare; original specific activity of 25 Ci mmol^{-1}, diluted to 15 Ci mmol^{-1} by the addition of nonradioactive IAA) was placed in contact with the apical end of the tissue section, while a receiver agar block containing 0.2 M MES (pH 6.5) was placed in contact with the basal end. Receiver blocks containing 0.2 M MES (pH 6.5) and 10 μM NPA (ChemService) were used as the +NPA control, and a second control was used where the orientation of the tissue section was inverted (acropetal control). Two strips of polyethylene film (Saran Original; S.C. Johnson & Sons) were placed between the agar blocks and the support agar on the plates to avoid diffusion of [^{3}H]IAA through the support agar and thus prevent an undesirable increase in background counts. The agar plates were placed vertically with donor blocks down in a chamber with high humidity for 3 h, and each of the hypocotyl sections was then divided into apical and basal halves. The receiver block and each half-section of the hypocotyl were extracted individually in scintillation cocktail (Econo-Safe; Research Products International) overnight, and the radioactivity was determined by liquid scintillation counting (LS 6500; Beckman). All the manipulations before scintillation cocktail extraction were done in a dark room under dim green safelight.

Measurement of Auxin Transport Velocity in Hypocotyls

The setup used for the assay was similar to the PAT assay described above. Two centimeters of a tomato hypocotyl section cut from 2 mm below the hook tip was incubated for 20 min with an auxin donor agar block containing 10^{-7} M [^{3}H]IAA on its apical end and a receiver agar block on the basal end. Next, the auxin donor agar block was replaced by a new auxin donor agar block containing 10^{-7} M unlabeled IAA (Sigma) and again placed in the humid chamber. After different incubation time periods, each 2-cm hypocotyl section was cut into 3-mm segments, except that the apical top segment was 2 mm. Each segment of the hypocotyl and the receiver block was incubated individually in scintillation cocktail overnight, and the radioactivity was determined by liquid scintillation counting.

Quantification of Free IAA and Conjugated IAA

Six tomato seedlings were dissected into different tissue sections as shown in Figure 3-7D, and the six replicates from each tissue section were pooled into one microcentrifuge tube, weighed, frozen in liquid nitrogen, and stored in a 280 °C freezer. For every 10 mg of frozen tissue, 70 µL of homogenization buffer (35% 0.2 M imidazole, 65% isopropanol, pH 7) containing 1.4 ng of [$^{13}C_6$] IAA was added, and tissues were homogenized using a Mixer Mill (MM 300; Qiagen) with tungsten carbide beads (3-mm beads for 1.5-mL tubes and 2.3-mm beads for 0.5-mL tubes; Craig Ball Sales).

Micro solid phase extraction (SPE) methods were modified from methods described in Chapter 2. Each SPE resin (5 mg of NH_2 and 20 mg of polymethylmethacrylate epoxide) was packed into 200 µL of TopTips (TT2EMT.96; Glygen Corp) that were placed over 2-mL microcentrifuge tubes with adaptors, and solvents were added and passed through the tips by centrifugation at 3,000 g to 6,000 g for a few seconds.

After 1 h on ice, 20 µL of the homogenate was diluted with 180 µL of water and the extract was purified by micro SPE, similar to that described in Chapter 2. Free IAA was eluted using methanol and methylated by ethereal diazomethane in a 250-µL glass insert. The solvents were evaporated under a stream of N_2 gas and the sample was redissolved in 15 µL of ethyl acetate.

For the rest of the homogenate, 10 µL was hydrolyzed in 1 N NaOH (1 h, room temperature; Baldi *et al*., 1989) for measurement of free plus ester-linked IAA and 10 µL was hydrolyzed in 7 N NaOH (3 h, 100 °C under N_2; Bialek and Cohen, 1989) for measurement of total IAA (free plus ester-linked and amidelinked IAA). After hydrolysis, the pH of the hydrolysate was adjusted to 2.7, and the free IAA plus that released from the conjugates was purified from the extracts using TopTips containing 7.5 mg of C18 resin (12213020; Varian), washed twice with 60 µL of water, eluted twice with 50 µL of methanol, collected in 250-µL glass inserts, and methylated as described above.

The methylated IAA was analyzed using gas chromatography (GC)-selected reaction monitoring-mass spectrometry (MS) on a Thermo Trace GC Ultra coupled to a TSQ Vantage triple quadrupole MS system (Thermo Scientific). The GC column and separation conditions were as described in Chapter 2. Compounds eluted from the GC device were ionized in the electron impact mode with electron emission at 70 eV and emission current of 100 mA. The molecular ions (mass-to-charge ratio [m/z] 189 for endogenous IAA and m/z 195 for [$^{13}C_6$]IAA) were selected by the first quadrupole and collided with argon in the second quadrupole using 10 V of collision energy and a 1.5-mTorr collision gas pressure. The quinolinium ions produced from the molecular ions (m/z 130 from m/z 189 and m/z 136 from m/z 195) were selected by the third quadrupole and detected using 0.025-s scan times. Levels of free IAA, free plus ester-linked IAA, and total IAA were quantified by isotope dilution analysis based on the [$^{13}C_6$]IAA internal standard, as described previously (Barkawi *et al*., 2010).

Stable Isotope Labeling and Isotopic Enrichment Analysis

Tomato seeds were planted on vertical agar plates on a sheet of 20-µm nylon filter screen (146510; Spectrum Laboratories) that had been placed on top of the agar medium. The nylon screen allowed tomato seedlings to grow straight on the surface and prevented root hairs from penetrating into the agar medium. This procedure ensured that a rapid switch of the tomato plants from normal growth agar to growth agar containing stable isotope-labeled compounds could be accomplished. It also minimized the effects of wounding and gravitropic responses during seedling movement. The growth conditions and light treatments were the same as those described above. To start the labeling process, tomato plants were transferred to labeling medium by picking up the filter screen with sterile forceps and transferring the screen and the attached tomato seedlings onto agar medium containing either 0.1 mM [2-^{13}C]indole (CLM-1863; Cambridge Isotope Laboratories) or 0.5 mM L-[^{13}C-indole 2]Trp (CLM-1543; Cambridge Isotope Laboratories). To uniformly label all the tissues, the entire seedlings were attached to the nylon filter. Seedlings fed by [$^{13}C_1$]Trp (four per plate) were covered by a 11-cm × 11-cm

piece of KimWipe tissue (Kimberly-Clark) moistened with labeling medium, as this was found to prevent shoots from bending away from the screen and labeling medium, which otherwise was a consequence of asymmetric growth induced by the supplied Trp. The plates were then placed vertically during the labeling period. At the end of the labeling period, the four seedlings were dissected, pooled, and collected as described above. All the manipulations prior to storing the samples in a -80 °C freezer were done in a physiological dark room under dim green light.

Free IAA was extracted and analyzed similarly to IAA quantification, but the quinolinium ions m/z 130 and 131 produced from the molecular ions m/z 189 and 190, respectively, were monitored for analysis of isotopic enrichment in the free IAA pool. Indole was partitioned from diluted plant homogenate before the anion-exchange resin extraction, using 80 µL of hexane, and ions m/z 117 and 118 were monitored in the selected ion monitoring mode for analysis of isotopic enrichment in the indole pool (Chapter 2). To analyze the Trp pool, the flow-through of the plant homogenate, after it passed through the anion-exchange resin, was collected. Extraction and GC-MS analysis of Trp were similar to those described by Chen *et al*. (2010) using methyl chloroformate derivatization, and ions m/z 276 and 130 as well as m/z 277 and 131 were monitored in the selected ion monitoring mode for analysis of isotopic enrichment in the Trp pool. The natural abundance of ^{13}C was determined using unlabeled chemical standards (Sigma) and is corrected for in the calculations and the data reported (Chapter 2).

Results

Measurement of PAT in Hypocotyls of Etiolated Seedlings

It was reported that the transport of IAA in dark-grown Arabidopsis hypocotyls was very low and not inhibited by NPA (Rashotte *et al*., 2003), suggesting that a very sensitive method is necessary to measure PAT in etiolated seedlings. Thus, I modified the method described by Rashotte *et al*. (2003) to increase the signal-to-noise ratio, and I established a sensitive assay that allowed us to measure PAT in excised etiolated Arabidopsis hypocotyl sections. As shown in Figure 3-1A, 6-mm hypocotyl sections

were used to measure PAT, and [^{3}H]IAA tracer was added in the donor agar block adjacent to the apical end of the section while a receiver agar block was placed adjacent to the basal end of the section. After a 3-h transport period, the hypocotyl section was cut into halves (Fig. 3-1B), and the basipetal transport of IAA was determined as a percentage of radioactivity in the basal section and the receiver block divided by the total radioactivity in the tissue plus the receiver block.

As shown in Figure 3-1C, about 10% of the [^{3}H]IAA taken up by the etiolated Arabidopsis hypocotyl section was transported to the basal end of the hypocotyl section. This transport was reduced by at least 50% when 10 mM of the transport inhibitor NPA was added to the receiver agar block, indicating that the measured transport of [^{3}H]IAA was polar and inhibited by NPA.

In the acropetal control, auxin transport was as low as 1% of the total, showing a low amount of diffusion of [^{3}H]IAA in the assay, and percentage PAT was determined by subtracting the apparent acropetal auxin transport from the basipetal auxin transport. This assay was also successfully applied to dark-grown tomato hypocotyls and similar results were obtained, except that PAT in etiolated tomato seedlings was about twice as much as in etiolated Arabidopsis seedlings (Fig. 3-1C).

PAT in Etiolated Seedlings Was Increased by Light

To explore the light effect on PAT in etiolated seedlings, Arabidopsis plants were kept in the dark for 4 d after sowing and tomato plants were kept in the dark for 3 d after germination before light exposure. Seedlings were then exposed to continuous white (W) light for 2 d, while control plants were kept in the dark for the same length of time. As shown in Figure 3-2, A and B, 2 d of continuous W light doubled the PAT in Arabidopsis hypocotyls and increased PAT in tomato hypocotyls by about 60%. When the W light exposure period was shortened to 1 d, the promotion of PAT in Arabidopsis still occurred but was reduced relative to a 2-d exposure, while tomato showed the same amount of PAT promotion as with 2 d of W. I further shortened the light exposure period to 1 h and then returned plants to the dark for an additional 1 d (tomato) or 2 d (Arabidopsis) to

allow the same time period for biochemical processes to occur as in the long light exposure treatments, and I found that the light-induced PAT promotion completely disappeared in Arabidopsis, but it still occurred at the same level as after 1- or 2-d light exposure treatment in tomato (Fig. 3-2B). Because a short light exposure period minimized the effects of deetiolation and photosynthesis, and thus would allow analyses of a variety of photobiological features, and because the size of tomato seedlings was more amenable to physical manipulation and analytical analysis of IAA, I continued ,my research using tomato as the primary system.

Promotion of PAT in Tomato Was Sensitive to B and R Light

Because W light includes a large range of wavelengths, I analyzed whether light quality affected the promotion of PAT in etiolated tomato seedlings. As shown in Figure 3-2C, when W light was replaced by either R light or B light, a 1-h light exposure followed by 1 d of darkness increased PAT to a similar level, suggesting that R or B light alone was sufficient to trigger the response. I then varied the fluence of R or B light to determine the minimum fluence followed by 1 d of darkness that was required to promote PAT. When R light was applied, as shown in Figure 3-3A, a significant PAT promotion was found when the fluence was as low as 3 μmol m^{-2} ($P< 0.05$), and the maximal promotion was achieved with 10 μmol m^{-2} R light, corresponding to a duration of 5 s. As shown in Figure 3-3B, when the fluence of B light was reduced to 100 μmol m^{-2}, a significant PAT promotion was found ($P<0.05$). The promotion became more pronounced when higher fluences were applied and reached the maximal level when the B light fluence was 14,400 μmol m^{-2} (equivalent to 1 h of B in the previous experiment). These results suggested that the promotion of PAT in tomato hypocotyls was very sensitive to the amount of B and R light and was more sensitive to R light than to B light.

Phytochrome Involvement in the Promotion of PAT

Phytochromes absorb and respond to both R and FR light and, to a lesser extent, B light as well (Pratt and Briggs, 1966; Cordonnier and Pratt, 1982; Weller *et al*., 2001).

Because the promotion of PAT was more sensitive to R light than B light, it is likely that both the B and R light responses were mediated by phytochromes. To test this hypothesis, I analyzed the promotion of PAT in available tomato photoreceptor mutants, including *cry1*, *phyA*, *phyB1*, and *phyB2* (Van Tuinen *et al*., 1995a, 1995b; Weller *et al*., 2001), and the wild-type plants of the same background. When plants were treated with 10 μmol m^{-2} R light followed by 1 d of darkness (Fig. 3-4A), PAT in wild-type tomato seedlings was significantly increased compared with the corresponding dark controls, and the increase was significantly reduced in *phyA*, *phyB1*, or *phyB2* mutants. After being treated with 3,000 μmol m^{-2} B light followed by 1 d of darkness, PAT in wild-type and *cry1* tomato seedlings was also significantly increased compared with the corresponding dark controls ($P<0.0005$; Fig. 3-4C), suggesting that cryptochrome was not involved in the promotion of PAT induced by B light. On the other hand, B light exposure did not increase PAT significantly in *phyA*, *phyB1*, or *phyB2* mutants ($P<0.2$), suggesting that phytochrome was involved in this B light response.

To further evaluate the phytochrome dependence of the light-induced promotion of PAT, I tested if the light response was FR light reversible, a distinguishing property of many phytochrome responses (Casal *et al*., 1998). As shown in Figure 3-4B, 10 μmol m^{-2} R light followed by 1 d of darkness induced a significant increase in PAT, and this increase was significantly reversed by 1 μmol m^{-2} FR light applied immediately after the R light exposure ($P<0.05$) and thus was not different from the dark control. The FR treatment alone had no significant effect. Similarly, the promotion of PAT induced by 100 μmol m^{-2} B light was significantly reversed by 10 μmol m^{-2} FR light applied immediately after B light (Fig. 3-4D). These results support the conclusion that the PAT promotion induced by R or B light exposure in tomato seedlings was mediated by phytochrome photoreceptors.

Promotion of PAT by Light Required Time to Develop

I found in a preliminary experiment that the promotion of PAT in tomato seedlings occurred 1 d after the light exposure but not 2 h after the light exposure, so I

asked what was the minimum lag time following the light exposure that was required for plants to develop the response. Therefore, I analyzed PAT in seedlings at different time points following the light exposure along with their corresponding dark controls. I found that PAT was significantly increased after 15 h in darkness following the R light exposure ($P<0.005$; Fig. 3-5). The increase continued and reached the maximal level 18 h after R light exposure. Similar results were also obtained using B light exposure (Fig. 3-12A). These results suggested that a dark period greater than 12 h following the light exposure was required for the PAT promotion to occur.

The Velocity of PAT was Increased by Light

A pulse-chase experiment was carried out to compare the velocity of PAT in tomato seedlings treated with 100 μmol m^{-2} R light exposure followed by 1 d of darkness and in the dark control plants. The 2-cm excised tomato hypocotyl sections were given a 20-min [^{3}H]IAA pulse followed by unlabeled IAA chase periods. The localization of [^{3}H]IAA in each hypocotyl section was analyzed 1, 2, and 3 h after the start of the chase. The front and the peak of [^{3}H]IAA taken up by hypocotyls moved away from the IAA source over time, and Figure 3-6 shows the result after a 3-h chase period. In R light-treated seedlings, the front of [^{3}H]IAA movement reached tissue section 17 to 20 mm below the IAA source, and the peak was located in or slightly after tissue section 11 to 14 mm below the IAA source. However, in the dark control plants, the front of [^{3}H]IAA reached tissue section 14 to 17 mm below the IAA source, and the peak was located in tissue section 8 to 11mm below the IAA source. These results showed that IAA in plants exposed to R light moved faster than in dark control plants and that IAA was transported about 3 mm farther than in the dark control plants during the 3-h transport period. Similar results were also obtained using B light exposure followed by 1 d of darkness (Fig. 3-12B).

The Level of Free IAA was Increased by Light in Some Tissue Sections

Because altered PAT can be associated with an altered distribution of free IAA among different plant tissues, I quantified the levels of IAA in different tomato tissue sections. In a preliminary experiment, when levels of free IAA were measured in the 6-mm hypocotyl sections used for the PAT assay and in tissues above (meristem, cotyledons, and hook) and below (remaining hypocotyl tissues) the sections, no change in free IAA was found after plants were treated by light followed by 1 d of darkness. However, because the change in IAA levels might be very localized, I measured IAA levels in more discrete tissue sections, as shown in Figure 3-7D. Consistent with the preliminary result, the level of free IAA was not changed in the top section (consisting of meristem, cotyledons, and hook), H1, and H5 sections, but free IAA was increased 20% to 30% in H2, H3, and H4 sections after 100 μmol m^{-2} R light followed by 1 d of darkness ($P<0.05$; Fig. 3-7A). I also measured the level of conjugated IAA, including ester-linked IAA and amide-linked IAA, but neither type of IAA conjugate showed significant changes (Fig. 3-7, B and C), suggesting that the increased free IAA was not due to a change in the rate of release of free IAA from IAA conjugates via hydrolysis.

Biosynthesis of IAA in the Top Section was Increased by Light

IAA can be synthesized from [$^{13}C_1$]indole directly via the Trp-independent pathway or, following [$^{13}C_1$] indole conversion to Trp, the [$^{13}C_1$]indole-derived Trp can be used in the Trp-dependent pathways. IAA can be synthesized from supplied labeled Trp only via Trp-dependent pathways (Fig. 3-8C). To understand if IAA biosynthesis was altered by R light followed by 1 d of darkness, I used stable isotope-labeled indole or Trp to feed tomato seedlings, and I analyzed the enrichment of labeled IAA derived from each labeled precursor. I found that 100 μmol m^{-2} R light followed by 1 d of darkness induced a significant increase of [$^{13}C_1$]indole-derived IAA in the top section ($P<0.05$; Fig. 3-8A; Fig. 3-13A) and a marginally significant increase of [$^{13}C_1$]indole-derived IAA in H3 ($P<0.6$; Fig. 3-8A). This R light-induced increase of [$^{13}C_1$]indole-derived IAA in the top section does not occur in *phyA*, *phyB1*, or *phyB2* mutants (Fig. 3-9), suggesting

that phytochromes are involved in the regulation of IAA biosynthesis. Importantly, the level of [$^{13}C_1$]indole-derived IAA in the top section after R exposure was significantly higher than the level of [$^{13}C_1$]indole-derived Trp ($P<0.05$), while the levels were the same in dark control plants (Fig. 3-8A); this difference was more obvious when a shorter labeling period was applied (Fig. 3-13B), and these results suggest that TI biosynthesis of IAA was increased by R light and became the predominant path for de novo IAA biosynthesis. Similarly, a significant increase of [$^{13}C_1$]Trp-derived IAA was found in the top section after R light exposure ($P<0.05$; Fig. 3-8B). I also found that the isotopic enrichment in the indole or Trp pool was not different in plants with or without light treatment (Fig. 3-14), supporting the conclusion that the increased amount of labeled IAA was not due to increased availability of labeled precursors but because the biosynthesis of IAA was increased by light. Interestingly, when plants were fed with [$^{13}C_1$]indole and 10 mM NPA simultaneously, labeled IAA was greatly reduced in tissue sections H1, H2, H3, and H4 compared with controls without NPA (Fig. 3-10), suggesting that IAA synthesized in the top section moved basipetally in the PAT stream while IAA was also synthesized locally in hypocotyl tissues and/or that NPA directly affected IAA biosynthesis as well.

Discussion

A goal of this study was to understand the effects of light on the transport, biosynthesis, and distribution of IAA in etiolated seedlings. It was reported previously that auxin transport in dark-grown Arabidopsis seedlings was not reduced by NPA (Rashotte *et al*., 2003). Here, I found that 10% of the IAA taken up by dark-grown Arabidopsis hypocotyls was transported basipetally and that transport was reduced by 50% when NPA was applied to the basal end of the sections (Fig. 3-1C). This suggested that, similar to other etiolated dicotyledonous plants such as cucumber and tomato, PAT occurs in dark-grown Arabidopsis hypocotyls, and the lack of measured NPA inhibition of PAT in Rashotte *et al*. (2003) was likely due to the sensitivity limit of the transport

assay used. My results are consistent with those of Nagashima *et al*. (2008), who showed that NPA inhibited the elongation of 3-d dark-grown Arabidopsis seedlings, but the inhibition was not as great in 5-d dark-grown seedlings. Because hypocotyl growth approached a maximum in 5-d dark-grown etiolated Arabidopsis, probably due to the exhaustion of seed reserves (Gardner *et al*., 2009), it seemed that NPA-treated dark-grown seedlings could still growat a lower rate and finally reach their maximal lengths; this may explain why Jensen *et al*. (1998) found no effect of NPA on the elongation of 7-d-old Arabidopsis seedlings. The slow growth of dark-grown seedlings treated with NPA could be a contribution of the local biosynthesis of IAA (discussed below), but local IAA biosynthesis alone was not sufficient to support the growth of light-grown seedlings, which had a higher level of PAT (Fig. 3-2A). Therefore, it would appear that auxin transport is required for hypocotyl elongation in both dark-grown and light-grown Arabidopsis seedlings, but it limits the growth of light-grown seedlings to a greater extent.

The promotion of PAT by light seems to be regulated differently in Arabidopsis and tomato seedlings. In tomato, the promotion could be achieved using light fluences in the range of 1 to 1,000 μmol m^{-2}, which fits the definition of a low-fluence response (LFR; Neff *et al*., 2000), and this response was further confirmed by the R/FR reversibility test. However, the promotion in Arabidopsis required a much longer period of light exposure and also a higher fluence rate; thus, effects such as greening and active photosynthesis could also play an important role in this promotion. LFR has often been considered to be controlled by phyB (Shinomura *et al*., 1996; Casal *et al*., 1998), while LFR controlled by phyA has also been reported (Long and Iino, 2001; Stowe-Evans *et al*., 2001; Shen *et al*., 2009). I found that the promotion of PAT induced by low-fluence R light was greatly reduced in *phyA*, *phyB1*, and *phyB2* tomato mutants (Fig. 3-4A), providing an additional example of LFR mediated by both phyA and phyB. B light-induced PAT promotion was also reduced in these phytochrome mutants (Fig. 3-4C), which is consistent with the role of phytochromes in B light perception in tomato (Weller *et al*., 2001). This response was not reduced in a *cry1* mutant, and PAT was significantly

increased in the *cry1* mutant after B exposure (Fig. 3-15), suggesting a negative role of cryptochrome in PAT, as reported previously (Zeng *et al*., 2010). In the absence of tomato mutants defective in phototropin functions, I could not test for effects of phototropins on the B light induced PAT promotion, but I found that a FR light pulse following the B light pulse reversed the B light effects (Fig. 3-4D), suggesting that this B light response was mostly, if not entirely, mediated by phytochromes.

The low-fluence-induced PAT promotion did not occur immediately after light exposure but required a dark period of over 12 h to develop (Fig. 3-5). This means that the effect of the light pulse persisted over a long period of time, and a series of downstream changes triggered by the light signal, such as changes in the expression and localization of PAT transporters and facilitators, were required to increase PAT. Keuskamp *et al*. (2010) showed regulation of PIN3 by phytochrome signaling in a shade-avoidance response, and Ding *et a*l. (2011) showed that unilateral W light (which induced phototropic curvature) polarized PIN3 localization to the inner side of hypocotyl endodermis cells (facing the vasculature). These studies suggest that R light could induce polarly localized PIN3, which restricts IAA to the basipetal transport stream in the stele (Petrášek and Friml, 2009), and thus this could increase the basipetal transport of IAA. Interestingly, I found that a brief light pulse increased PAT velocity (Fig. 3-6), which was also reported in cucumber seedlings after a long period of R light treatment (Shinkle *et al*., 1998). Although a mechanism for regulating the auxin transport rate in hypocotyls has not been established as yet, light was shown to change the intracellular distribution of PIN2 in Arabidopsis roots (Laxmi *et al*., 2008). Thus, light may increase the PAT rate by promoting the plasma membrane localization of auxin transporters and facilitators as well as by increasing the turnover rate of these proteins.

PAT is usually considered as a means of controlling the distribution of free IAA, so the transport direction may imply the relative level of free IAA. Thus, when PAT was promoted in the hypocotyl segment by a light pulse, I expected the level of free IAA to be increased in lower regions of the hypocotyl and decreased in the top section. My free IAA measurement was partially consistent with this expectation, which showed that the

free IAA level was significantly increased in H2, H3, and H4 segments (Fig. 3-7A), but this difference was not significant when all tissues below H1 were pooled together, suggesting that the significant increase in free IAA was localized. On the other hand, the free IAA levels in H1 and in the top section above H1 were not changed by the light pulse, suggesting that transporting IAA away from these tissue sections did not necessarily decrease the level of free IAA. This result was not surprising given that Jones *et al*. (2005) found no change in the distribution of free IAA in the upper and lower regions of inflorescence stems of the Arabidopsis *pin1-1* mutant, where PAT was dramatically decreased (Okada *et al*., 1991). Furthermore, this result could be explained when IAA biosynthesis was taken into consideration (discussed below). Indeed, the lack of light effects on free IAA levels in these tissues was a result of the combined effects of increased IAA biosynthesis and increased PAT, and transporting newly synthesized IAA basipetally to lower regions of the hypocotyls maintained a constant level of free IAA in the top section.

I used both [^{13}C]indole and [^{13}C]Trp to label the seedlings in order to explore if light had different effects on the TI and TD IAA biosynthetic pathways. The rationale for this approach is that [^{13}C]Trp forms IAA only via TD pathways while [^{13}C]indole forms IAA directly via the TI pathway or, alternatively, can be converted to Trp and subsequently used by the TD pathways. Because the level of [^{13}C]Trp-derived IAA was increased in the top section, it can be concluded that TD IAA biosynthesis was increased by R light (Fig. 3-8B). In addition, the enrichment of [^{13}C]indole-derived [^{13}C]IAA in the top section in dark control plants was equal to the [^{13}C]indole-derived [^{13}C]Trp, so the [^{13}C]IAA in dark tissue could all have been derived from [^{13}C]Trp via TD pathways; thus, the TD pathways could be the predominant path for de novo IAA biosynthesis in dark-grown plants. On the other hand, in the case of R light-exposed plants, an increased enrichment of [^{13}C]indole-derived [^{13}C]IAA was noted, while the enrichment of [^{13}C]indole-derived [^{13}C]Trp in the same samples was unaffected. This resulted in the enrichment of [^{13}C]IAA exceeding that of [^{13}C]Trp (Fig. 3-8A). Therefore, it can be concluded that the TI IAA biosynthesis was also increased by R light, and that the TI

IAA biosynthetic pathway was the predominant path for de novo IAA biosynthesis in the top section after R light exposure. Moreover, when the enrichment of [^{13}C]indole-derived [^{13}C] IAA was analyzed in the top section of *phyA*, *phyB1*, and *phyB2* mutants, I found that IAA biosynthesis in these tissues did not change in response to low-fluence R light (Fig. 3-9), suggesting that the R light effect on IAA biosynthesis is under the control of phytochrome. Additionally, IAA biosynthesis in these phytochrome mutants was lower than in the wild type both in the presence and absence of R light exposure (Fig. 3-9). Thus, in addition to the *red1*/*cyp83b1* mutant (Hoecker *et al*., 2004) and the shade avoidance response (Tao *et al*., 2008), my work provides an additional link between phytochrome signaling and auxin biosynthesis, confirming that auxin biosynthesis plays an important role in phytochrome-regulated photomorphogenesis.

I also noticed that the predominance of TI IAA biosynthesis after R light exposure was even more evident when a shorter labeling period was analyzed (Fig. 3-13B). This result suggests the possibility that one could fail to see the differential labeling if too long a labeling period was used and the Trp pool became saturated by [^{13}C]Trp derived from [^{13}C]indole. Changes in the use of TI and TD IAA biosynthetic pathways were reported previously as a result of plant organ development and as a response to stress (Ljung *et al*., 2001b; Epstein *et al*., 2002; Rapparini *et al*., 2002; Sztein *et al*., 2002), indicating that the different IAA biosynthetic pathways play distinct roles under different developmental and environmental conditions. Additionally, my data showed that the biosynthesis of [^{13}C]Trp from [^{13}C]indole was also increased by R light exposure in sections H1 and H2 but not in any other tissue section (Fig. 3-8A). This change could potentially be hidden if the whole seedling was used for analysis, as was done for microarray analyses (where both R and FR exposure decrease Trp synthase-β At1g01010 gene expression in Arabidopsis; http://bbc.botany.utoronto.ca/efp/cgi-bin/efpWeb.cgi). The change in Trp biosynthesis was not associated with changes in TD IAA biosynthesis in these tissue sections (Fig. 3-8B), suggesting that it is a consequence or trigger for photomorphogenic changes other than IAA biosynthesis. While, to my knowledge, phytochrome regulation of Trp synthase-b activity has not been reported, phytochrome is known to regulate the

expression, translation, and thus activity of a plethora of other plastid-localized enzymes (Christopher, 2003).

It is worth pointing out that the amount of [^{13}C]IAA derived from [^{13}C]Trp or [^{13}C]indole was different in different tissue sections, and one might conclude that the utilization of these precursors for IAA biosynthesis was different in different tissues. However, the enrichment of [^{13}C]Trp was not uniform among the tissue sections (Fig. 3-13B), and the relative abundance corresponded to that of [^{13}C]Trp-derived IAA, suggesting that the amount of [^{13}C]Trp-derived IAA was associated with the availability of [^{13}C]Trp in the tissue. However, the enrichment of [^{13}C]indole was uniform in all tissue sections (Fig. 3-14A), so the abundance of [^{13}C]indole-derived IAA in each tissue section represented IAA biosynthesis activity. Therefore, compared with Trp, indole is a better precursor for comparative study of IAA biosynthesis across different tissues, not only because it covers both TD and TI biosynthetic pathways but also because it labels the endogenous pool uniformly.

The role of localized IAA biosynthesis in different regions of the hypocotyl was further explored using NPA to disrupt PAT. When seedlings were treated with NPA to inhibit PAT (Fig. 3-10), the enrichment of newly synthesized labeled IAA in the H1, H2, H3, and H4 segments was greatly reduced, and the slight increase of labeled IAA by the light pulse was also abolished in these segments but not in the top section, suggesting that light increased IAA biosynthesis only in the top section and thus the increased amount of free IAA in the H2, H3, and H4 segments resulted from increased IAA biosynthesis in the top section. Because IAA has been found to promote the plasma membrane localization of PIN proteins and therefore increase IAA's own efflux from cells (Paciorek *et al*., 2005), the increased IAA biosynthesis at the top section may be the driving force for increased PAT triggered by light exposure. Although it was expected that the level of labeled IAA at the top section might be increased by NPA due to disrupted PAT, it was actually unchanged, suggesting a feedback regulation of IAA biosynthesis by IAA itself, which has also been reported in other systems (Ribnicky *et al*., 1996; Ljung *et al*., 2001a). The level of labeled IAA in the major portion (H5) of the hypocotyls was not

changed by NPA during the 4-h feeding period, suggesting that the enrichment of labeled IAA in this tissue section was primarily due to local biosynthesis of IAA at a rate that was lower than that found in the upper part of the shoot. In fact, the enrichment of labeled IAA in the H5 tissue section in untreated plants could be detected in a 2-h feeding period (Fig. 3-13A), and it would be impossible for IAA synthesized at the top section to reach this region within a 2-h period, because the transport rate in hypocotyls was at most 6 mm h^{-1} (calculated from Fig. 3-5). Therefore, the top section of the seedling was not the only tissue for de novo IAA biosynthesis, and local biosynthesis of IAA might also contribute to hypocotyl growth. Although the hypocotyl tissues were capable of synthesizing IAA, the top section contained the majority of the IAA conjugates (Fig. 3-7, B and C), which could serve as IAA precursors that slowly release free IAA (Nowacki and Bandurski, 1980; Chisnell and Bandurski, 1988; Bialek and Cohen, 1992; Ljung *et al*., 2001b). Thus, PAT plays an important role in supplying free IAA to lower parts of seedlings by basipetal transport of newly synthesized and conjugate-derived IAA in the top section.

The increase of free IAA in a region of tomato hypocotyls after a R light pulse was consistent with what Behringer and Davies (1992) reported in pea. However, in this work, the increase in free IAAwas not associated with a differential hypocotyl elongation rate, and the growth of hypocotyls in plants that were exposed to R light followed by 1 d of darkness was not different from dark control plants (Fig. 3-16). Thus, instead of regulating hypocotyl elongation, it is likely that the redistribution of free IAA triggered other developmental changes, such as promoting vascular development in the stem tissues (Mattsson *et al*., 1999; Aloni, 2010). Alternatively, the altered PAT might be a way to tightly regulate the level of free IAA in the top section, where growth was most active, or to supply free IAA in root tissues to initiate lateral root formation and promote root development (Bhalerao *et al*., 2002; Ljung *et al*., 2005; Salisbury *et al*., 2007). Although I have found that a single very brief R light pulse was sufficient to alter auxin biosynthesis and transport in etiolated tomato seedlings, no dramatic change in hypocotyl elongation was observed in this LFR (Fig. 3-16). However, it was previously shown that

hypocotyl elongation was decreased when dark-grown tomato seedlings were exposed to R light pulses with hourly repeats (Van Tuinen *et al*., 1995a), which was also defined as a LFR (Casal *et al*., 1998), and the R light effect was reversible by FR light pulses following each R light pulse (Van Tuinen *et al*., 1995a). The mechanism related to the requirement of repeated R light pulses for the inhibition of hypocotyl elongation during the de-etiolation process remains to be further studied.

In summary (Fig. 3-11), I have found that in the absence of light, IAA is synthesized in all regions in the shoot, with more synthesized at the top section, while PAT also occurs to transport IAA produced at the top section to lower regions in the hypocotyl, maintaining free IAA gradients across the shoot with maxima at the top section. When etiolated seedlings are exposed to low-fluence R light, IAA biosynthesis at the top section is increased and PAT in the adjacent hypocotyl tissue is also increased to transport more IAA to the basal part of the seedling, leading to an unchanged level of free IAA in the top section and an increased level of free IAA in the lower regions of the hypocotyl.

Figures

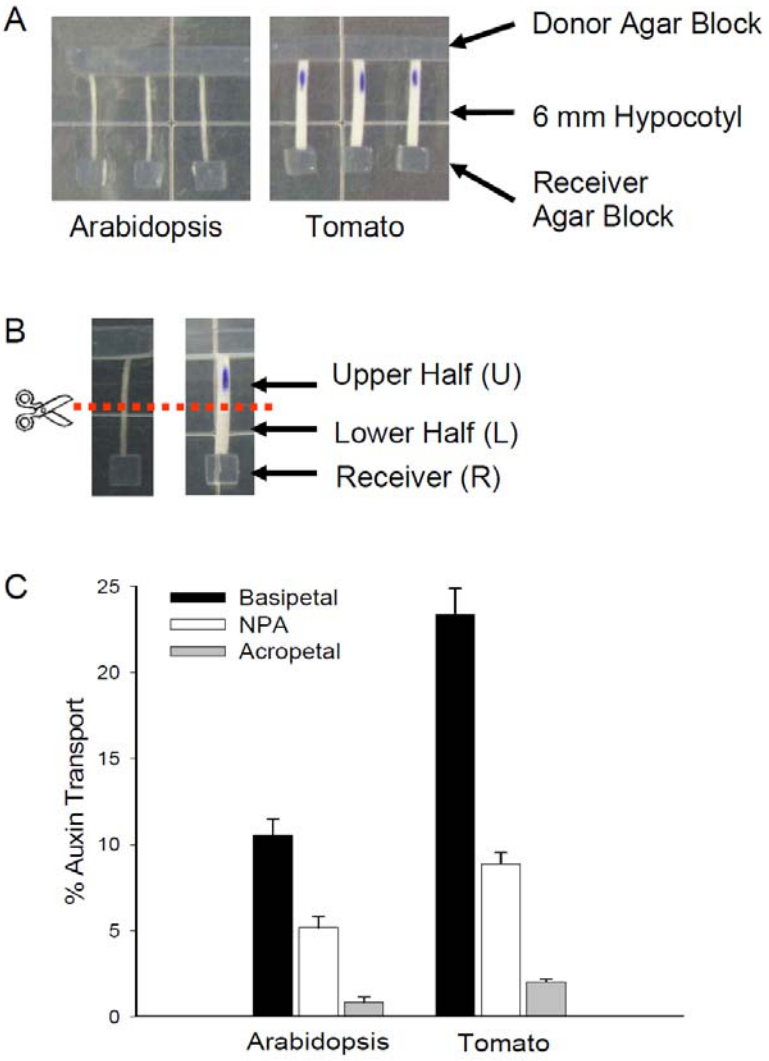

Figure 3-1. Etiolated Arabidopsis and tomato seedlings had measurable basipetal polar auxin transport (PAT) in excised hypocotyl sections. (A) The PAT assay: Donor agar block contained 10^{-7} M [^{3}H]IAA; 10 µM NPA was added to the receiver agar block in the NPA control. **(B)** Radioactivity in the upper half (U), lower half (L), and receiver (R) was determined separately at the end of the transport period. **(C)** Polar auxin transport in 6-d dark-grown Arabidopsis and 4-d dark-grown tomato hypocotyls after a 3-h transport period (n=10). Similar results were also obtained using 8-d dark-grown Arabidopsis plants. Percent auxin transport equals the percentage of radioactivity in L and R divided by the sum of L, R, and U. Error bars represent standard errors.

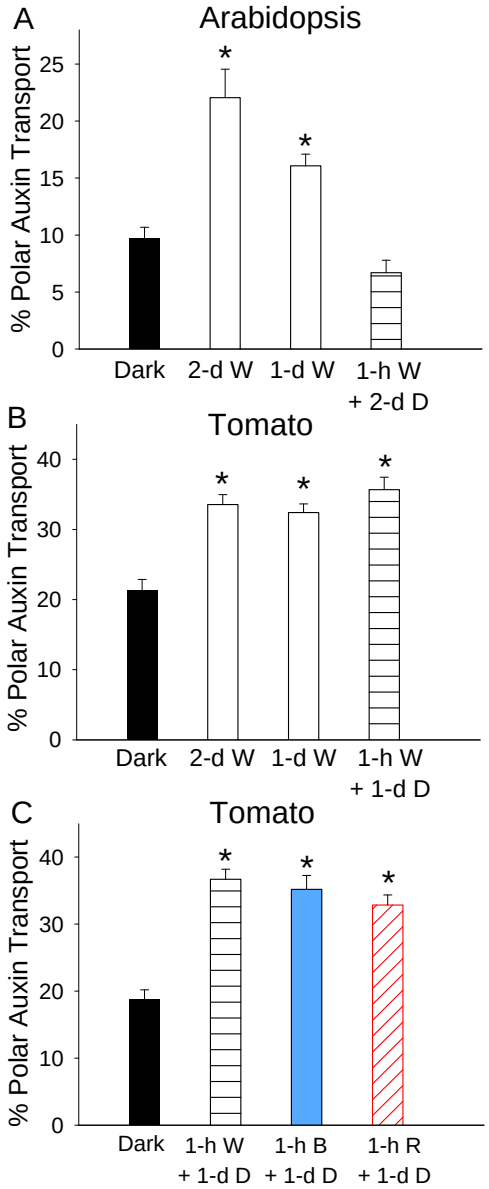

Figure 3-2. Light increased PAT in etiolated Arabidopsis and tomato seedlings. % PAT equals percent basipetal auxin transport minus the percent acropetal auxin transport. W: white light; B: blue light; R: red light. * indicates significant changes. **(A)** PAT in Arabidopsis hypocotyls was significantly increased by 2 d or 1 d continuous 80 µmol m^{-2} s^{-1} W light ($P<0.0005$, n=10, student's t-test), but not by 1 h W light followed by 2 d darkness. **(B)** PAT in tomato hypocotyls was significantly increased by 2 d or 1 d continuous 21 µmol m^{-2} s^{-1} W light and by 1 h W light followed by 1 d darkness ($P< 0.0001$, n=10, student's t-test). (C) PAT in tomato hypocotyls was significantly increased by 1 h of 21 µmol m^{-2} s^{-1} W light or by 1 h of 4 µmol m^{-2} s^{-1} B or R light followed by 1 d darkness ($P< 0.0001$, n=10, student's t-test).

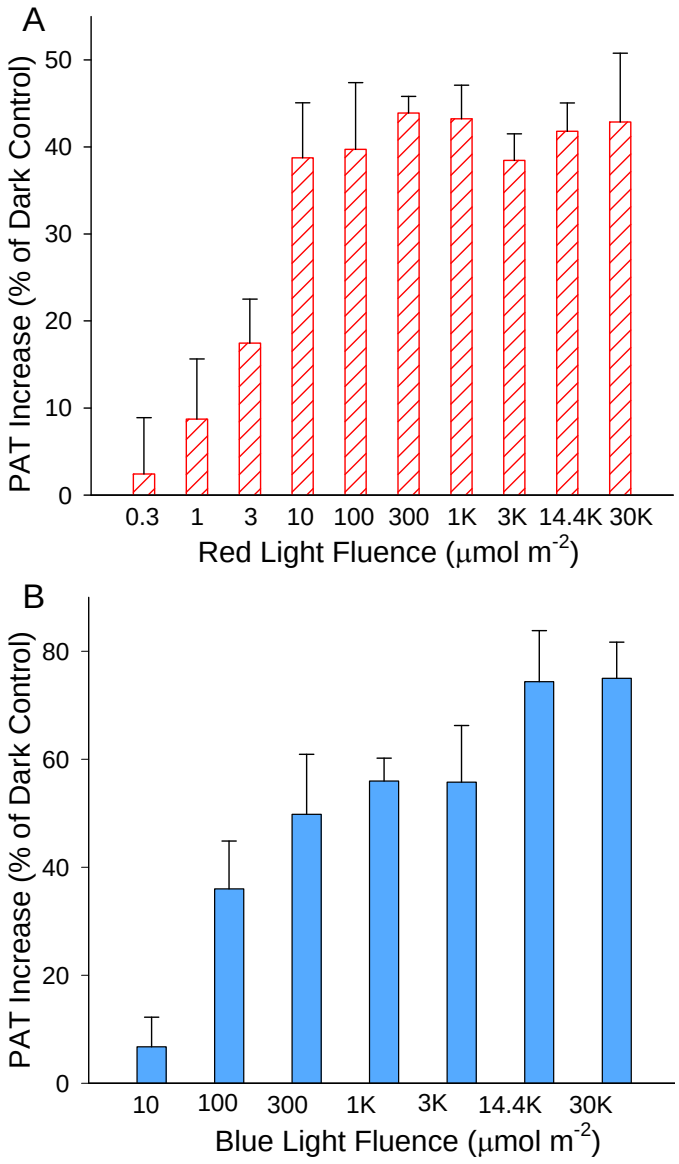

Figure 3-3. Increase of PAT in etiolated tomato hypocotyls in response to different blue and red light fluences followed by 1-d darkness. The increase in PAT is shown as percent of the dark control. **(A)** Increase of PAT in etiolated tomato seedlings when different red light fluences were applied. The increase was significant when red light fluence was equal to or higher than 3 μmol m^{-2} ($P<0.05$, n=8, student's t-test). **(B)** Increase of PAT in etiolated tomato seedlings when different blue light fluences were applied. The increase was significant when blue light fluence was equal to or higher than 100 μmol m^{-2} ($P<0.05$, n=8, student's t-test).

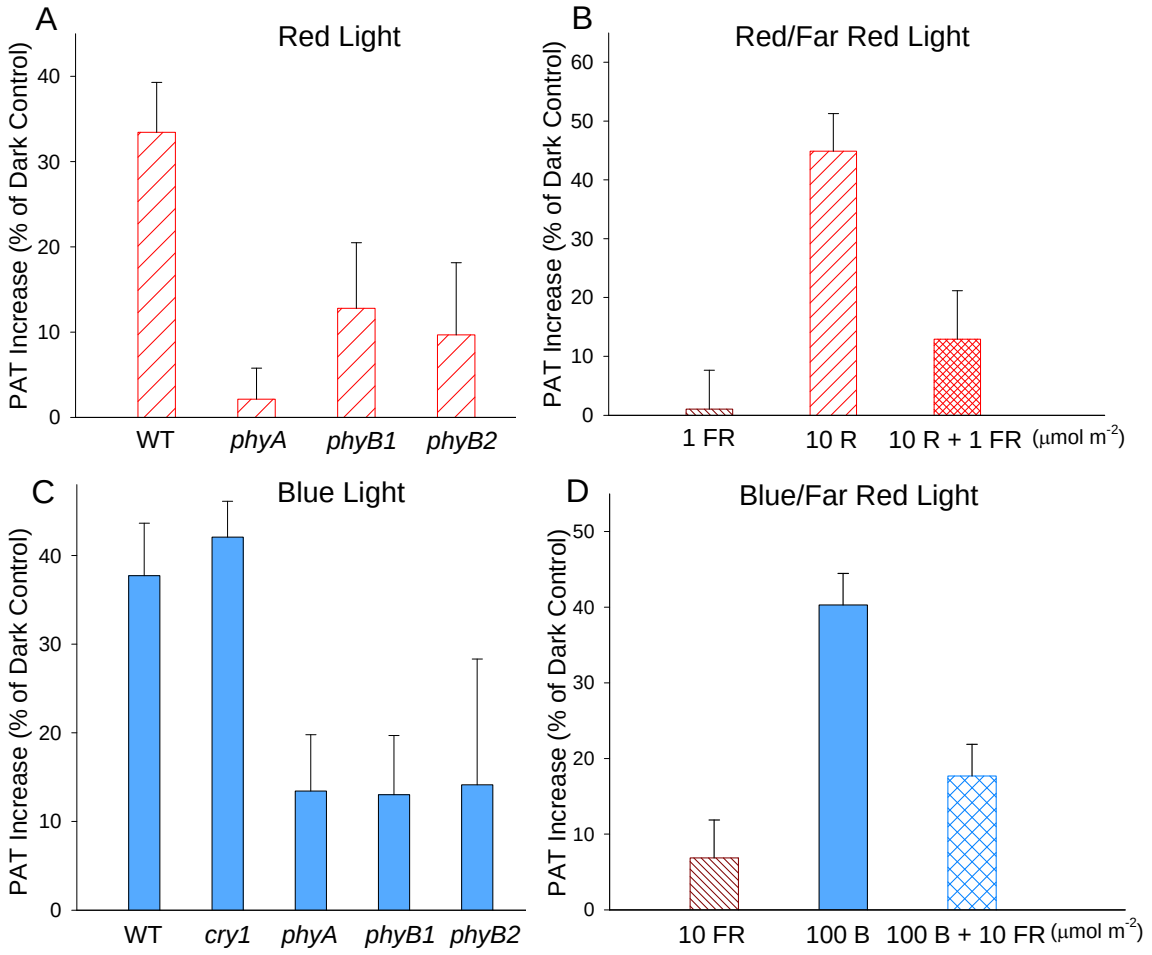

Figure 3-4. Red and blue-light induced increase of PAT in etiolated tomato seedlings was mediated by phytochrome. R: red light; B: blue light; FR: far red light. **(A)** The increase in PAT in wild type tomato seedlings by 10 μmol m^{-2} red light exposure was reduced or abolished in *phyA*, *phyB1*, or *phyB2* tomato seedlings. **(B)** 1 μmol m^{-2} far red light applied immediately after 10 μmol m^{-2} red light reversed the increase in PAT induced by 10 μmol m^{-2} red light ($P<0.05$, n=10, student's t-test). **(C)** 3000 μmol m^{-2} blue light exposure significantly increased PAT in wild type and *cry1* tomato seedlings, but not in *phyA*, *phyB1*, or *phyB2* tomato seedlings ($P>0.2$, n=8, student's t-test). **(D)** 10 μmol m^{-2} far red light applied immediately after 100 μmol m^{-2} blue light reversed the increase in PAT induced by 100 μmol m^{-2} blue light ($P<0.05$, n=10, student's t-test). 10 μmol m^{-2} far red light alone did not show significant effects on PAT. ($P>0.3$, student's t-test). In A and C, all tomato plants were in the cv. MoneyMaker background. Data shown are increased PAT as percent of dark control in corresponding genotypes.

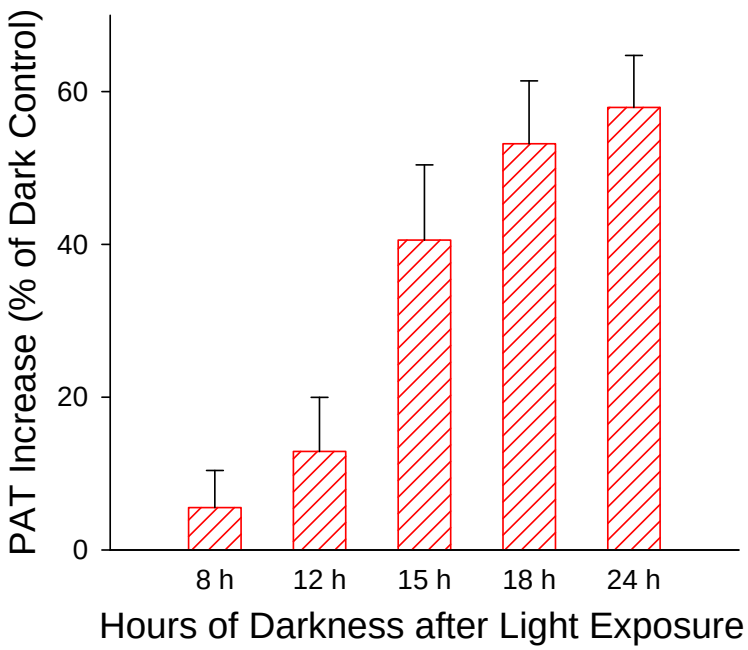

Figure 3-5. Greater than 12-hour darkness after the red light exposure was required for the increase in PAT to occur. When the dark period following 10 μmol m^{-2} red light exposure equaled or exceeded 15 hours, PAT was significantly increased in etiolated tomato seedlings ($P<0.005$, $n=10$; student's t-test). A similar result was also obtained using 3000 μmol m^{-2} blue light exposure.

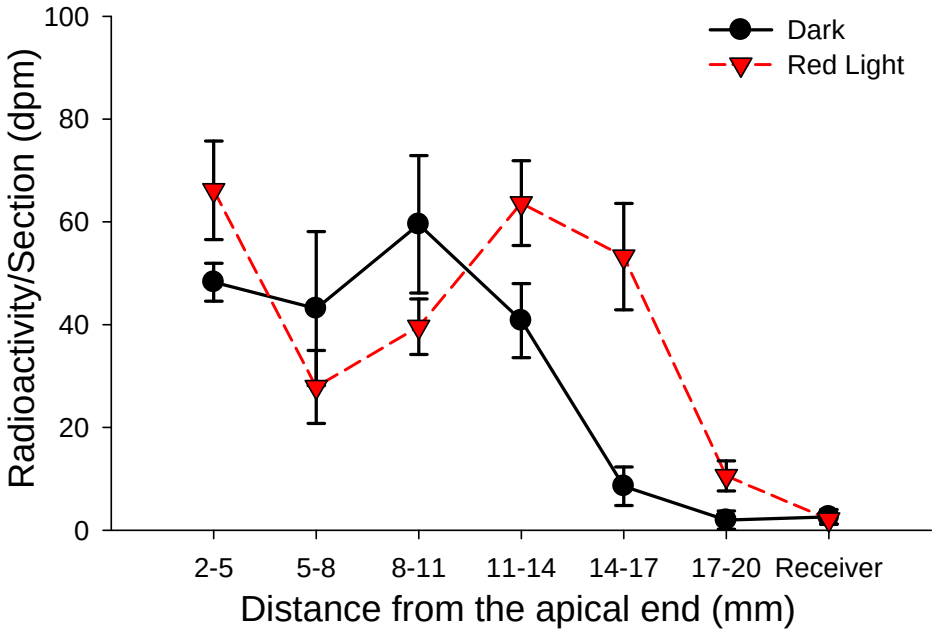

Figure 3-6. PAT velocity was increased by red light exposure. In tomato seedlings treated with 100 µmol m^{-2} red light exposure followed by 1-day darkness, the pulse of [^{3}H]IAA reached the tissue section 17 mm below the IAA source after a 3-hour chase period, while the pulse of [^{3}H]IAA reached the tissue section 14 mm below the IAA source in dark control plants (n=4). A similar result was obtained using blue light exposure.

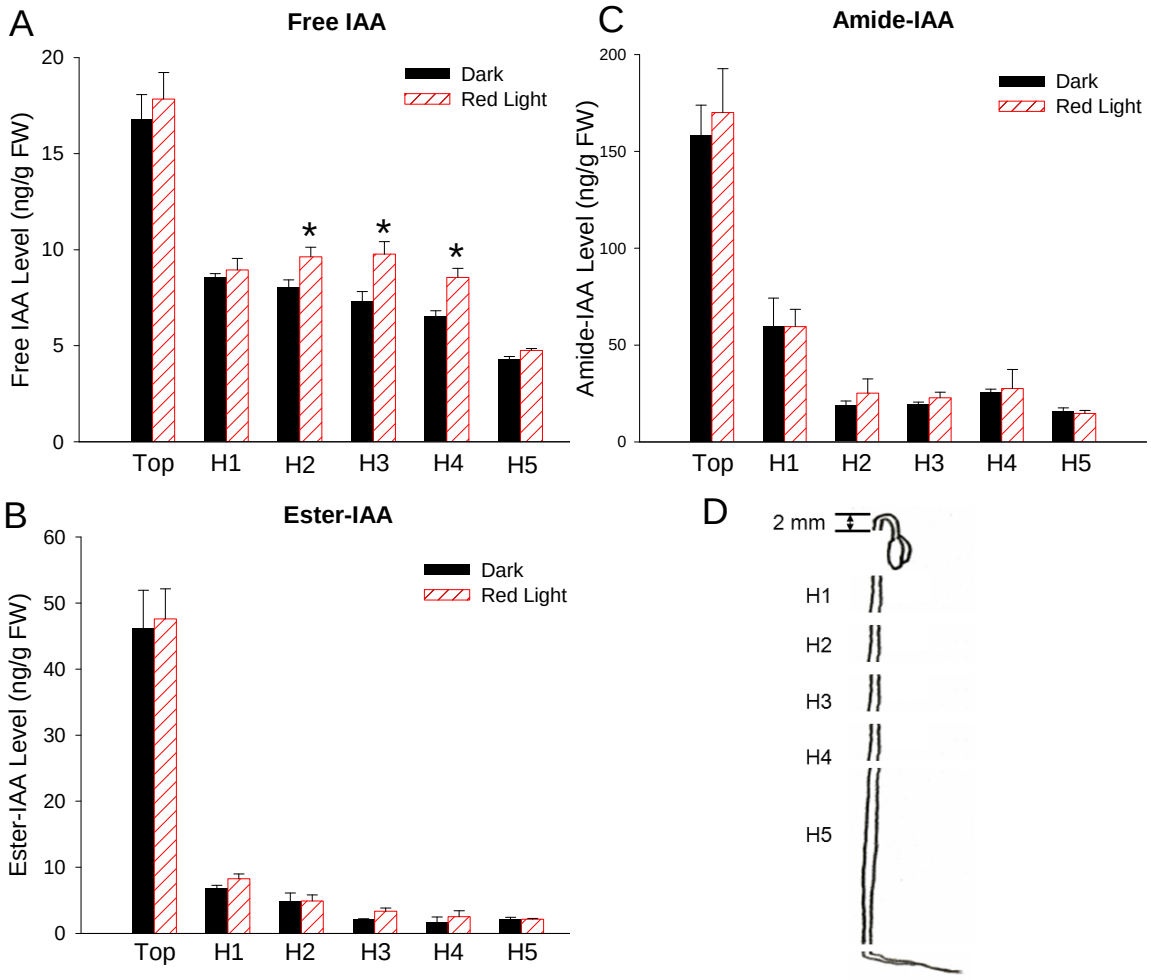

Figure 3-7. Light increased the level of free IAA in specific regions of etiolated tomato hypocotyls. Tissue sections that displayed a significant change in IAA level after 100 µmol m^{-2} red light exposure followed by 1-d darkness are indicated by * ($P<0.05$, n=4; student's t-test). **(A)** Level of free IAA in etiolated tomato tissue sections with or without red light exposure. **(B)** Level of ester-linked IAA (determined following a 1 h 1 N NaOH hydrolysis at room temperature and then subtracting the level of free IAA) in etiolated tomato tissue sections with or without red light exposure. No significant change in response to red light was found in any tissue sections. **(C)** Level of amide-linked IAA (determined following a 3 h 7 N NaOH hydrolysis at 100°C and then subtracting the level of free + ester IAA) in etiolated tomato tissue sections with or without red light exposure. No significant change in response to red light was found in any tissue section. **(D)** Tissue sections analyzed in A-C. Top section: meristem, cotyledons and the hook region; H1-H4: 6-mm hypocotyl sections adjacent to each other; H5: the remaining hypocotyl below H4.

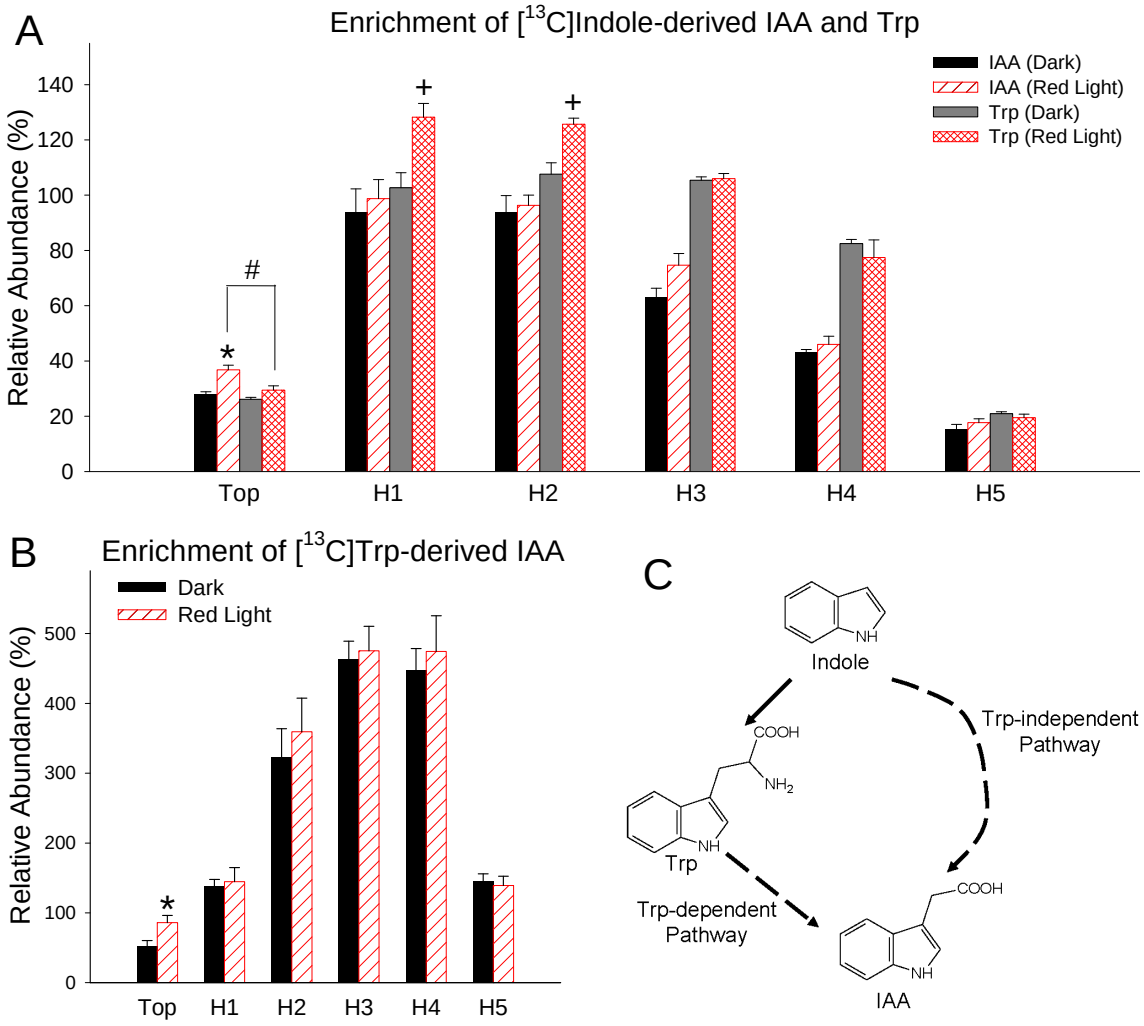

Figure 3-8. Light increased biosynthesis of IAA from labeled precursors in the top section of etiolated tomato seedlings. Tissue sections that show significant change in IAA biosynthesis after 100 µmol m^{-2} red light exposure followed by 1-d darkness are indicated by * ($P<0.05$, n=4; student's t-test). Relative abundance is defined as the ratio of the ion abundance of ([m/z 131]/[m/z 130]·100) corrected for the natural abundance of ^{13}C in the unlabeled IAA. **(A)** Relative enrichment of the unlabeled pools by labeled IAA and Trp synthesized from [^{13}C]indole during a 4-h feeding period. The enrichment of label in Trp in H1 and H2 was significantly increased after red light exposure (indicated by +, $P<0.05$, n=4; student's t-test). In the top section after red light exposure, the enrichment of label in IAA was significantly higher than that of Trp (indicated by #, $P<0.05$, n=4; student's t-test). **(B)** Enrichment of labeled IAA from that synthesized from [^{13}C]Trp during a 4-h feeding period. **(C)** A simplified summary of IAA biosynthetic pathways. A solid arrow represents a single step process; dashed arrows indicate multiple steps; and thus the pathways are shown in abbreviated form.

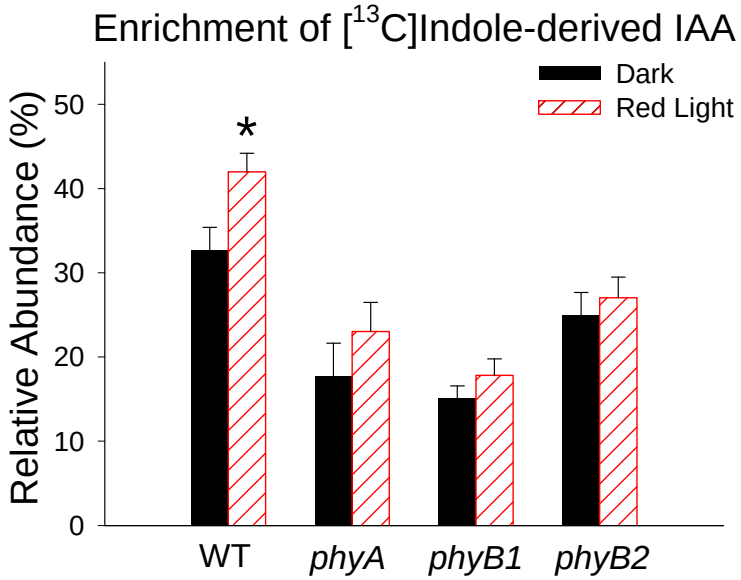

Figure 3-9. Red-light induced increase in IAA biosynthesis in the top section (meristem, cotyledons, and hook) of tomato seedlings was mediated by phytochrome. IAA biosynthesis was significantly increased after 100 µmol m^{-2} red light exposure followed by 1-d darkness in the top section of wild type (indicated by *, $P<0.05$, n=6; student's t-test), but not in *phyA*, *phyB1*, or *phyB2* mutants. In dark-grown seedlings, IAA biosynthesis in *phyA* and *phyB1* was significantly lower than in the wild type ($P<0.01$, n=6; student's t-test); after red light exposure, IAA biosynthesis in all three mutants was significantly lower than in the wild type ($P<0.001$, n=6; student's t-test). Relative abundance is defined as described in Fig. 3-8. All tomato plants were in the cv. MoneyMaker background, and only the top section as described in Fig. 3-7D was used for analysis.

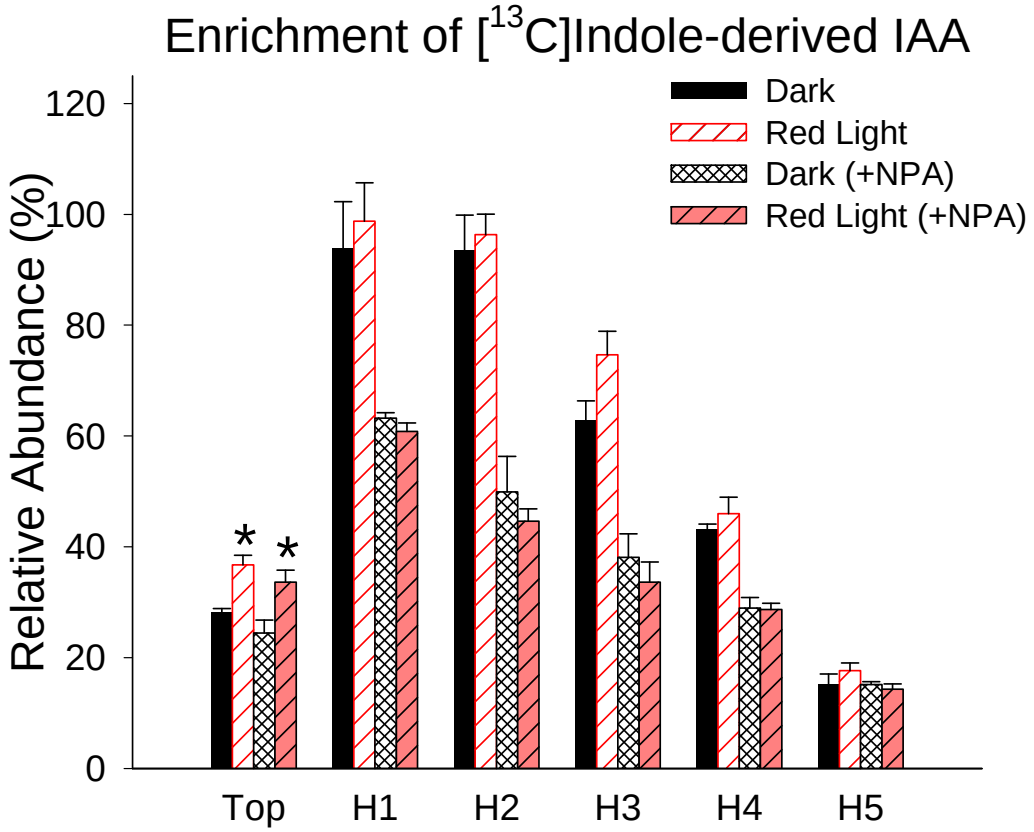

Figure 3-10. The effect of NPA on IAA biosynthesis from labeled precursors. Enrichment of label in IAA from that synthesized from [^{13}C]indole during a 4-h feeding period in the presence and absence of NPA is shown. Relative abundance is defined as described in Fig. 3-8. When 10 µM NPA was supplied along with [^{13}C]indole, the level of labeled IAA in H1, H2, H3, and H4 sections was significantly reduced compared with controls without NPA ($P<0.01$, n=4; student's t-test), as predicted from inhibiting PAT. However, the significant labeling in H5 confirms localized biosynthesis of IAA in this tissue. Red light increased the enrichment of [^{13}C]indole–derived IAA in the top section in the presence and absence of NPA (indicated by *; $P<0.05$, n=4; student's t-test).

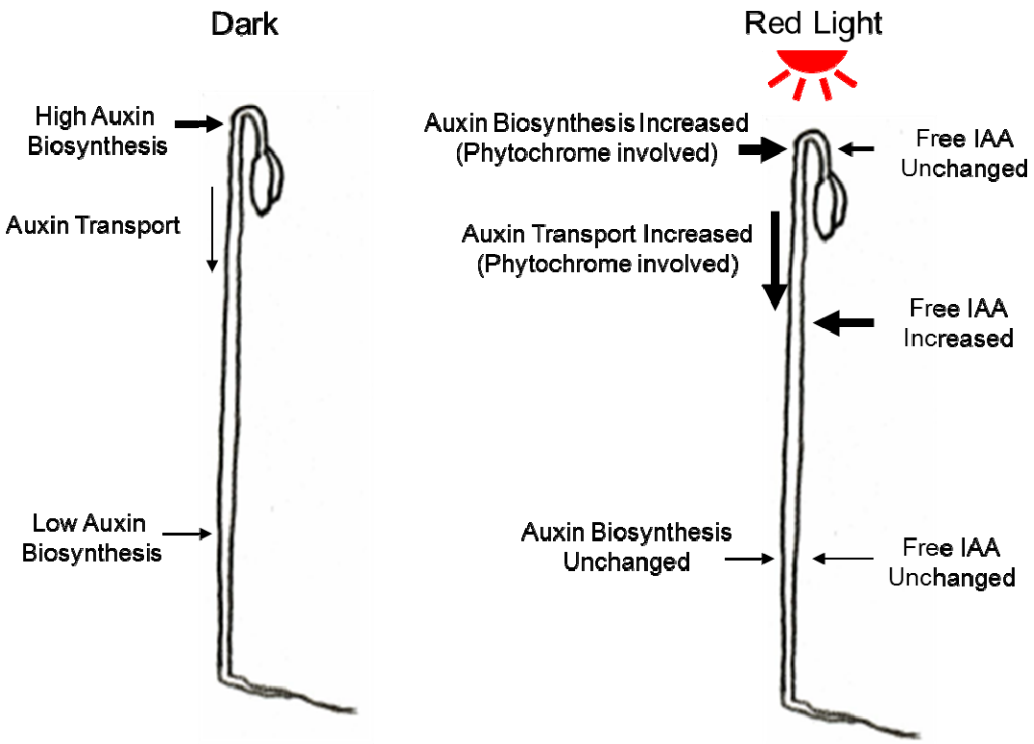

Figure 3-11. A summary of the low fluence red light effect on the transport and biosynthesis of IAA. In dark-grown seedlings, IAA biosynthesis is high at the top of the hypocotyl and is low in the lower part of the hypocotyl. IAA synthesized in the top section moves basipetally in the polar auxin transport steam to supply free IAA to lower hypocotyl regions. When seedlings were exposed to red light, IAA biosynthesis at the top section increased, and IAA transport in the adjacent hypocotyl region also increased to move newly synthesized IAA to the lower hypocotyl regions, which maintained constant free IAA level at the top section and increased free IAA in the lower portion of the hypocotyl.

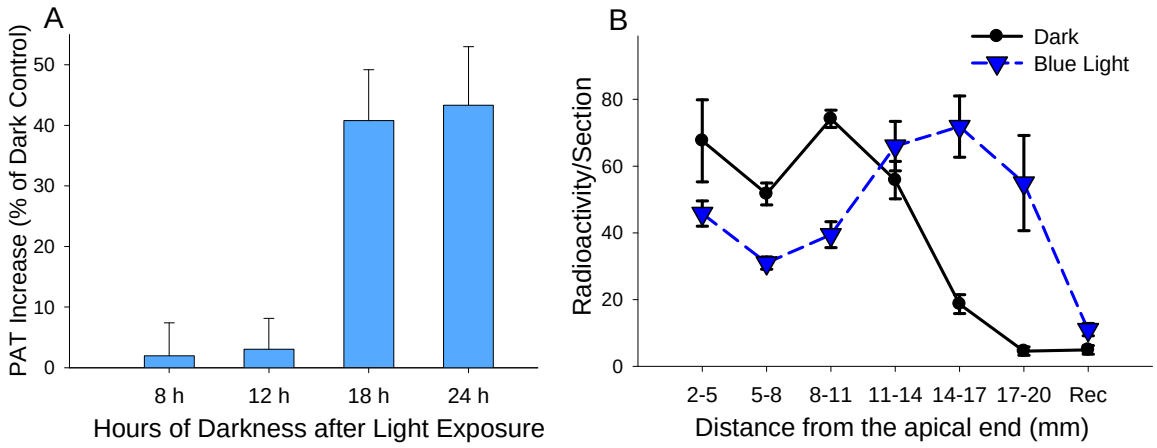

Figure 3-12. **Increase in PAT following blue light exposure. (A)** Greater than 12-hour darkness after blue light exposure was required for the increase in PAT to occur. When the dark period following 3000 µmol m^{-2} blue light exposure equaled or exceeded 18 hours, PAT was significantly increased in etiolated tomato seedlings ($P<0.005$, n=8; student's t-test). **(B)** PAT velocity was increased by blue light exposure. In tomato seedlings treated with 14,400 µmol m^{-2} blue light exposure followed by 1-day darkness, the pulse of [^{3}H]IAA reached the tissue section 17 mm below the IAA source after a 3-hour chase period, while the pulse of [^{3}H]IAA reached the tissue section 14 mm below the IAA source in dark control plants (n=4).

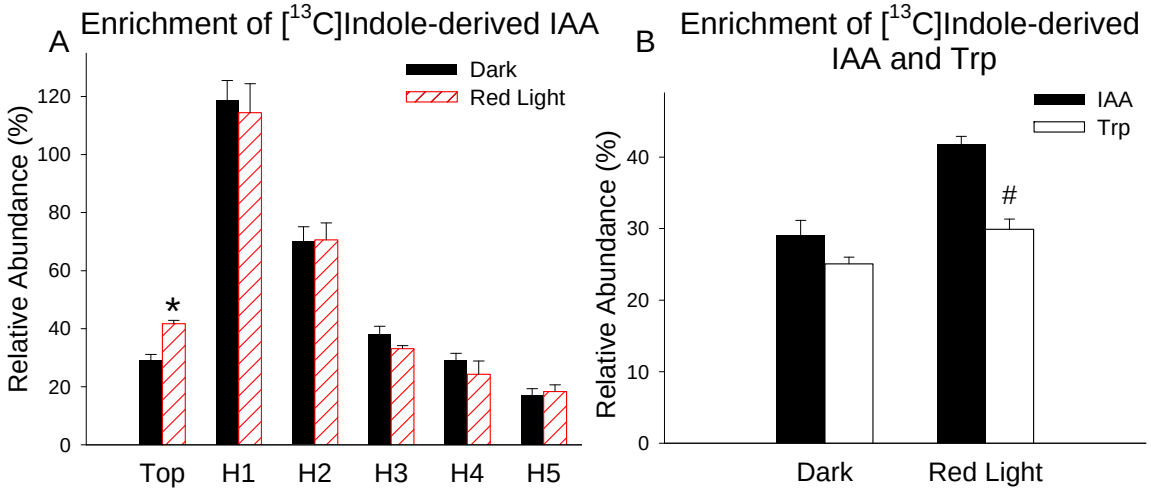

Figure 3-13. Light increased Trp-independent biosynthesis of IAA in the top section of etiolated tomato seedlings. Relative abundance is defined as the ratio of the ion abundance of ([m/z 131]/[m/z 130]·100) corrected for the natural abundance of ^{13}C in the unlabeled IAA or Trp. **(A)** Enrichment of [^{13}C]IAA synthesized from [^{13}C]indole after a 2-h feeding period. The enrichment of [^{13}C]IAA in the top section was significantly increased after 100 µmol m^{-2} red light exposure followed by 1-d darkness (indicated by *, $P<0.05$, n=3; student's t-test). **(B)** Enrichment of [^{13}C]IAA and [^{13}C]Trp synthesized from [^{13}C]indole in the top section after a 2-h feeding period. After 100 µmol m^{-2} red light exposure followed by 1-d darkness, the level of [^{13}C]IAA was significantly higher than that of [^{13}C]Trp (indicated by #, $P<0.05$, n=3).

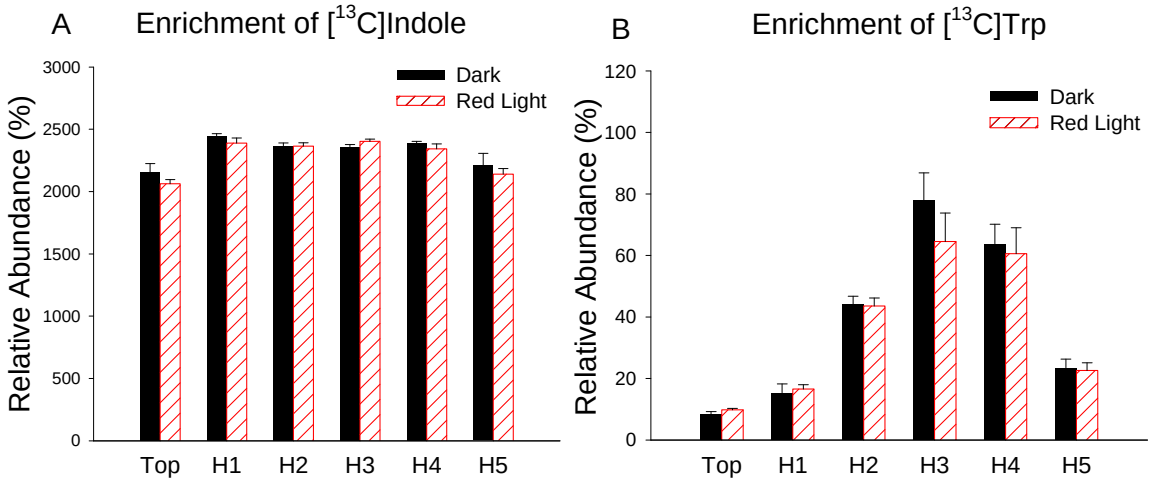

Figure 3-14. Enrichment of [^{13}C] labeled precursors in tissues that synthesize IAA from these precursors. (A) Enrichment of [^{13}C]indole after 4-h [^{13}C]indole labeling. The enrichment in all the tissue sections and treatments was uniform. Relative abundance is defined as the ratio of the ion abundance of ([m/z 131]/[m/z 130]·100) corrected for the natural abundance of ^{13}C in the unlabeled indole. **(B)** Enrichment of [^{13}C]Trp after 4-h [^{13}C]Trp labeling. No difference in enrichment was found between red light treated plants and the dark control plants, but the enrichment was different in different tissue sections. Relative abundance is defined as described in Fig. 3-12B.

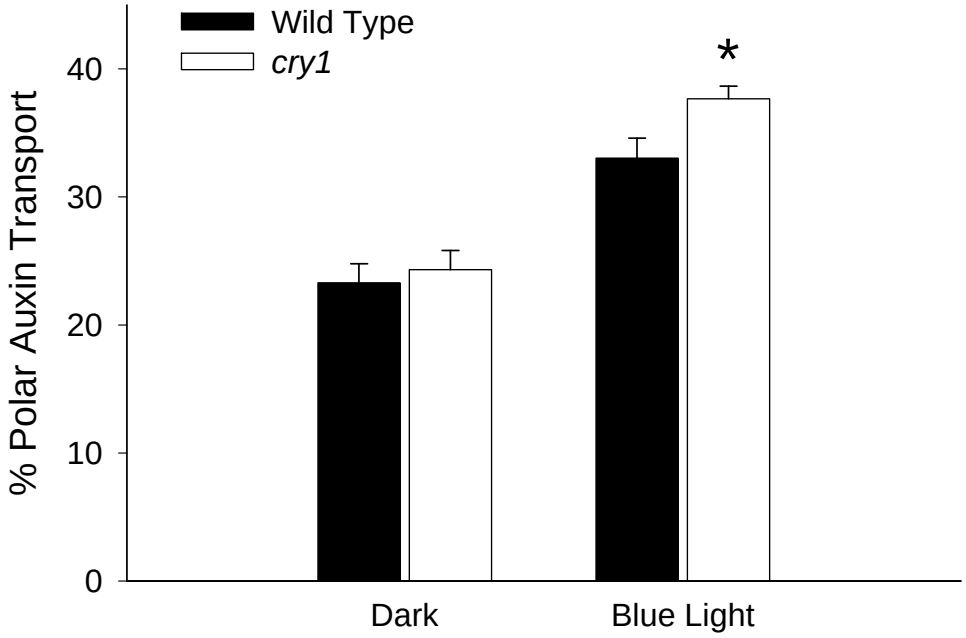

Figure 3-15. Polar auxin transport was significantly increased in *cry1* mutant tomato hypocotyls treated with 3000 µmol m^{-2} blue light exposure followed by 1-day darkness (indicated by *; P<0.05, n=8; student's t-test).

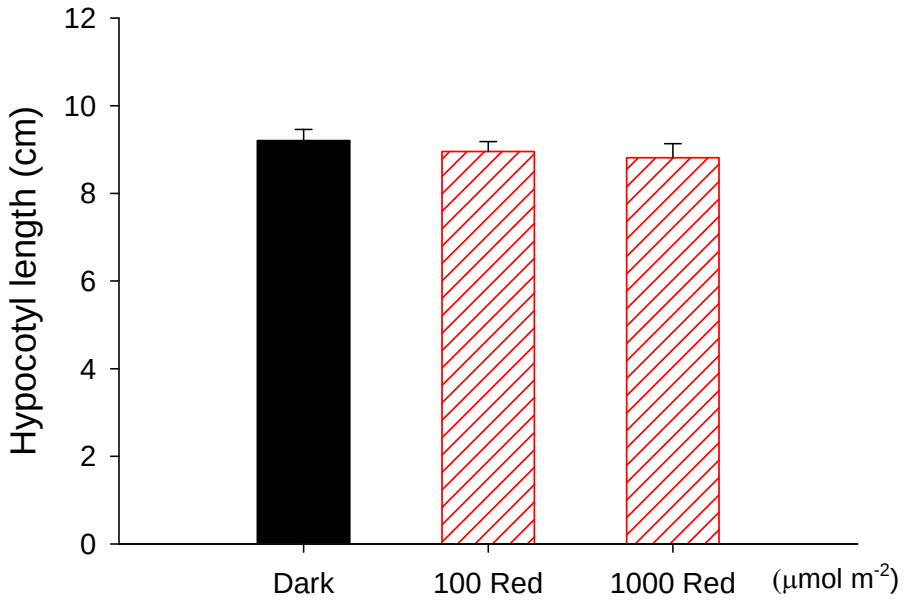

Figure 3-16. Red light exposure followed by 1-day darkness did not alter hypocotyl length. Three-day dark-grown tomato seedlings with similar hypocotyl lengths were irradiated with 100 μmol m^{-2} or 1000 μmol m^{-2} red light and returned to the dark, along with non-irradiated control plants. After one additional day in the dark, seedlings were photographed, and hypocotyl lengths were measured with the NIH image analysis program, ImageJ (http://rsb.info.nih.gov/ij/). No significant change as a result of red light exposure was observed ($P>0.3$, $n=20$; student's t-test).

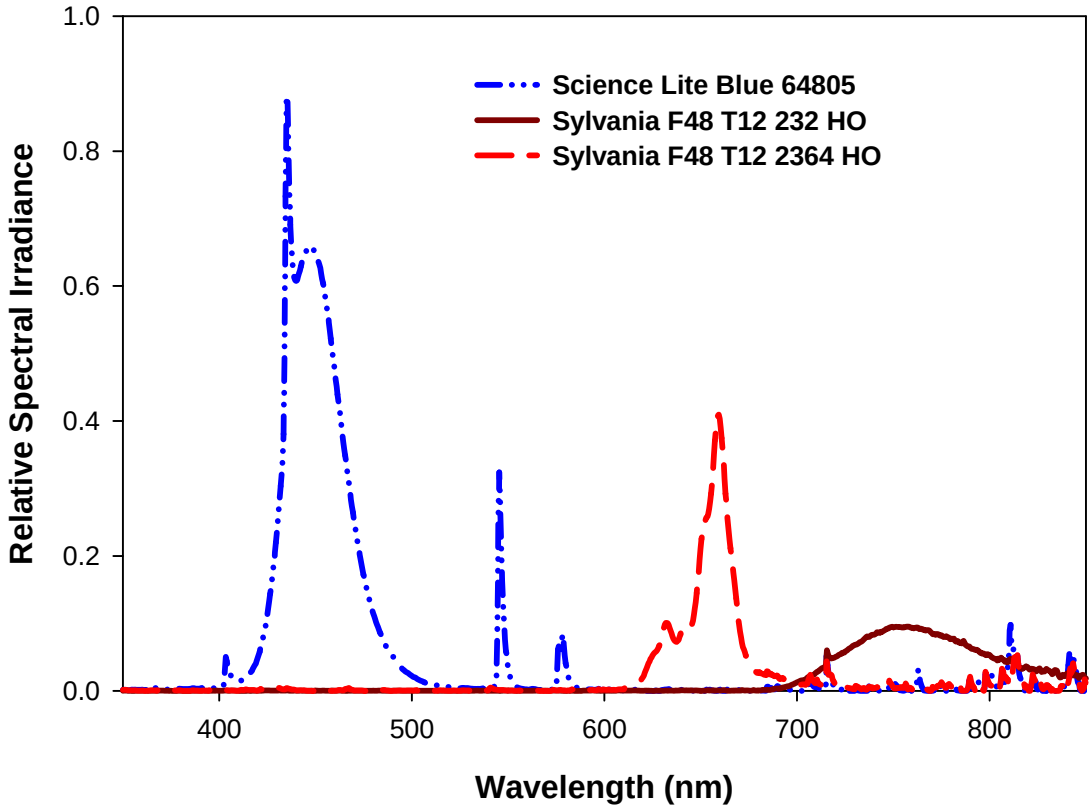

Figure 3-17. Spectral photon distributions of the red, far-red, and blue light sources. Red (R) light was provided by two R fluorescent lamps (Sylvania F48T12/2364/HO) filtered through an Encapsulite R tube guard and a single layer of Roscolux #66 cool blue filter; far red (FR) light was provided by two FR fluorescent lamps (Sylvania F48T12/232/HO) filtered through an Encapsulite FR tube guard and a single layer of Lee #85 deeper blue filter; and blue (B) light was provided by two B fluorescent lamps (Science-LiteTM Blue-64805, Rockville, MA). Spectral photon distributions were measured with an Apogee model SPEC-UV/PAR Spectroradiometer (Apogee Instruments, Logan, UT).

Chapter 4

Transport of Indole-3-Butyric Acid and Indole-3-Acetic Acid in Arabidopsis thaliana Hypocotyls Using Stable Isotope Labeling[2]

Introduction

Indole-3-acetic acid (IAA), the most abundant form of the plant hormone auxin, is critical for plant growth and development. IAA levels are regulated in plants by multiple means, including biosynthesis of IAA through both tryptophan (Trp) dependent and Trp-independent pathways, conjugation of IAA via ester or amide bonds that can be hydrolyzed to release free IAA, polar transport of IAA over long distances, and degradation of IAA (reviewed by Woodward and Bartel, 2005; Seidel *et al*., 2006).

Indole-3-butyric acid (IBA), which has had a long history of use as a synthetic auxin to promote root initiation, has been identified as an endogenous compound in a variety of plants (reviewed by Ludwig-Müller, 2000), including Arabidopsis (*Arabidopsis thaliana*) (Ludwig-Müller *et al*., 1993). IBA can be synthesized from IAA by a microsomal membrane preparation from maize (*Zea mays* L.) seedlings and by an enzyme preparation from Arabidopsis seedlings in the presence of acetyl CoA and ATP (Ludwig-Müller *et al*., 1995a; Ludwig-Müller, 2007), but no mutants defective in this IAA-to-IBA conversion have been identified. Similar to IAA, IBA can be conjugated via both ester and amide bonds (reviewed by Ludwig-Müller, 2000), and the major conjugate of exogenous IBA in Arabidopsis was identified as IBA-glucose (Ludwig-Müller and Epstein, 1993). Endogenous IBA-glucose was also found to be present in Arabidopsis at

[2] This chapter has been published in Plant Physiology, 2012, Vol. 158. All the work presented here was done by me, except that results in Figure 4-7 were generated by Dr. Lana Barkawi.

a high concentration, and this conjugation activity significantly affected plant development and tolerance to environmental stress (Tognetti *et al*., 2010). Importantly, IBA is converted to IAA via β-oxidation in a peroxisome-dependent manner (reviewed by Woodward and Bartel, 2005; Strader and Bartel, 2011), and the IBA-derived IAA has been shown to be important for organ development in Arabidopsis (Strader *et al*., 2010; Strader *et al*., 2011).

Distinct transport streams occur in plants to transport IAA in a polar fashion. In hypocotyls, IAA moves basipetally from the shoot apex towards the roots. The machinery for IAA polar transport includes passive diffusion of protonated IAA, influx proteins (AUX1/LAX) that transport IAA into the cell, and efflux proteins (PIN, ABCB/PGP) that transport IAA out of the cell (reviewed by Peer *et al*., 2011). The transport of IBA over long distances was suggested by an early study showing that IBA promotes growth of *Avena* tissue distant from the application site, and the transport of IBA was found to be lower than IAA (Went and White, 1938). A study using intact peas (*Pisum sativam* L.) led to similar conclusions (Yang and Davies, 1999). The transport of IBA was also directly measured using radioactive IBA tracers. In midrib sections of Cleopatra mandarin (*Citrus reticulate Blanco*), the basipetal transport of IBA was lower than IAA and was only about twice the acropetal transport (Epstein and Sagee, 1992). Using Arabidopsis inflorescence stems, Ludwig-Müller *et al*. (1995b) reported that [^{3}H]IBA was taken up to a greater extent than [^{14}C]IAA and was transported more rapidly. However, the acropetal transport of both [^{3}H]IBA and [^{14}C]IAA was greater than the basipetal transport in their system, suggesting that the measured transport was not polar (Rashotte *et al*., 2003). Also using radioactive IBA and IAA, Rashotte *et al*. (2003) performed a detailed study of auxin transport in different Arabidopsis tissues. They found basipetal transport of IAA but no transport of IBA in inflorescence stems, greater basipetal transport of IBA than IAA in hypocotyls, and both basipetal and acropetal transport of IAA and IBA in roots. Taken together, these reports suggest that similar to IAA, IBA can be transported over long distances in some plant tissues. However, knowing that IBA is converted to IAA (Strader *et al*., 2010) and that detecting

radioactivity alone in plant tissues cannot distinguish [^{3}H]IBA from its metabolites (Fig. 4-1), it is possible that the transported compound was a metabolite of [^{3}H]IBA, such as [^{3}H]IAA. Consistent with this hypothesis, using HPLC to distinguish [^{3}H]IBA from [^{3}H]IAA, Ruzicka *et al*. (2010) found that after [^{3}H]IBA was applied to Arabidopsis root columella cells, most of the [^{3}H]IBA was converted to [^{3}H]IAA when the radioactivity reached the region up to 4 mm above the root tip, which suggests that only IAA derived from IBA can be transported to areas distant from the IBA application site. To better distinguish IBA and IAA derived from IBA, I decided to use gas chromatography (GC)-mass spectrometry (MS) to analyze the transported compounds after application of stable-isotope labeled IBA, where both IAA and IBA from the same plant sample can be measured simultaneously (Sutter and Cohen, 1992; Barkawi *et al*., 2008). In preliminary studies (Fig. 4-7), my colleague Dr. Lana Barkawi found that when [$^{13}C_8$,$^{15}N_1$]IBA was applied to maize coleoptile sections, a significant portion of the stable-labeled compounds detected in the agar receiver block was [$^{13}C_8$,$^{15}N_1$]IAA derived from [$^{13}C_8$,$^{15}N_1$]IBA, and NPA inhibited the movement of [$^{13}C_8$,$^{15}N_1$]IAA into the receiver. She also found that a very small amount of [$^{13}C_8$,$^{15}N_1$]IBA moved basipetally in a polar fashion, but this movement was not inhibited by NPA. These results suggest that by using specific labeled compounds and GC-MS analysis, the movement and metabolic changes of the labeled compounds can be accurately measured.

To evaluate the role of IBA-to-IAA conversion and IBA metabolism in the transport of IBA in Arabidopsis hypocotyls, I applied [$^{13}C_1$]IBA instead of radioactive tracers in my established system for polar auxin transport measurement in Arabidopsis hypocotyls (Liu *et al*., 2011, see also Chapter 3), and I quantified the transported compounds by GC-MS/MS, using [$^{13}C_8$,$^{15}N_1$]IBA and [$^{2}H_4$]IAA as internal standards. As a comparison, I used the same approach and quantified the transport of [$^{13}C_6$]IAA in Arabidopsis hypocotyls. I found that a significant portion of [$^{13}C_6$]IAA taken up by Arabidopsis hypocotyls moved basipetally and the majority of the transported [$^{13}C_6$]IAA remained as free [$^{13}C_6$]IAA. In contrast, a large portion of [$^{13}C_1$]IBA was converted to [$^{13}C_1$]IAA and ester-linked [$^{13}C_1$]IBA during the transport period, and the proportion of

the applied [$^{13}C_1$]IBA transported basipetally was much lower than the proportion of applied [$^{13}C_6$]IAA transported basipetally, suggesting that long distance transport of IBA has a much smaller effect on IBA pools than transport of IAA has on IAA pools.

Materials and Methods

Plant Materials and Growth Conditions

Wild-type Arabidopsis (*Arabidopsis thaliana*) and *ibr 1 ibr 3 ibr 10* seeds were a gift from Dr. Bonnie Bartel (Rice University, TX), and *nakr1* seeds were from Dr. John Ward (University of Minnesota). All experiments were performed with ecotype Columbia. Seeds were imbibed in distilled water for a few hours, surface sterilized in 2.0-mL microcentrifuge tubes with 1 mL 70% ethanol for 2 min followed by 1 mL 30% commercial bleach (to yield 2% sodium hypochlorite) for 5 min, and washed with sterile water five times. Seeds were sown onto MS medium (4.33 g/L Murashige and Skoog salts, MSP01-50LT; Caisson Labs, North Logan, UT), 0.8% (w/v) Phytoblend agar (PTP01-500GM; Caisson Labs), 1.5% (w/v) sucrose (Sigma-Aldrich, Inc., St. Louis, MO), pH 5.7. After seeding, agar plates were wrapped with Parafilm® (Pechiney Plastic Packaging, Menasha, WI) and kept at 4°C for three days, and seedlings were grown vertically on the plates at room temperature (22°C) under 5 μmol m^{-2} (photosynthetically active radiation) continuous cool white fluorescent light for five days before the measurement of auxin transport. These growth conditions were similar to those described in Rashotte *et al.* (2003).

Synthesis of Stable Isotope Labeled IBA

Synthesis of [$^{13}C_8$,$^{15}N_1$]IBA was as described in Chapter 2. The same synthesis and purification methods were used to synthesize [$^{13}C_1$]IBA, using [2-^{13}C]indole (CLM-1863; Cambridge Isotope Laboratories) as the starting material for synthesis. The concentration of the [$^{13}C_1$]IBA product was determined by UV absorbance at 282 nm (ε = 6,060) and confirmed by reverse-isotope dilution selected ion monitoring GC-MS with an unlabeled IBA standard.

Hypocotyl Auxin Transport Assays

The hypocotyl basipetal IAA transport assay was modified from that described in Chapter 3. Six mm of an Arabidopsis hypocotyl section harvested directly below the shoot apex was placed on an agar plate after excision, and an auxin donor block of 1.5% agar (Sigma-Aldrich, Inc.) containing 0.2 M 2-(N-morpholine)-ethanesulfonic acid (MES; Sigma-Aldrich, Inc.) and 10^{-5} M [$^{13}C_6$]IAA (CLM-1896; Cambridge Isotope Laboratories) or 10^{-5} M [$^{13}C_1$]IBA was placed in contact with the apical end of the tissue section, while a receiver agar block containing 0.2 M MES (pH 6.5) was placed in contact with the basal end. Receiver blocks containing 0.2 M MES (pH 6.5) and 10 μM NPA (ChemService, Inc., West Chester, PA) were used as the +NPA control, and a second control was used in which the orientation of the tissue section was inverted (acropetal control). Two strips of polyethylene film (Saran™ Original, S.C. Johnson & Sons, Inc., Racine, WI) were placed between the agar blocks and the support agar on the plates to avoid diffusion of stable-labeled auxin through the support agar and thus prevent an undesirable increase in background. The agar plates were placed vertically with donor blocks down for 5 h in a chamber with high humidity provided by moist filter paper, and each of the hypocotyl sections was then divided into apical and basal halves. When [$^{13}C_6$]IAA was added in the donor blocks, five replicates of basal half hypocotyl sections and receiver blocks were pooled into one microcentrifuge tube, and the corresponding apical half hypocotyl sections were pooled into another microcentrifuge tube. Samples were collected in a similar way when [$^{13}C_1$]IBA was added in the donor blocks, but 20 replicates of hypocotyl sections were pooled into one microcentrifuge tube. The samples were frozen in liquid nitrogen quickly after collection and stored in a -80 °C freezer before quantification of free stable-labeled auxins. When conjugated stable-labeled auxins were quantified, sample sizes were doubled and twice the number of tissue sections were pooled into one sample.

Quantification of Free Stable Isotope Labeled IAA and IBA

The quantification methods were modified from methods described in Chapter 2 and Chapter 3. For samples that were treated with [$^{13}C_6$]IAA in the donor block, 20 µL homogenization buffer (35% 0.2 M imidazole, 65% isopropanol, pH 7) containing 0.2 ng of [$^{2}H_4$]IAA (a gift from Prof. R.S. Bandurski; Magnus *et al.*, 1980) and 0.2 ng of [$^{13}C_8$,$^{15}N_1$]IBA was added; for samples that were treated with [$^{13}C_1$]IBA, 40 µL homogenization buffer containing 0.2 ng of [$^{2}H_4$]IAA and 0.2 ng of [$^{13}C_8$,$^{15}N_1$]IBA was added. Tissues were homogenized using a Mixer Mill (MM 300; Qiagen, Valencia, CA) with tungsten carbide beads (3 mm beads for 1.5-mL tubes, and 2.3 mm beads for 0.5-mL tubes; Craig Ball Sales, Seaford, DE). After 1 hr on ice, the homogenate was diluted ten times by adding water and then centrifuged at 10,000 g for 10 min. The supernatant was passed through a 200 µL TopTips (TT2EMT.96; Glygen Corp) solid phase extraction (SPE) column containing 5 mg NH_2 anion exchange resin (12213020, Varian) and then washed by a series of solvents and solutions essentially the same as that described in Chapter 2. To reduce the loss of IBA during extraction, IAA and IBA were both eluted from the NH_2 SPE tip by 3 x 80 µL 0.25% phosphoric acid (A242; Fisher Chemicals), and the eluate was partitioned against 100 µL ethyl acetate (E195-4; Fisher Chemicals). The ethyl acetate layer was collected and transferred to a 250-µL glass insert (CTI-9425; ChromTech), and the sample was methylated in the insert by adding ethereal diazomethane in the presence of 10% methanol (34860; Sigma-Aldrich) and waiting 5 min, and then the solvents were evaporated under a stream of N_2 gas and the sample was redissolved in 15 µL ethyl acetate. The methylated IAA and IBA were analyzed using gas chromatography-selected reaction monitoring-mass spectrometry (GC-SRM-MS) on a Thermo Trace GC Ultra coupled to a TSQ Vantage triple quadrupole MS system (Thermo Scientific, San Jose, CA) under conditions described in Chapter 2 and Chapter 3. The quinolinium ions produced from the molecular ions of IAA (Fig. 4-2B) (m/z 130 from m/z 189, m/z 131 from m/z 190, m/z 134 from m/z 193, and m/z 136 from m/z 195) were selected by the third quadrupole and monitored for the first 10.5 min of the chromatographic run. The quinolinium ions produced from the molecular ions of IBA

(Fig. 4-2C) (m/z 130 from m/z 217, m/z 131 from m/z 218, m/z 136 from m/z 223, and m/z 139 from m/z 226) were selected and monitored starting at 10.5 min until the end of the run. Levels of [$^{13}C_6$]IAA or [$^{13}C_1$]IAA derived from [$^{13}C_1$]IBA were quantified by isotope dilution analysis based on the [$^{2}H_4$]IAA internal standard; levels of [$^{13}C_1$]IBA were quantified by isotope dilution analysis based on the [$^{13}C_8$,$^{15}N_1$]IBA internal standard. The natural abundance of [^{13}C] was determined using unlabeled chemical standards (Sigma) and is corrected for in the calculations and the data reported.

Quantification of [$^{13}C_6$] IAA and [$^{13}C_1$]IBA in Donor Agar Blocks

Donor agar blocks containing 10^{-5} M [$^{13}C_6$]IAA and 10^{-5} M [$^{13}C_1$]IBA were placed on top of the apical end of Arabidopsis hypocotyl sections as described above. The agar blocks were collected into microcentrifuge tubes after 0-h and 5-h transport periods, and the tubes were weighed and quickly frozen in liquid N_2. The agar blocks were homogenized using the Mixer Mill as described above, after adding 400 µL of methanol containing 10 µL each of 10^{-5} M IAA and 10^{-5} M [$^{13}C_8$,$^{15}N_1$]IBA as the internal standards. After 1-h incubation on ice, 100 µL of supernatant from the homogenate was transferred into a 2-ml glass vial and was methylated by ethereal diazomethane. The methylated samples were dried under a stream of N_2 gas, re-suspended in 20 µL of ethyl acetate, and analyzed by GC-MS. The amounts of [$^{13}C_6$]IAA and [$^{13}C_1$]IBA present per mg of the donor agar block were calculated based on the internal standards and the weight of the agar block. Finally, the percent of [$^{13}C_6$]IAA and [$^{13}C_1$]IBA remaining in the 5-h samples (divided by the initial 0-h time point) was determined.

Quantification of Ester-linked and Amide-linked [$^{13}C_6$] IAA and [$^{13}C_1$]IBA

For samples that were treated with [$^{13}C_6$]IAA in the donor block, 40 µL homogenization buffer containing 0.6 ng of [$^{2}H_4$]IAA and 0.6 ng of [$^{13}C_8$,$^{15}N_1$]IBA was added. After homogenization and 1 hr on ice as described above, 20 µL of the homogenate was used for quantification of free [$^{13}C_6$]IAA in the same way as that described above. Of the remainder of the homogenate, 15 µL was hydrolyzed in 1 N

NaOH (1 hr, room temperature) for measurement of free plus ester-linked [$^{13}C_6$]IAA, and 10 μL was hydrolyzed in 7 N NaOH (3 h, 100°C under N_2) for measurement of total [$^{13}C_6$]IAA (free plus ester-linked and amide-linked [$^{13}C_6$]IAA). Extraction and methylation of free IAA plus that released from the conjugates were the same as described in Chapter 3, and the method for GC-SRM-MS analysis was the same as described above. Levels of free [$^{13}C_6$]IAA, free plus ester-linked [$^{13}C_6$]IAA, and total [$^{13}C_6$]IAA were quantified by isotope dilution analysis based on the [$^{2}H_4$]IAA internal standard, as described above. The results were displayed as pg IAA eq. since the chemical structures of every conjugate formed are not known.

For samples that were treated with [$^{13}C_1$]IBA in the donor block, 80 μL homogenization buffer containing 0.6 ng of [$^{2}H_4$]IAA and 0.6 ng of [$^{13}C_8$,$^{15}N_1$]IBA was added, and the homogenate was divided into three parts: 40 μL was used for quantitation of free [$^{13}C_1$]IBA and [$^{13}C_1$]IAA derived from the [$^{13}C_1$]IBA; 30 μL was used for measurement of free plus ester-linked [$^{13}C_1$]IBA; and 10 μL was used for measurement of total [$^{13}C_1$]IBA. Hydrolysis, extraction, methylation, GC-SRM-MS analysis, and quantification of free and conjugated [$^{13}C_1$]IBA were the same as described above.

Results

Absolute Quantification of Auxin Transport using Stable Isotope Labeled Tracers

I previously established a sensitive [^{3}H]IAA transport assay with low background noise to measure the transport of IAA in Arabidopsis hypocotyls (Liu *et al.*, 2011, see also Chapter 3). To achieve better compound identification, isotope analysis, and the quantification of transported IAA and IBA, I modified the assay and changed from a radioactive auxin tracer to a stable isotope system using either [$^{13}C_6$]IAA or [$^{13}C_1$]IBA (Fig. 4-2A). In order to recover a sufficient quantity of transported [$^{13}C_6$]IAA and [$^{13}C_1$]IBA for GC-MS/MS analysis, I applied stable-labeled auxin in the donor agar block at 10^{-5} M, a concentration that was reported to yield maximal basipetal auxin transport (Rashotte *et al.*, 2003). After a five-hour transport period, auxins were determined in pools of lower hypocotyl sections and receivers. Five plants were needed for facile

detection of [$^{13}C_6$]IAA, while 20 plants were needed for detection of [$^{13}C_1$]IBA and [$^{13}C_1$]IAA derived from [$^{13}C_1$]IBA. As shown in Figure 4-2B, when [$^{13}C_6$]IAA was added in the donor agar block, unlabeled endogenous IAA, [$^{13}C_6$]IAA tracer, and the [$^{2}H_4$]IAA internal standard were detected separately, thus the [$^{13}C_6$]IAA tracer could be distinguished from endogenous IAA, and the amount of [$^{13}C_6$]IAA could be quantified based on the [$^{2}H_4$]IAA internal standard. Potential [$^{13}C_6$]IBA derived from [$^{13}C_6$]IAA was also monitored but was not detected, which may be due to a low rate of conversion of [$^{13}C_6$]IBA that may require more tissue for detection. Similarly, when [$^{13}C_1$]IBA was added in the donor agar block (Fig. 4-2C), both IAA and IBA were monitored, and their retention times on GC were about 1 min apart. Therefore, unlabeled endogenous IBA and IAA, [$^{13}C_1$]IBA tracer and its metabolic product [$^{13}C_1$]IAA, and [$^{13}C_8$,$^{15}N_1$]IBA and [$^{2}H_4$]IAA internal standards were all detected separately, and the amount of [$^{13}C_1$]IBA and [$^{13}C_1$]IAA could be quantified based on the internal standards. Clearly, using stable isotope labeled auxins and GC-MS/MS, I are able to quantify the absolute amount of both endogenous and applied IAA and IBA transported.

Transport of Free [$^{13}C_6$]IAA and [$^{13}C_1$]IBA in Arabidopsis Hypocotyls

When [$^{13}C_6$]IAA was supplied in donor agar blocks and incubated with Arabidopsis hypocotyl sections for 5 h, 42 pg [$^{13}C_6$]IAA was detected per upper section (Fig. 4-3A), and 17 pg [$^{13}C_6$]IAA was detected per lower section and receiver (Fig. 4-3B). Therefore, about 29%[3] of the [$^{13}C_6$]IAA in the hypocotyl section was transported basipetally to the lower section and receiver (Fig 4-3C). When 10 μM of the auxin transport inhibitor N-1-naphthylphthalamic acid (NPA) was added in the receiver block, the level of [$^{13}C_6$]IAA per lower section and receiver was reduced to 1 pg without a concomitant reduction in the level of [$^{13}C_6$]IAA per upper section (Fig. 4-3,A and B).

[3] The percent transport is defined for [$^{13}C_6$]IAA as the amount of free auxin in the lower section and receiver (17 pg, Fig. 3B) divided by the sum of free auxin in upper + lower sections and the receiver (59 pg) and, similarly, for [$^{13}C_1$]IBA, 0.26 pg in the lower section and receiver divided by 42.26 pg in upper + lower sections and the receiver.

This result suggests that NPA diffused into the hypocotyl tissue from the receiver and thus dramatically inhibited the polar transport of [$^{13}C_6$]IAA into the lower hypocotyl section without resulting in an over-accumulation of [$^{13}C_6$]IAA in the upper hypocotyl section. In the acropetal control, each upper section contained 85 pg [$^{13}C_6$]IAA, and each lower section and receiver contained only 1 pg [$^{13}C_6$]IAA, suggesting a very low background level of diffusion in this transport assay.

In a parallel experiment, [$^{13}C_1$]IBA was supplied in donor agar blocks to quantify the transport of IBA. After a five-hour transport period, 42 pg [$^{13}C_1$]IBA was detected per upper section (Fig. 4-3D), which was similar to the amount of [$^{13}C_6$]IAA transported (described above). However, only 0.26 pg [$^{13}C_1$]IBA was found per lower section and receiver (Fig. 4-3E), and therefore, only 0.62%[1] of the [$^{13}C_1$]IBA in the hypocotyl section was transported basipetally to the lower section and receiver (Fig, 4-3F). Importantly, [$^{13}C_1$]IAA derived from [$^{13}C_1$]IBA was also detected in both sections, and 0.2 pg of [$^{13}C_1$]IAA was found per upper section while 0.34 pg [$^{13}C_1$]IAA was found per lower section and receiver (Fig. 4-3, G and H). Interestingly, adding NPA in the receiver did not change the level of [$^{13}C_1$]IBA in either section (Fig. 4-3, D and E), but NPA reduced the level of [$^{13}C_1$]IAA per lower section and receiver to 0.03 pg (Fig. 4-3H), suggesting that NPA inhibits the transport of [$^{13}C_1$]IAA derived from [$^{13}C_1$]IBA, but not the transport of [$^{13}C_1$]IBA itself. In the acropetal control, [$^{13}C_1$]IBA and [$^{13}C_1$]IAA were almost undetectable in the lower section and receiver, and the percent transport of [$^{13}C_1$]IBA was significantly lower than that found with the other two experimental groups ($p<0.01$; Fig. 4-3F). These results suggest that the transport of free IBA is much lower than the transport of free IAA in Arabidopsis hypocotyls (less than 1% compared to 29%) and shows that IAA synthesized from IBA also enters the IAA transport stream.

Because the transport of [$^{13}C_1$]IBA was very low and was not inhibited by NPA, it is possible that IBA was only transported in the phloem. To test this hypothesis, I quantified the transport of [$^{13}C_6$]IAA and [$^{13}C_1$]IBA in the *nakr1* mutant which was reported to be defective in phloem function but displays normal seedling growth (Tian *et al.*, 2010). As shown in Figure 4-4, the transport of [$^{13}C_6$]IAA and [$^{13}C_1$]IBA in the *nakr1*

mutant was the same as that in wild type plants, indicating that the aspect of phloem transport blocked in *nakr1* plants does not play an essential role in the transport of IAA or IBA.

Transport of Free [$^{13}C_6$]IAA and [$^{13}C_1$]IBA in *ibr1 ibr3 ibr10* Arabidopsis Hypocotyls

Because IAA and IBA can be converted to IBA and IBA can be converted back to IAA, each via specific metabolic pathways in vivo (Fig. 4-1), it is possible that the transport of IBA may be dependent on these interconversions. To test this possibility, I quantified the transport of [$^{13}C_6$]IAA and [$^{13}C_1$]IBA in the *ibr1 ibr3 ibr10* triple mutant, in which the capacity for the conversion of IBA to IAA is dramatically reduced (Strader *et al.*, 2010). As shown in Figure 4-5H, in the lower section and receiver, the level of [$^{13}C_1$]IAA derived from [$^{13}C_1$]IBA was significantly lower in *ibr1 ibr3 ibr10* than in the wild type ($p<0.002$), but there was no significant difference in the level of [$^{13}C_1$]IBA transported (Fig. 4-5E). Therefore, the transport of [$^{13}C_1$]IBA was not affected in the *ibr1 ibr3 ibr10* mutant (Fig. 4-5F), suggesting that the measured transport of [$^{13}C_1$]IBA in the wild type does not depend on the conversion between IBA and IAA. On the other hand, the transport of [$^{13}C_6$]IAA was significantly reduced in *ibr1 ibr3 ibr10* ($p<0.05$, Fig. 4-5C), and the amount of [$^{13}C_6$]IAA taken up by *ibr1 ibr3 ibr10* plants (sum of values in Fig. 4-5, A and B) was significantly lower than the wild type ($p<0.002$, n=3, student's *t* test), suggesting that disruption of IBR1, IBR3, and IBR10 affects aspects of IAA distribution.

Transport and Metabolism of [$^{13}C_6$]IAA and [$^{13}C_1$]IBA in Arabidopsis Hypocotyls

Free IAA and IBA can be released from their conjugated forms via chemical hydrolysis: weak base hydrolysis breaks the ester linkage (Baldi *et al.*, 1989), while strong base hydrolysis breaks both ester and amide linkages (Bialek and Cohen, 1989). Using different strengths of base hydrolysis, I quantified the level of [$^{13}C_6$]IAA and [$^{13}C_1$]IBA released from their ester- and amide-linked conjugates, in both upper section

and lower section plus receiver, after a five-hour transport period. When [$^{13}C_6$]IAA was supplied in the donor agar block, each upper section of the basipetal group contained 35 pg [$^{13}C_6$]IAA, 17 pg IAA equivalents (eq.) ester-linked [$^{13}C_6$]IAA, and 37 pg IAA eq. amide-linked [$^{13}C_6$]IAA (Fig. 4-6A); each lower section and receiver contained 22 pg [$^{13}C_6$]IAA, and a very small amount of conjugated [$^{13}C_6$]IAA (Fig. 4-6B). Interestingly, when NPA was added in the receiver, the level of [$^{13}C_6$]IAA and ester-linked [$^{13}C_6$]IAA was not changed per upper section, but the amount of amide-linked [$^{13}C_6$]IAA was significantly increased ($p<0.05$, Fig. 4-6A) and reached 208 pg/plant. Similarly, in the upper section from the acropetal control, the level of amide-linked [$^{13}C_6$]IAA was significantly higher than in the basipetal group. On the other hand, a very small amount of free and conjugated [$^{13}C_6$]IAA was detected in the lower section and receiver of the NPA and acropetal groups (Fig. 4-6B). These results confirm that amide-linked IAA is the major conjugate derived from exogenous IAA (reviewed in Slovin *et al.*, 1999; see also Staswick *et al.*, 2005), and show that free IAA is the primary form of transported IAA.

When [$^{13}C_1$]IBA was supplied in the donor agar block, each upper section of the basipetal group contained 25 pg [$^{13}C_1$]IBA, 458 pg IBA eq. ester-linked [$^{13}C_1$]IBA, 27 pg IBA eq. amide-linked [$^{13}C_1$]IBA, and 0.17 pg [$^{13}C_1$]IAA (Fig. 4-6C). A similar pattern of these components was also found in the NPA group (Fig. 4-6C). In each lower section and receiver of the basipetal group, there was 0.16 pg [$^{13}C_1$]IBA, 0.52 pg ester-linked [$^{13}C_1$]IBA, 0.09 pg amide-linked [$^{13}C_1$]IBA, and 0.31 pg [$^{13}C_1$]IAA (Fig. 4-6D); adding NPA in the receiver did not change levels of free and conjugated [$^{13}C_1$]IBA significantly but reduced the level of [$^{13}C_1$]IAA to 0.01 pg/plant (Fig. 4-6D). These results suggest that a large portion of exogenous IBA is converted to ester-linked IBA, and an extremely small portion of free and/or ester-linked IBA is transported to the lower hypocotyl sections.

Discussion

The aim of this study was to evaluate the transport of IBA and IAA in Arabidopsis hypocotyls, using methods that provide accurate compound identification and absolute quantification. To my knowledge, this is the first time that the polar transport of auxins and their metabolites has been measured using the stable-isotope labeling approach. Rashotte *et al*. (2003) found that when various concentrations of [^{3}H]IAA or [^{3}H]IBA were applied in an agar donor block, both [^{3}H]IAA and [^{3}H]IBA move basipetally in Arabidopsis hypocotyls, and the transport of [^{3}H]IBA was higher than the transport of [^{3}H]IAA. They argued that the conversion from [^{3}H]IBA to [^{3}H]IAA did not contribute to the measured transport of [^{3}H]IBA, because no transport of [^{3}H]IBA was detected in the Arabidopsis inflorescence axis where basipetal transport of [^{3}H]IAA occurred, and because no [^{3}H]IAA was detected using thin layer chromatography (TLC) after incubating Arabidopsis seedlings with [^{3}H]IBA. However, the metabolism of [^{3}H]IBA in the inflorescence might be different from that in hypocotyls, and detection of radioactivity on a TLC plate does not provide a sensitive and precise measurement of [^{3}H]IBA and its metabolites. Indeed, in a more recent study using GC-MS for IAA and IBA quantification, Strader *et al*. (2010) found a significant amount of stable-labeled IAA derived from stable-labeled IBA in Arabidopsis seedlings. Using HPLC to separate [^{3}H]IAA from [^{3}H]IBA, Ruzicka *et al*. (2010) showed that although [^{3}H]IBA was transported out of the root apex in an ABCG37 dependent manner, most of the [^{3}H]IBA was converted to [^{3}H]IAA in root tissue above the apex, suggesting that IAA, but not IBA, is the compound responsible for long distance transport of radioactivity derived from [^{3}H]IBA. However, detection of radioactivity after HPLC does not provide quantitative information about the transported compounds, so it is difficult to evaluate the contribution of the transport activity. Also, HPLC retention time alone does not provide precise compound identification. Therefore, I decided to replace the radioactive tracers with stable isotope labeled IBA and IAA, which can be distinguished from the endogenous compounds by GC-MS/MS based on their mass differences (Fig. 4-2), and I

can quantify the amount of transported compounds using differently labeled internal standards and the isotope dilution technique.

Rashotte *et al*. (2003) found that when concentrations of IAA and IBA in the donor agar block were increased from 10^{-7} M to 2 x 10^{-5} M, the transport of [^{3}H]IAA and [^{3}H]IBA in Arabidopsis hypocotyls was also increased and saturated at high concentrations. Because sufficient amounts of transported [$^{13}C_6$]IAA and [$^{13}C_1$]IBA are required for GC-MS analysis but high concentrations of auxin can significantly induce auxin conjugation activities (Sudi, 1966; Li *et al*., 1999), I applied 10^{-5} M [$^{13}C_6$]IAA or [$^{13}C_1$]IBA in the donor agar block, a concentration that does not seem to increase auxin conjugation dramatically during a short period of treatment (Sudi, 1966; Venis, 1972) and also yielded detectable amounts of labeled auxins from pooled hypocotyl sections (the amount of transported [$^{13}C_1$]IBA from 20 hypocotyl sections was just above the detection limit). Using Arabidopsis seedlings grown under conditions similar to those used by Rashotte *et al*. (2003), I found that a significant portion (29%) of the free [$^{13}C_6$]IAA in the hypocotyl sections was transported basipetally, and this basipetal transport was dramatically inhibited by NPA (Fig. 4-3, A, B and C). This is consistent with results from assays using [^{3}H]IAA tracers previously described (Liu *et al*., 2011, see also Chapter 3), and it confirms that transport of IAA plays an important role in regulating levels of free IAA. In contrast, very little (0.26 pg/plant, less than 1%) free [$^{13}C_1$]IBA was transported, and the amount of transported [$^{13}C_1$]IBA was dramatically lower than the [$^{13}C_6$]IAA (Fig. 4-3, D, E and F). This result does not agree with the previous findings where [^{3}H]IBA was used (Rashotte *et al*., 2003), suggesting that a large portion of the transported radioactivity in hypocotyls was not [^{3}H]IBA. Interestingly, similar to Rashotte *et al*. (2003), the transport of [$^{13}C_1$]IBA was not inhibited by NPA (Fig. 4-3E). Because NPA is an auxin-efflux inhibitor (Thomson *et al*., 1973; Goldsmith, 1982), this result suggests that IBA is not transported by the same efflux proteins that transport IAA. This conclusion is consistent with Ruzicka *et al*. (2010), which illustrated that the heterologously expressed IAA efflux proteins (PINs and ABCBs) did not use IBA as their substrates, and the heterologously expressed ABCG37 protein displayed substrate

specificity for IBA but not IAA. On the other hand, Rashotte *et al*. (2003) showed that the transport of [^{3}H]IBA was not reduced in Arabidopsis *aux1* mutant roots, and both Yang *et* al. (2006) and Swarup *et al*. (2008) showed that 20 μM IBA did not competitively inhibit the uptake of 0.1 μM [^{3}H]IAA by heterologously expressed AUX1 protein, suggesting that the transport influx protein AUX1 recognizes only IAA but not IBA. Swarup *et al*. (2008) also showed that 20 μM IBA reduced the uptake of 0.1 μM [^{3}H]IAA by heterologously expressed LAX3 protein, but not as effectively as 20 μM IAA, suggesting that IBA may be a substrate for IAA influx protein LAX3, with a lower affinity than IAA. However, considering that the endogenous level of free IBA is dramatically lower than free IAA (Tognetti *et al*., 2010), it is not likely that IBA can be transported by LAX3 under physiological conditions. Taken together, my results and previous reports support the conclusion that the mechanisms of IAA and IBA transport are partially, if not completely, distinct.

It is difficult to distinguish the low percentage of [$^{13}C_1$]IBA transported from diffusion or phloem transport. Even though I found that [$^{13}C_1$]IBA transport was not altered in the *nakr1* mutant (Fig. 4-4), which is defective in some aspects of long-distance phloem transport (Tian *et al*., 2010), this does not exclude the possibility that [$^{13}C_1$]IBA transport might be reduced in mutants that have defects in other aspects of phloem transport. The Arabidopsis *suc2* mutant, defective in loading sucrose into the phloem, could be a candidate for such a test, however the mutant seedlings are severely dwarfed (Srivastava *et al*., 2008; Gottwald *et al*., 2000) and are thus not easily applicable for use in the hypocotyl transport assay (Dr. John Ward, personal communication). Nevertheless, it would be useful to measure IBA transport in mutants that are defective in long-distance phloem transport if the seedlings are either not dramatically stunted or alternative methods can be devised. Such studies could potentially reveal aspects of the mechanism of IBA transport. The low rates of movement I measured, however, are also consistent with a primarily diffusion-mediated mechanism, and the passive diffusion of protonated IBA can be greater than protonated IAA due to the higher hydrophobicity of IBA. On the

other hand, basipetal transport of over 60%[4] of the [$^{13}C_1$]IAA derived from [$^{13}C_1$]IBA was detected in the hypocotyl tissues (Fig. 4-3, G, H and I), and this transport was significantly inhibited by NPA, suggesting that [$^{13}C_1$]IAA was synthesized from [$^{13}C_1$]IBA before it transported basipetally in the hypocotyl, and thus the IBA-to-IAA conversion could partially contribute to the transported radioactivity found by Rashotte *et al*. (2003).

There is an important distinction between the use of radiolabeled auxin measurement of transport and that using stable isotopes and GC-MS. With both procedures the amount of IAA in the upper hypocotyl section is likely overestimated due to labeled IAA adhering to the plant surfaces and, thus, the percent transported IAA is potentially underestimated. With stable labels, however, catabolism of IAA or IBA results in compounds, such as oxidized IAA and its conjugates (Ostin *et al*., 1998; Kai *et al*., 2007), not detected by the analytical methods used here. Thus, oxidative degradation at the cut hypocotyl surface (Sanchez-Bravo *et al*., 1988) could result in an underestimate of total transport only when using the radioisotope method (since with [^{3}H]IAA its catabolites would still be radioactive, localized to the top section, and would contribute to the calculated IAA content). Similarly, catabolism of IAA in the lower section following transport would result in an underestimate of transport by the stable isotope method. The products of IAA and IBA catabolism could potentially be identified by using a modified extraction and derivatization method prior to GC-MS analysis, or by using liquid chromatography (LC)-MS based methods (Ostin *et al*., 1998; Tam *et al*., 2000; Kowalczyk and Sandberg, 2001; Kai *et al*., 2007), but the stable labeled standards for each corresponding compound would need to be synthesized for quantification. Nevertheless, I found that the percent transport of [$^{13}C_1$]IBA-derived [$^{13}C_1$]IAA (Fig. 4-3I) was twice as much as the percent transport of [$^{13}C_6$]IAA (Fig. 4-3C). However,

[4] The percent transport is defined for [$^{13}C_1$]IAA as the amount of [$^{13}C_1$]IAA in the lower section and receiver (0.34 pg, Fig. 3H) divided by the sum of [$^{13}C_1$]IAA in upper + lower sections and the receiver (0.54 pg).

because of these adhesion and metabolic concerns I cannot be certain that the IBA-derived IAA is preferentially used for polar transport.

Although I could not detect [$^{13}C_6$]IBA derived from [$^{13}C_6$]IAA from five Arabidopsis hypocotyl sections, IAA was previously found to be converted to IBA by enzyme preparations from Arabidopsis seedlings (Ludwig-Müller, 2007). Therefore, the transported [$^{13}C_1$]IBA measured in my assay might also contain [$^{13}C_1$]IBA derived from transported [$^{13}C_1$]IAA. To gain a clearer view of the transport of IBA itself, I analyzed IBA transport in mutants that are defective in the conversions between IAA and IBA (Fig. 4-1). Because no mutants have been demonstrated to show defects in IAA-to-IBA conversion *in vivo*, I only analyzed [$^{13}C_1$]IBA transport in *ibr1 ibr3 ibr10* triple mutant Arabidopsis hypocotyls defective in IBA-to-IAA conversion (Strader *et al*., 2010; Fig. 4-5, G, H and I). I found that [$^{13}C_1$]IBA transport was not altered in the *ibr1 ibr3 ibr10* mutant (Fig. 4-5, D, E and F), suggesting that the small amount of transport of IBA does not depend on the inter-conversion between IBA and IAA. Interestingly, I found that the transport of [$^{13}C_6$]IAA in the *ibr1 ibr3 ibr10* mutant was significantly lower than the wild type (Fig. 4-5C). Although I do not know how the IBR proteins might play a role in the transport of IAA, this result could partially explain why the *ibr1 ibr3 ibr10* mutant does not respond to exogenous IAA in a wild-type manner (Strader *et al*., 2011).

Because both IAA and IBA can be converted to their conjugate forms (Fig. 4-1), and because the ester-linked IAA conjugate IAA-*myo*-inositol was found to be transported in maize seedlings (Chisnell and Bandurski, 1988), it is also possible that both IAA and IBA conjugates are transported over long distances and thus contributed to the transported radioactivity measured by Rashotte *et al*. (2003) but were excluded in my assay where only free IAA and IBA were measured (Fig. 4-3, Fig. 4-4, and Fig. 4-5). Therefore, I further quantified the pools of IAA and IBA conjugates, using base hydrolysis that selectively breaks ester and amide conjugate bonds. Although the base hydrolysis treatment is relatively harsh, it provides unbiased quantification of the entire IAA and IBA conjugate pools. However, if specific IAA and IBA conjugates had been of interest, alternative methods using either GC-MS or LC-MS could have been applied. As

shown in Figure 4-6B, free [$^{13}C_6$]IAA was the dominant form of transported IAA, and only a very small amount of conjugated [$^{13}C_6$]IAA could be detected after transport. Although my analysis did not include metabolites of [$^{13}C_6$]IAA that do not maintain the indole ring and the two-carbon side chain, this result, together with the percent of transported free [$^{13}C_6$]IAA (discussed above), leads to the conclusion that IAA itself is the major substrate in the polar transport system. Therefore, transported radioactivity measured in assays with [^{3}H]IAA tracers primarily represents the transport of free IAA in Arabidopsis hypocotyls. However, this does not exclude the possibility that the transport of some IAA conjugates occurs in some plant tissues during some developmental periods to provide free IAA in the target tissue, such as the transport of IAA-*myo*-inositol from the maize kernel to the shoot (Epstein *et al*., 1980; Nowacki and Bandurski, 1980; Chisnell and Bandurski, 1988). When pools of IBA conjugates were quantified in the lower hypocotyl section and receiver block (Fig. 4-6D), ester-linked [$^{13}C_1$]IBA was detected at a level significantly higher than free [$^{13}C_1$]IBA, and its level was not affected by NPA applied in the receiver. This result suggests that ester-linked IBA may also be transported basipetally in Arabidopsis hypocotyls and is consistent with what Epstein and Ackerman (1993) found in *Leucadendron discolor*, except that the movement was in a different direction. However, the sum of transported [$^{13}C_1$]IBA and its metabolites analyzed in my assay was still significantly lower than the amount of transported [$^{13}C_6$]IAA, suggesting that the majority of the transported radioactivity derived from [^{3}H]IBA measured by Rashotte *et al*. (2003) was not from [^{3}H]IBA or [^{3}H]IBA-derived conjugates and [^{3}H]IAA. Therefore, unlike IAA, measurement of transported radioactivity does not represent the transport of IBA.

Although I found a small amount of transported free and conjugated IBA, the amount is considerably lower than that of IAA, so it is difficult to consider IBA transport as an important means of IBA regulation, in comparison with IAA transport. Because over 29% of the free IAA was transported basipetally (Fig. 4-3C; discussed above), changes in IAA transport can significantly change the level of free IAA (Liu *et al*., 2011, see also Chapter 3) and play important roles in root development (Reed *et al*., 1998;

Bhalerao *et al.*, 2002; Salisbury *et al.*, 2007). In contrast, with less than 1% transport of exogenous IBA (Fig. 4-3I), it is not likely that this transport contributes substantially to the IBA pools at sites distant from where the IBA is applied. In addition, Strader *et al*. (2011) found that only IAA, but not IBA, could induce lateral root formation in Arabidopsis mutants that were defective in IBA-to-IAA conversion, suggesting that IBA is essentially an auxin precursor rather than active auxin. Because plants have developed a robust and tightly regulated system to transport the active auxin IAA over long distance (reviewed by Peer *et al*., 2011), it may not be necessary to develop another system to continuously transport the auxin precursor IBA similarly over long distances. Additionally, similar to what was suggested by Ruzicka *et al*. (2010), the transport of IBA may only serve as an additional way to regulate the production of IAA, and the transport may be altered when environmental conditions are changed and IAA production is differently regulated.

The exogenous IAA and IBA were converted to their conjugates in the upper hypocotyl section after the five-hour period (Fig. 4-6, A and C). IAA formed more amide-linked conjugates than ester-linked conjugates, while IBA was mostly converted to ester-linked conjugates. Interestingly, the level of amide-linked [$^{13}C_6$]IAA in the upper section was significantly increased when NPA was added in the receiver block, while the level of free [$^{13}C_6$]IAA was not changed (Fig. 4-6A). Because transport of [$^{13}C_6$]IAA into the lower section was significantly inhibited by NPA (Fig. 4-6B) and thus [$^{13}C_6$]IAA could accumulate in the upper section, this result suggests that conjugating IAA via amide linkages might be a way to regulate the level of free IAA by removing the excess amount of IAA, and at least for the amide-linked IAA conjugates IAA-apartate and IAA-glutamate, they may be further metabolized by oxidative degradation (Tuominen *et al*., 1994).

The formation of the large amount of ester-linked IBA is consistent with what was found previously, and the major conjugate is most likely to be IBA-glucose (Ludwig-Müller and Epstein, 1993; Epstein and Ackerman, 1993; Baraldi *et al*., 1995). On the other hand, the total amount of free and conjugated [$^{13}C_1$]IBA in the upper section was

dramatically higher than the amount of total [$^{13}C_6$]IAA, suggesting the uptake of [$^{13}C_1$]IBA through the cut surface was greater than that for [$^{13}C_6$]IAA. However, it was found that the uptake of [^{3}H]IBA was the same as the uptake of [^{3}H]IAA in intact Arabidopsis seedlings (Ludwig-Müller *et al*., 1995b). I also analyzed the stability of [$^{13}C_1$]IBA and [$^{13}C_6$]IAA in the donor agar block and found that the same proportion (65%) of [$^{13}C_1$]IBA and [$^{13}C_6$]IAA remained in the donor agar block after the five-hour transport period, suggesting that the higher uptake of [$^{13}C_1$]IBA is not due to a higher stability of [$^{13}C_1$]IBA in the donor agar block. Because Tognetti *et al.* (2010) found that the gene encoding the IBA-glucose conjugating enzyme (*UGT74E2*) was rapidly and strongly induced by oxidative stress and the level of IBA-glucose was dramatically increased under stress conditions, it is possible that the IBA-glucose conjugating activity was significantly induced at the cut surface of the hypocotyl, and the formation of IBA-glucose conjugates led to more IBA taken up into the plant tissue. This finding can also be linked to the phenomenon that IBA is better than IAA in stimulating adventitious root formation in plant cuttings, possibly because plant tissues store more exogenous IBA than IAA in a conjugate form, which can release free IBA over a long period of time after the application of exogenous IBA (Epstein *et al*., 1993) and eventually provide free IAA for root primordia induction (Liu and Reid, 1992).

In summary, I evaluated the transport of IAA and IBA in Arabidopsis hypocotyls using stable isotope labeled tracers and GC-MS/MS. I found that, in contrast to previous reports using radioactive assays, the transport of free IBA was much lower than the transport of free IAA and was not inhibited by NPA; and IBA was metabolized to IAA and IBA conjugates during the transport, while IAA remained as free IAA after transport. I conclude that the mechanism of IBA transport is fundamentally different from IAA, and the transport and metabolism of IBA can be an additional means to regulate levels of free IAA which can trigger physiological responses.

My study also shows that by using stable isotope labeling and mass spectrometry, the movement and metabolism of both endogenous and applied compounds in plants can be accurately identified and quantified. Therefore, in addition to analysis of auxin

transport and metabolism, I have also demonstrated a model system that should prove useful for the analysis of the transport and metabolism of other plant hormones and small molecules that have potential regulatory activity.

Figures

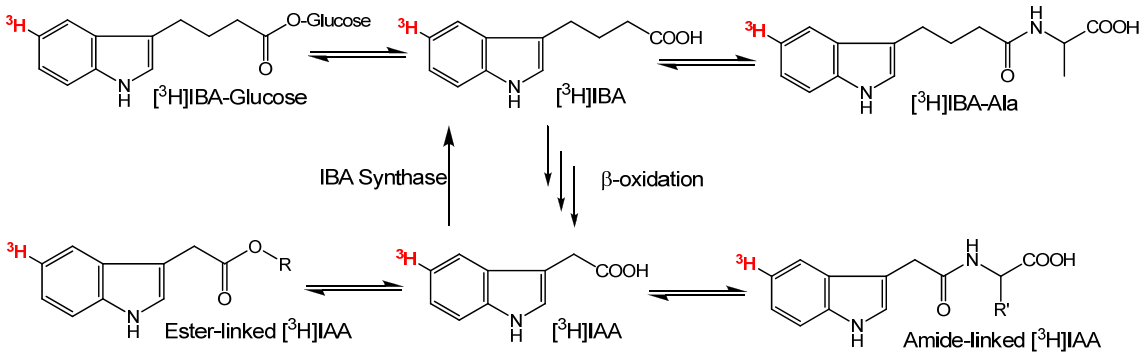

Figure 4-1. Possible metabolic pathways of [^{3}H-5]IBA and [^{3}H-5]IAA (adapted from Woodward and Bartel, 2005). [^{3}H]IBA can be converted to [^{3}H]IAA via β-oxidation through multiple steps, and [^{3}H]IBA can also be synthesized from [^{3}H]IAA via IBA synthase. Both [^{3}H]IBA and [^{3}H]IAA can be converted to ester-linked and amide-linked conjugated forms.

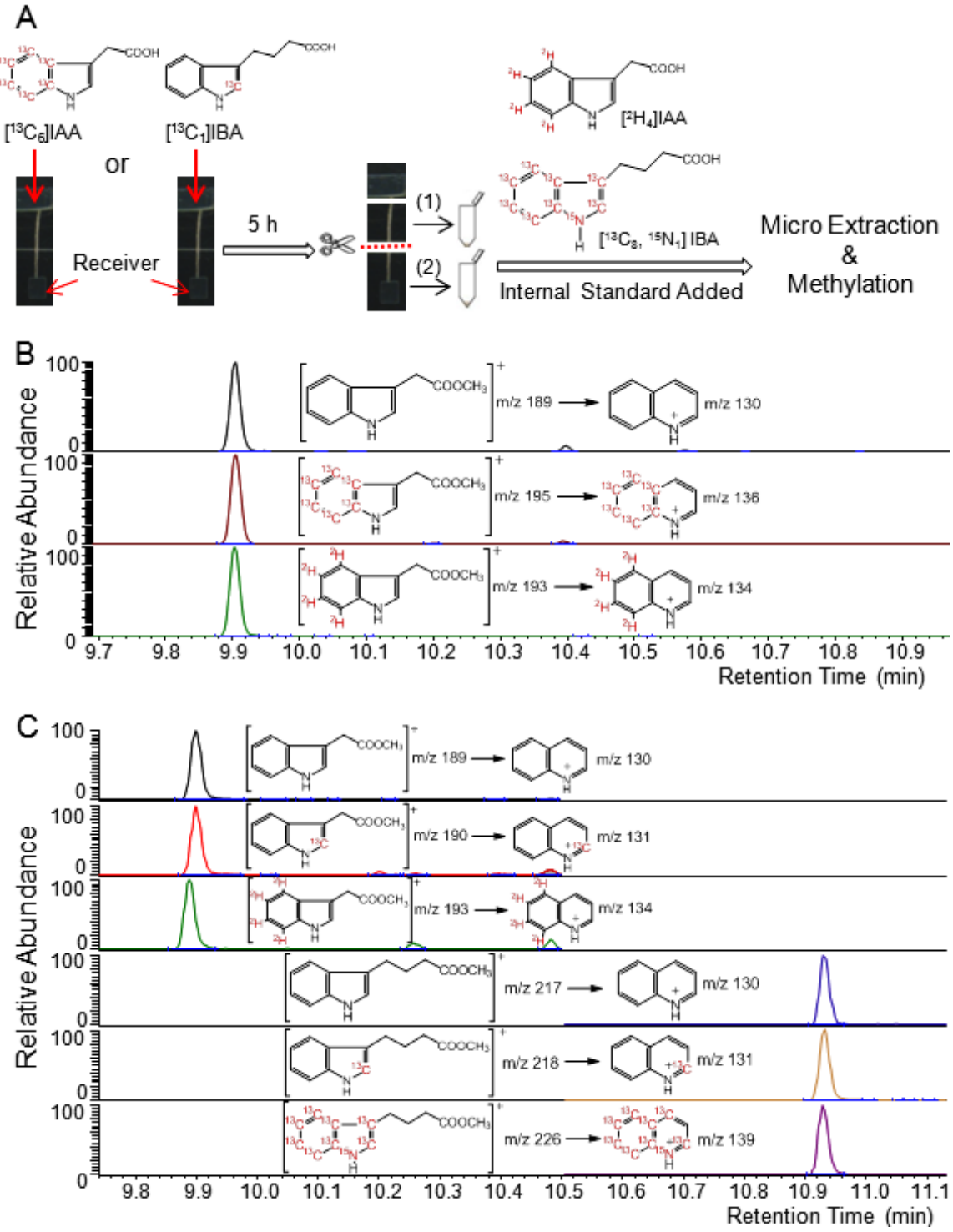
A
[13C6]IAA
[13C1]IBA
or
Receiver
5 h
(1)
(2)
[2H4]IAA
[13C8, 15N1] IBA
Internal Standard Added
Micro Extraction
&
Methylation
B
Relative Abundance
m/z 189
m/z 130
m/z 195
m/z 136
m/z 193
m/z 134
Retention Time (min)
C
Relative Abundance
m/z 189
m/z 130
m/z 190
m/z 131
m/z 193
m/z 134
m/z 217
m/z 130
m/z 218
m/z 131
m/z 226
m/z 139
Retention Time (min)

Figure 4-2. Summary of experimental procedures. Selected reaction monitoring mass spectrometry was used to detect molecular ion to major fragment ion transitions produced by methylated IAA and IBA. The major fragment ion for both 3-substituted indoles involves a ring expansion to form the relatively stable quinolinium ion in high yield (see Marx and Djerassi, 1968). **(A)** Donor agar blocks containing 10^{-5} M [$^{13}C_6$]IAA or [$^{13}C_1$]IBA were placed on top of 6-mm *Arabidopsis* hypocotyl sections. After 5 h, the hypocotyl sections were cut horizontally into halves. Samples (1) containing upper half hypocotyl sections and (2) containing lower half hypocotyl sections plus receivers were collected and extracted with known amounts of [$^{2}H_4$]IAA and [$^{13}C_8$,$^{15}N_1$]IBA added as internal standards. **(B)** Chromatographic results of samples labeled by [$^{13}C_6$]IAA. From top to bottom: unlabeled endogenous IAA, [$^{13}C_6$]IAA from donor block, and [$^{2}H_4$]IAA internal standard. **(C)** Chromatographic results of samples labeled by [$^{13}C_1$]IBA. From top to bottom: unlabeled endogenous IAA, [$^{13}C_1$]IAA derived from [$^{13}C_1$]IBA, [$^{2}H_4$]IAA internal standard, unlabeled endogenous IBA, [$^{13}C_1$]IBA from donor block, and [$^{13}C_8$,$^{15}N_1$]IBA internal standard.

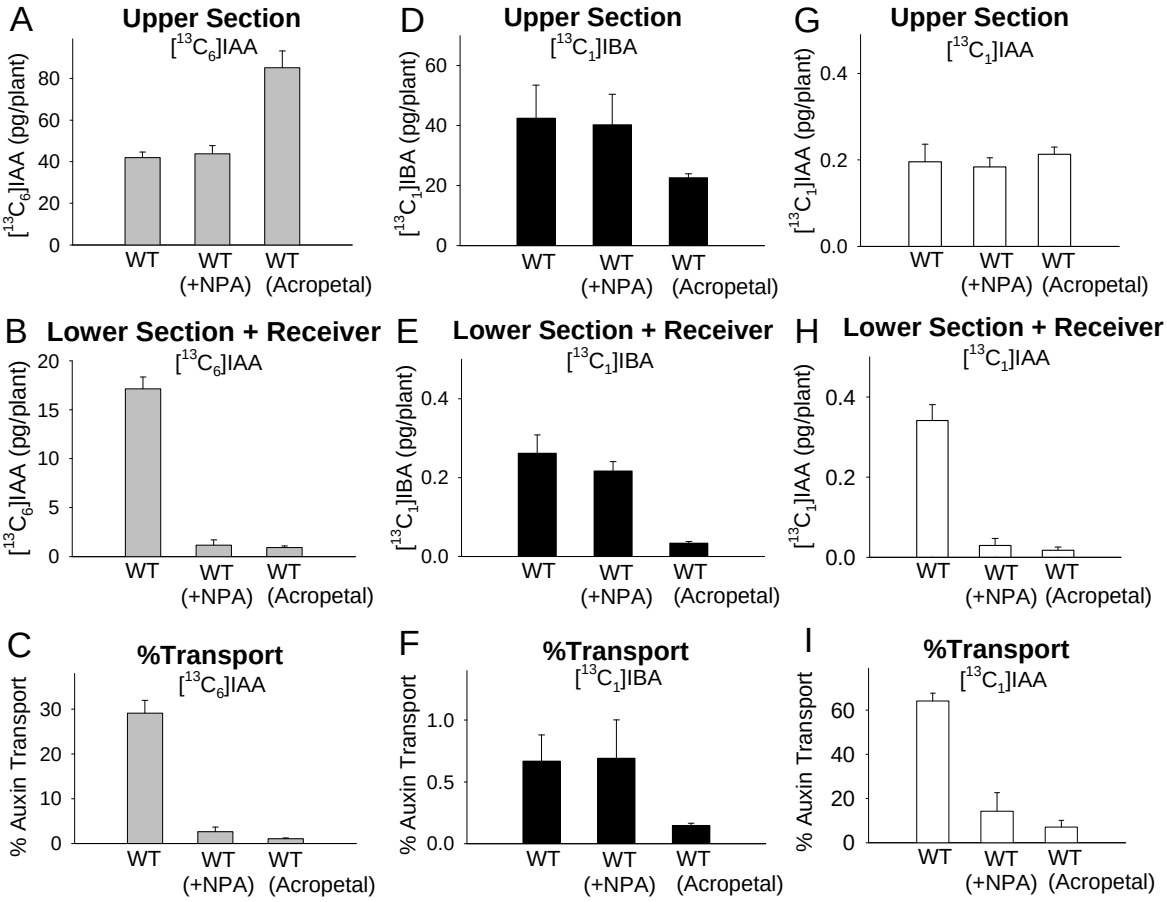

Figure 4-3. Polar auxin transport and quantification of free [$^{13}C_6$]IAA, [$^{13}C_1$]IBA, and [$^{13}C_1$]IAA derived from [$^{13}C_1$]IBA in wild type Arabidopsis hypocotyls after 5-h transport periods. WT: wild type; WT (+NPA): 10 μM NPA was added in receivers; WT (Acropetal): control with reversed orientation of hypocotyl sections. Error bars represent standard errors. **(A)** Amounts of [$^{13}C_6$]IAA in the upper half hypocotyl sections. **(B)** Amounts of [$^{13}C_6$]IAA transported into the lower half hypocotyl sections and receiver. **(C)** Percent transport of [$^{13}C_6$]IAA, calculated as values in (B) divided by the sum of values in (A) and (B). Transport of [$^{13}C_6$]IAA was dramatically reduced by NPA ($p<0.001$, n=3, student's *t* test), which was similar to the acropetal control. **(D)** Amounts of [$^{13}C_1$]IBA in the upper half hypocotyl sections. **(E)** Amounts of [$^{13}C_1$]IBA transported into the lower half hypocotyl sections and receiver. **(F)** Percent transport of [$^{13}C_1$]IBA, calculated as values in (E) divided by the sum of values in (D) and (E). Transport of [$^{13}C_1$]IBA transport in WT (+NPA) was not different from WT, but was significantly higher than in WT (Acropetal) ($p<0.01$, n=3, student's *t* test). **(G)** Amounts of [$^{13}C_1$]IAA derived from [$^{13}C_1$]IBA in the upper half hypocotyl sections. **(H)** Amounts of [$^{13}C_1$]IAA derived from [$^{13}C_1$]IBA transported into the lower half hypocotyl sections and receiver. [$^{13}C_1$]IAA was detected in WT, and the amounts were significantly reduced in WT (+NPA) and WT (Acropetal) ($p<0.002$, n=3, student's *t* test). **(I)** Percent transport of [$^{13}C_1$]IAA, calculated as values in (H) divided by the sum of values in (G) and (H).

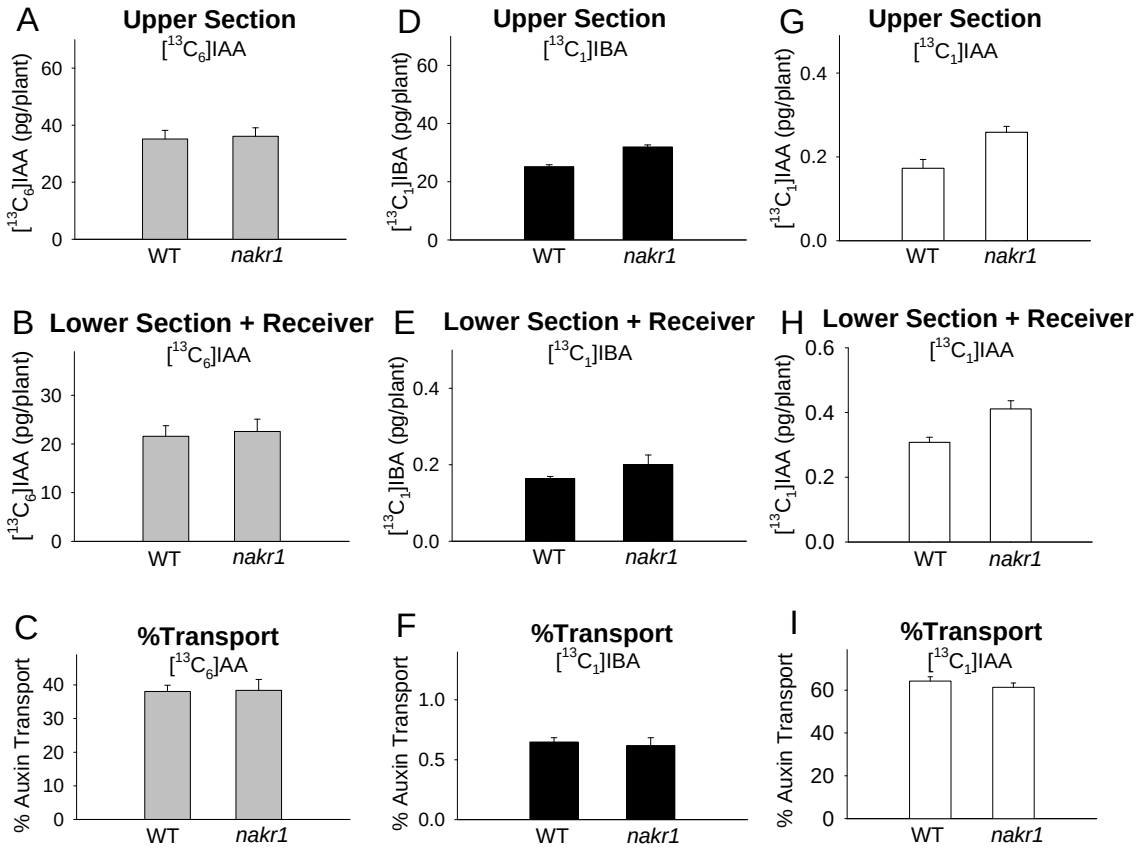

Figure 4-4. Polar auxin transport and quantification of free [$^{13}C_6$]IAA, [$^{13}C_1$]IBA, and [$^{13}C_1$]IAA derived from [$^{13}C_1$]IBA in wild type and *nakr1* mutant Arabidopsis hypocotyls after 5-h transport periods. WT: wild type. Error bars represent standard errors. **(A)** Amounts of [$^{13}C_6$]IAA in the upper half hypocotyl sections. **(B)** Amounts of [$^{13}C_6$]IAA transported into the lower half hypocotyl sections and receiver. **(C)** Percent transport of [$^{13}C_6$]IAA, calculated as values in (B) divided by the sum of values in (A) and (B). Transport of [$^{13}C_6$]IAA in *nakr1* mutant was not different from WT. **(D)** Amounts of [$^{13}C_1$]IBA in the upper half hypocotyl sections. **(E)** Amounts of [$^{13}C_1$]IBA transported into the lower half hypocotyl sections and receiver. **(F)** Percent transport of [$^{13}C_1$]IBA, calculated as values in (E) divided by the sum of values in (D) and (E). Transport of [$^{13}C_1$]IBA in *nakr1* mutant was not different from WT. **(G)** Amounts of [$^{13}C_1$]IAA derived from [$^{13}C_1$]IBA in the upper half hypocotyl sections. **(H)** Amounts of [$^{13}C_1$]IAA derived from [$^{13}C_1$]IBA transported into the lower half hypocotyl sections and receiver. **(I)** Percent transport of [$^{13}C_1$]IAA, calculated as values in (H) divided by the sum of values in (G) and (H).

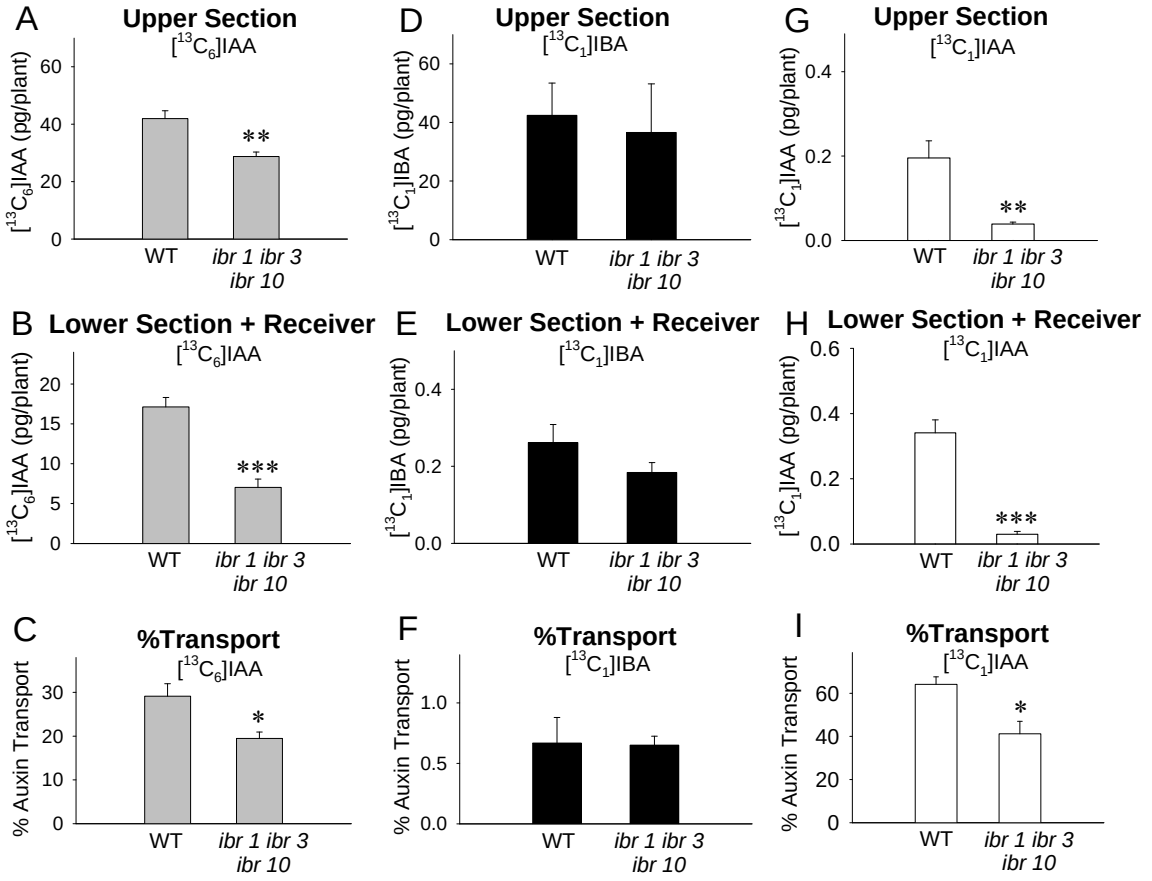

Figure 4-5. Polar auxin transport and quantification of free [$^{13}C_6$]IAA, [$^{13}C_1$]IBA, and [$^{13}C_1$]IAA derived from [$^{13}C_1$]IBA in wild type and *ibr1 ibr3 ibr10* mutant Arabidopsis hypocotyls after 5-h transport periods. WT: wild type. Error bars represent standard errors. The +NPA and acropetal controls were also performed using *ibr1 ibr3 ib10* mutant plants, and the results were similar to the wild type shown in Figure 3. **(A)** Amounts of [$^{13}C_6$]IAA in the upper half hypocotyl sections. **(B)** Amounts of [$^{13}C_6$]IAA transported into the lower half hypocotyl sections and receiver. **(C)** Percent transport of [$^{13}C_6$]IAA, calculated as values in (B) divided by the sum of values in (A) and (B). Transport of [$^{13}C_6$]IAA in *ibr1 ibr3 ibr10* mutant was significantly lower than in the WT (indicated by *; $p<0.05$, n=3, student's *t* test). **(D)** Amounts of [$^{13}C_1$]IBA in the upper half hypocotyl sections. **(E)** Amounts of [$^{13}C_1$]IBA transported into the lower half hypocotyl sections and receiver. **(F)** Percent transport of [$^{13}C_1$]IBA, calculated as values in (E) divided by the sum of values in (D) and (E). Transport of [$^{13}C_1$]IBA in *ibr1 ibr3 ibr10* mutant was not different from WT. **(G)** Amounts of [$^{13}C_1$]IAA derived from [$^{13}C_1$]IBA in the upper half hypocotyl sections. **(H)** Amounts of [$^{13}C_1$]IAA derived from [$^{13}C_1$]IBA transported into the lower half hypocotyl sections and receiver. The amount of [$^{13}C_1$]IAA was significantly reduced in *ibr1 ibr3 ibr10* mutant compared with the WT (indicated by ***; $p<0.002$, n=3, student's *t* test). **(I)** Percent transport of [$^{13}C_1$]IAA, calculated as values in (H) divided by the sum of values in (G) and (H).

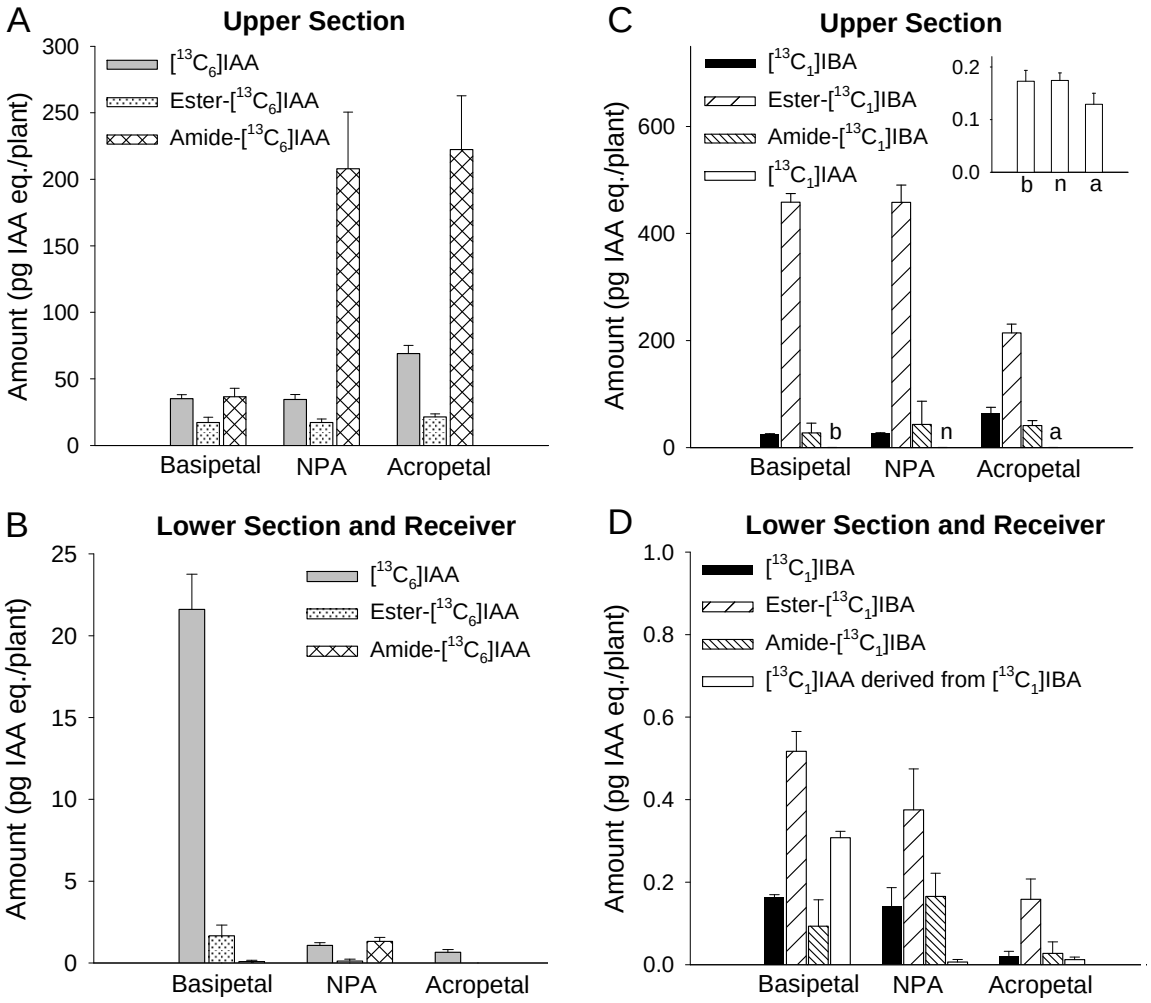

Figure 4-6. Quantification of free [$^{13}C_6$]IAA, free [$^{13}C_1$]IBA, and the ester- or amide-linked conjugates they formed in wild type Arabidopsis hypocotyls after 5-h transport periods. (A) Amounts of free, ester-linked, and amide-linked [$^{13}C_6$]IAA in the upper half hypocotyl sections. Levels of amide-linked [$^{13}C_6$]IAA in NPA and Acropetal groups were significantly higher than in the basipetal group ($p<0.05$, n=3, student's *t* test). **(B)** Amounts of free, ester-linked, and amide-linked [$^{13}C_6$]IAA in the lower half hypocotyl sections and receivers. Free [$^{13}C_6$]IAA was the dominant form of transported auxin. **(C)** Amounts of free, ester-linked, amide-linked [$^{13}C_1$]IBA, and [$^{13}C_1$]IAA derived from [$^{13}C_1$]IBA in the upper half hypocotyl sections. The lettered bars are shown in the insert graph using an expanded scale for better visualization of the values. Ester-linked [$^{13}C_1$]IBA was the dominant metabolic product of [$^{13}C_1$]IBA. **(D)** Amounts of free, ester-linked, amide-linked [$^{13}C_1$]IBA, and [$^{13}C_1$]IAA derived from [$^{13}C_1$]IBA in the lower half hypocotyl sections and receivers. The level of ester-linked [$^{13}C_1$]IBA was significantly higher than free [$^{13}C_1$]IBA ($p<0.005$, n=3, student's *t* test) in the basipetal group, and the level was not significantly reduced by NPA.

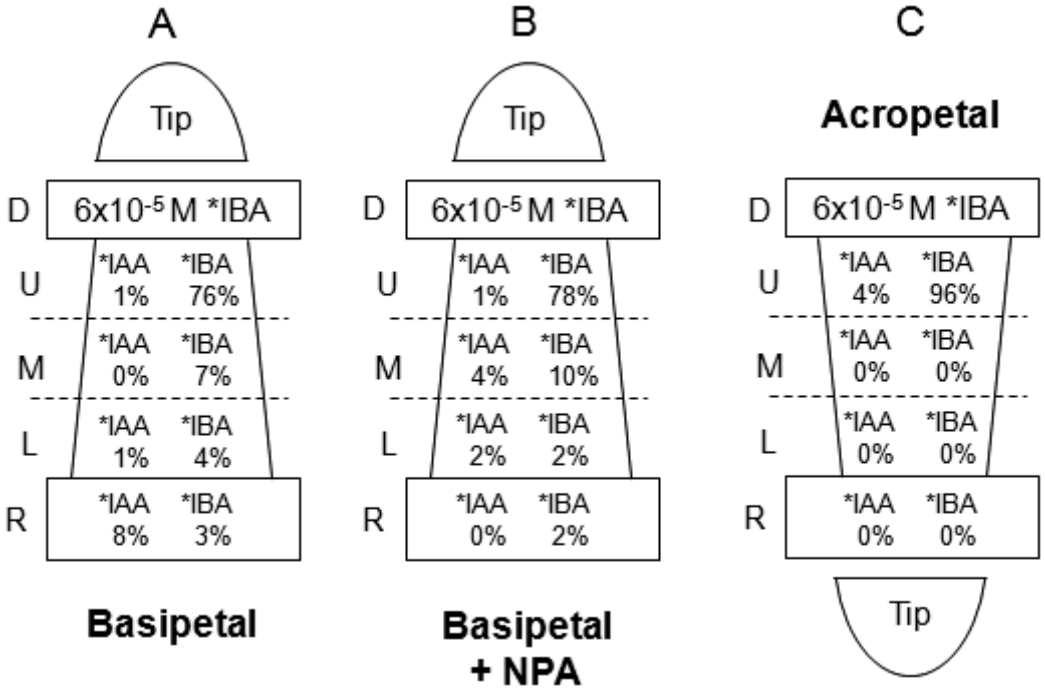

Figure 4-7. Transport of free [$^{13}C_8$,$^{15}N_1$]IBA, and [$^{13}C_8$,$^{15}N_1$]IAA derived from [$^{13}C_8$,$^{15}N_1$]IBA in maize coleoptiles after 3.5-h transport periods. Coleoptile tissues were collected from 6-day old dark-grown maize seedlings (cv. Silverqueen), and 6-mm sections were dissected 2-mm below the apical tips. Donor agar blocks containing 6 x 10^{-5} M [$^{13}C_8$,$^{15}N_1$]IBA were placed on the apical end of coleoptile sections, while receiver agar blocks were placed on the basal end. After 3.5-h transport period, the coleoptile sections were dissected into three 2-mm segments and collected separately for analysis. IBA and IAA were extracted and quantified from each of the 2-mm coleoptile segment and the receiver block exactly as previously described (Barkawi *et al*., 2008). The enrichment of [$^{13}C_8$,$^{15}N_1$]IBA and [$^{13}C_8$,$^{15}N_1$]IAA over the unlabeled endogenous IBA and IAA pool was determined, and average values of three replicates are presented in the figure. Tip: the uppermost 2-mm coleoptile tissue; D: donor agar block; U: upper 2-mm coleoptile segment; M: middle 2-mm coleoptile segment; L: lower 2-mm coleoptile segment; R: receiver agar block. *IBA represents [$^{13}C_8$,$^{15}N_1$]IBA; *IAA represents [$^{13}C_8$,$^{15}N_1$]IAA derived from [$^{13}C_8$,$^{15}N_1$]IBA. (A) Basipetal transport of auxin. Both [$^{13}C_8$,$^{15}N_1$]IBA and [$^{13}C_8$,$^{15}N_1$]IAA derived from [$^{13}C_8$,$^{15}N_1$]IBA was transported into the receiver agar block. (B) Basipetal transport of auxin in the presence of 20 μM NPA. NPA added in the receiver agar block significantly reduced the transport of [$^{13}C_8$,$^{15}N_1$]IAA into the receiver agar block, but did not reduce the transport of [$^{13}C_8$,$^{15}N_1$]IBA. (C) Acropetal transport of auxin, a negative control where the orientation of coleoptile sections was reversed. [$^{13}C_8$,$^{15}N_1$]IBA or [$^{13}C_8$,$^{15}N_1$]IAA was not detected in the receiver, lower or middle coleoptile segment.

Addenda

The following sections provide information about six of my collaborative projects, which are all aimed at better understand in the role of auxin transport and auxin metabolism in plant growth and development. Each section starts with an abstract summarizing the goals and conclusions of the project, followed by a detailed description of the work I contributed. Figures showing my experimental results are also presented, which have been or will be included in research journal articles.

A.

Genetic Dissection of the Role of Ethylene in Regulating Auxin-dependent Lateral and Adventitious Root Formation in Tomato

Sangeeta Negi, Poornima Sukumar, Xing Liu, Jerry D. Cohen and Gloria K. Muday[§]

§ Corresponding author; Department of Biology, Wake Forest University, Winston-Salem, North Carolina, USA

Published in *The Plant Journal* (2010) **61:** 3-15

Abstract

In this study we investigated the role of ethylene in the formation of lateral and adventitious roots in tomato (*Solanum lycopersicum*) using mutants isolated for altered ethylene signaling and fruit ripening. Mutations that block ethylene responses and delay ripening -*Nr* (*Never ripe*), *gr* (*green ripe*), *nor* (*non ripening*), and *rin* (*ripening inhibitor*) - have enhanced lateral root formation. In contrast, the *epi* (*epinastic*) mutant, which has elevated ethylene and constitutive ethylene signaling in some tissues, or treatment with the ethylene precursor 1-aminocyclopropane carboxylic acid (ACC), reduces lateral root formation. Treatment with ACC inhibits the initiation and elongation of lateral roots, except in the *Nr* genotype. Root basipetal and acropetal indole-3-acetic acid (IAA) transport increase with ACC treatments or in the *epi* mutant, while in the *Nr* mutant there is less auxin transport than in the wild type and transport is insensitive to ACC. In contrast, the process of adventitious root formation shows the opposite response to ethylene, with ACC treatment and the *epi* mutation increasing adventitious root formation and the *Nr* mutation reducing the number of adventitious roots. In hypocotyls, ACC treatment negatively regulated IAA transport while the *Nr* mutant showed increased IAA transport in hypocotyls. Ethylene significantly reduces free IAA content in roots, but only subtly changes free IAA content in tomato hypocotyls. These results indicate a negative role for ethylene in lateral root formation and a positive role in adventitious root

formation with modulation of auxin transport as a central point of ethylene-auxin crosstalk.

Quantification of Free IAA in Tomato Roots and Hypocotyls

The *Nr* mutant in the Pearson background was provided by Harry Klee (University of Florida, Gainesville, FL) (Wilkinson *et al*., 1995); *epi* (in the VFN8 background) mutant seeds were provided by Jim Giovannoni (Boyce Thompson Institute, Ithaca, NY) (Barry *et al*., 2001). All seeds were sterilized by incubation for 5 min in 95% ethanol, then for 30 min in freshly prepared 20% (v/v) bleach plus 0.01% (v/v) Triton X-100, and then washed with sterile water. The sterilized seeds were sown on sterilized blue filter papers and after emergence of the radicle they were transferred to control plates: 0.8% (w/v) Type M agar (A-4800; Sigma), MS nutrients (macro and micro salts, MSP0501; Caisson Labs) (Murashige and Skoog, 1962), vitamins (1 μg ml^{-1} thiamine, 1 μg ml^{-1} pyridoxine HCl, and 0.5 μg ml^{-1} nicotinic acid), 0.05% (w/v) 2-(N-morpholine)-ethanesulfonic acid (MES), with pH adjusted to 5.8. For root samples, seeds were germinated and after radicle emergence transferred to control or 1 μM ACC plates for 48 h. Roots were excised and frozen in liquid nitrogen. For hypocotyl tissues, samples were grown in low light for 3 days and transferred to high-light conditions onto media with and without 1 or 10 μM ACC for 48 h; hypocotyls were collected and frozen. For both types of sample, 50-80 mg of frozen tissue was homogenized with a bead beater in 150 μL of homogenization buffer (35% of 0.2 M imidazole, 65% isopropanol, pH 7), containing 4 ng of [$^{13}C_6$]IAA as an internal standard. The level of free IAA was analyzed by solid phase extraction followed by GC-SIM-MS as previously described (Barkawi *et al*., 2010).

As shown in Figure A-1, free IAA levels were higher in *Nr* roots than in wild-type plants, and consistent with these results, ACC-treated wild-type roots contained a significantly lower level of free IAA than untreated roots ($P<0.05$). The effect of ACC was similar in all backgrounds (Pearson, AC, and VFN8) with a statistically significant

1.5-fold decrease in free IAA content ($P<0.05$). These results suggest that ethylene plays a negative role in regulating the level of free IAA in tomato root tissues.

On the other hand, *Nr* hypocotyl tissues showed a slight (20%) reduction in free IAA content (Fig. A-2A), and *epi* showed a 40% reduction in free IAA levels compared with the wild type. But neither of the reductions was significant. When wild-type plants were treated with 1 or 10 μM of ACC for 48 h, no changes in free IAA levels were found in hypocotyls from treated plants compared with hypocotyls from untreated control plants (Fig. A-2B). These results suggest that although the ACC treatment was found to alter IAA transport in tomato hypocotyls (Negi *et al*., 2010), the treatment had little effect on free IAA levels in tomato hypocotyl tissues.

Figures

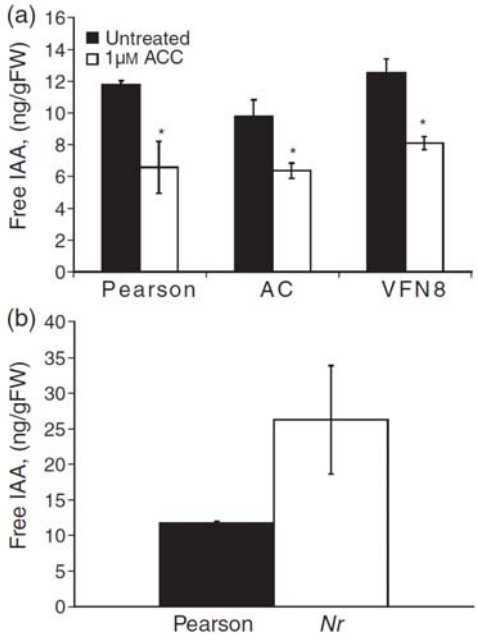

Figure A--1. In tomato roots, the free IAA content is reduced 2 days after treatment with 1 μM ACC. (A) Free IAA content in three different genotypes after treatment with 1 μM ACC. **(B)** Free IAA content in Pearson and the *Nr* mutant. The average and standard error of three replicates are shown. The asterisk (*) indicates a statistically significant difference relative to untreated wild-type as determined by student's *t* test ($P<0.05$).

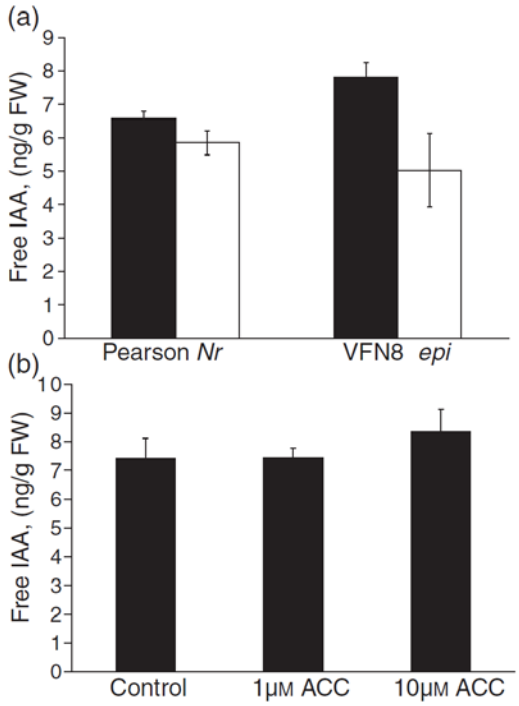

Figure A--2. Effect of ethylene on the free IAA content in tomato hypocotyls. (A) Free IAA in the ethylene mutants *Nr* and *epi* are compared with the respective wild types. **(B)** Free IAA in tomato hypocotyls treated with ACC for 48 h. In both panels the average and standard error of three replicates are reported.

B.

vanishing tassel2 Encodes a Grass-Specific Tryptophan Aminotransferase Required for Vegetative and Reproductive Development in Maize

Kimberly A. Phillips, Andrea L. Skirpan, Xing Liu, Ashley Christensen, Thomas L. Slewinski, Christopher Hudson, Solmaz Barazesh, Jerry D. Cohen, Simon Malcomber, and Paula McSteen[§]

§ Corresponding author; Department of Biology, Pennsylvania State University, University Park, Pennsylvania, USA

Published in *The Plant Cell* (2011) **23:** 550-566

Abstract

Auxin plays a fundamental role in organogenesis in plants. Multiple pathways for auxin biosynthesis have been proposed, but none of the predicted pathways are completely understood. Here, we report the positional cloning and characterization of the *vanishing tassel2* (*vt2*) gene of maize (*Zea mays*). Phylogenetic analyses indicate that *vt2* is a co-ortholog of *TRYPTOPHAN AMINOTRANSFERASE OF ARABIDOPSIS1* (*TAA1*), which converts Trp to indole-3-pyruvic acid in one of four hypothesized Trp-dependent auxin biosynthesis pathways. Unlike single mutations in *TAA1*, which cause subtle morphological phenotypes in *Arabidopsis thaliana*, *vt2* mutants have dramatic effects on vegetative and reproductive development. *vt2* mutants share many similarities with *sparse inflorescence1* (*spi1*) mutants in maize. *spi1* is proposed to encode an enzyme in the tryptamine pathway for Trp-dependent auxin biosynthesis, although this biochemical activity has recently been questioned. Surprisingly, *spi1 vt2* double mutants had only a slightly more severe phenotype than *vt2* single mutants. Furthermore, both *spi1* and *vt2* single mutants exhibited a reduction in free auxin levels, but the *spi1 vt2* double mutants did not have a further reduction compared with *vt2* single mutants. Therefore, both *spi1*

and *vt2* function in auxin biosynthesis in maize, possibly in the same pathway rather than independently as previously proposed.

Quantification of Free IAA in Maize Leaf Tissues

Maize families segregating for both *spi1* and *vt2* in the B73 genetic background were grown for 2 weeks and genotyped as described in Phillips et al (2011). Samples of leaf tissue were collected from the fifth leaf that was just emerging from the whorl. Leaf tissue (50 to 80 mg) was weighed, frozen in liquid nitrogen, and stored at -80 ºC. For each sample, 150 µL of homogenization buffer (35% of 0.2 M imidazole and 65% isopropanol, pH 7) containing 3 or 4 ng of [$^{13}C_6$]IAA was added before homogenization. The level of free IAA was analyzed by solid phase extraction followed by GC-SIM-MS as previously described (Barkawi *et al*., 2010).

As shown in Figure A-3, wild-type maize leaves contained 10 to 11 ng/g fresh weight of free IAA, while *spi1* and *vt2* single mutants had an average 82% and 34% of normal IAA levels, respectively. The reduction of free IAA levels in *spi1 vt2* double mutants was not statistically significantly different from that in *vt2* single mutants (P=0.845), which supported the conclusion from the genetic evidence that *spi1* acted downstream of *vt2* in the same IAA biosynthetic pathway. These results for the first time provide experimental support for the hypothesis that *vt2* (*TAA1*) and *spi1* (*YUCCA*) actually function in the same pathway for auxin biosynthesis, at least in maize leaf tissues.

Figure

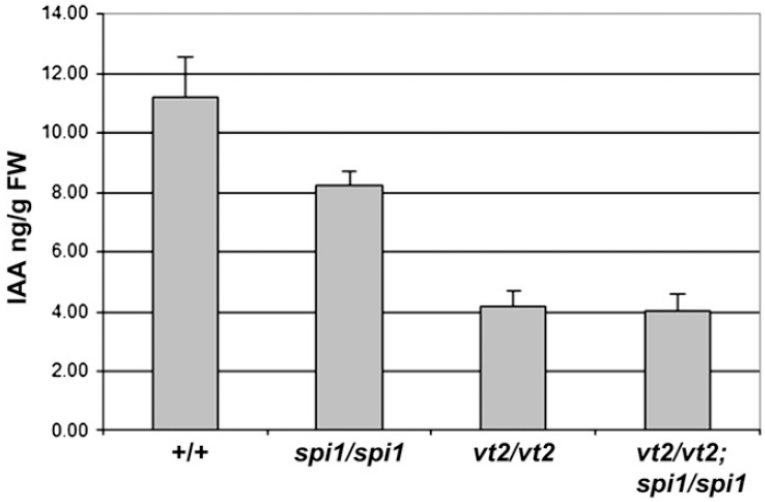

Figure A--3. Measurement of free IAA levels in normal, *spi1*, *vt2* and *spi1 vt2* mutants. Free IAA levels were measured in developing leaves of 2-week-old seedlings. Error bars represent the standard error, n=5 each of normal, *spi1*, *vt2*, and *vt2 spi1*. One replicate of three is shown. FW, fresh weight.

C.

Arabidopsis Monothiol Glutaredoxin, AtGRXS17, is Critical for Temperature-dependent Postembryonic Growth and Development via Modulating Auxin Response

Ning-Hui Cheng[§], Jian-Zhong Liu, Xing Liu, Qingyu Wu, Sean M. Thompson, Julie Lin, Joyce Change, Seven A. Whitham, Sunghun Park, Jerry D. Cohen, and Kendal D. Hirschi
§ Corresponding author; United States Department of Agriculture/Agricultural Research Service, Children's Nutrition Research Center, Baylor College of Medicine, Houston, Texas, USA

Published in *The Journal of Biological Chemistry* (2011) **286:** 20398-20406

Abstract

Global environmental temperature changes threaten innumerable plant species. Although various signaling networks regulate plant responses to temperature fluctuations, the mechanisms unifying these diverse processes are largely unknown. Here, we demonstrate that an *Arabidopsis* monothiol glutaredoxin, AtGRXS17 (At4g04950), plays a critical role in redox homeostasis and hormone perception to mediate temperature-dependent postembryonic growth. *AtGRXS17* expression was induced by elevated temperatures. Lines altered in *AtGRXS17* expression were hypersensitive to elevated temperatures and phenocopied mutants altered in the perception of the phytohormone auxin. We show that auxin sensitivity and polar auxin transport were perturbed in these mutants, whereas auxin biosynthesis was not altered. In addition, *atgrxs17* plants displayed phenotypes consistent with defects in proliferation and/or cell cycle control while accumulating higher levels of reactive oxygen species and cellular membrane damage under high temperature. Together, our findings provide a nexus between reactive oxygen species homeostasis, auxin signaling, and temperature responses.

Quantification of Free and Conjugated IAA in Arabidopsis Seedlings

Ten-day-old wild type, *atgrxs17* KO, and *AtGRXS17* RNAi seedlings were harvested after growth at 22 or 28 °C. For each seedling type, 150-200 mg of frozen tissue was homogenized using a Mixer Mill (MM 300; Qiagen, Valencia, CA), with a 3-mm tungsten carbide bead in 300 µl of homogenization buffer (35% of 0.2 M imidazole, 65% isopropanol, pH 7) containing 20 ng of [$^{13}C_6$]IAA and 200 ng of [^{13}C]indoleacetonitrile (IAN) as internal standards (Ilić *et al*., 1996).

After 1 h on ice, 150 µl of the homogenate was purified through two sequential solid phase extraction (SPE) columns, anion exchange and plastic affinity, using a Gilson SPE 215 system, methylated, dried, and redissolved in ethyl acetate exactly as described previously (Barkawi *et al*., 2010). The flow-through from the amino anion exchange SPE column was collected for IAN analysis. The samples were then analyzed using GC-SIM-MS on an Agilent 6890/5973 system. The level of free IAA was quantified by isotope dilution analysis based on the [$^{13}C_6$]IAA internal standard (Barkawi *et al*., 2010).

For IAN analysis, the flowthrough collected from the amino SPE column was passed through a C18 SPE column (100 mg; Varian) and then washed with 3 × 0.6 ml water, eluted with 3 × 0.3 ml acetonitrile, evaporated to complete dryness, and derivatized with 50 µl of bis(trimethylsily)trifluoroacetamide plus 1% trimethylchlorosilane at 45 °C for 45 min. The samples were analyzed using GC-SIM-MS, and the correction factor for nonenzymatic conversion of IAN to IAA was determined (Ilić *et al*., 1996).

For the rest of the homogenate, 100 µl was hydrolyzed in 1 N NaOH (1 h, room temperature) for measurement of free plus ester-linked IAA, and 50 µl was hydrolyzed in 7 N NaOH (3 h, 100 °C under nitrogen gas) for measurement of total IAA. After hydrolysis, the pH of the homogenate was adjusted to 2.7 and desalted by passing through a C18 SPE column (100 mg; Varian), washed with 3 × 0.6 ml water, eluted with 3 × 0.3 ml methanol, evaporated to dryness, and redissolved in 150 µl of homogenization buffer. The purification of IAA released from the conjugates was subsequently the same as used for the purification of free IAA. The samples were analyzed using GC-SIM-MS,

and the levels of free plus ester-linked IAA and total IAA were quantified with correction for IAN hydrolysis (Ilić *et al*., 1996).

As shown in Figure A-4, no significant difference in IAA levels was found in *atgrxs17* KO or RNAi seedlings compared with wild-type control plants, grown at either 22 °C or 28 °C. This result suggest that the auxin-related phenotypes observed in *atgrxs17* mutant plants (Cheng *et al*., 2011) were not due to altered IAA levels or auxin metabolism.

Polar Auxin Transport in Arabidopsis Hypocotyls

Wild type, *atgrxs17* KO, and AtGRXS17 RNAi line seeds were surface-sterilized and plated on one-half strength MS medium. After 3 days in the dark at 4 °C and 12 h under cool white fluorescent lights (photosynthetically active radiation = 80 μmol m^{-2} s^{-1}), the seeds were grown at either 22 or 28 °C continuously in darkness for 4 days and then exposed to continuous cool white fluorescent lights (photosynthetically active radiation = 80 μmol m^{-2} s^{-1}) for an additional 2 days. The basipetal IAA transport in hypocotyl tissues was measured as previously described (Liu *et al*., 2011, see also Chapter 3).

As shown in Figure A-4D, basipetal transport of auxin in the hypocotyls of *atgrxs17* KO and RNAi seedlings was reduced compared with wild-type controls at 22 °C, but this difference was not statistically significant. At 28 °C, basipetal transport of auxin in the hypocotyls of wild-type seedlings was increased but not in *atgrxs17* KO or RNAi seedlings, and therefore, the basipetal transport of auxin in *atgrxs17* mutant plants was significantly lower than that in wild-type seedlings ($p<0.001$). Additionally, the higher temperature promoted polar auxin transport in wild type controls, but not in either *atgrxs17* KO or RNAi seedlings, indicating that temperature-dependent promotion of polar auxin transport was lost in both *atgrxs17* KO and RNAi seedlings. These results suggest that the reduction of polar auxin transport activity in AtGRXS17 loss-of-function plants contributes to auxin-related growth defects under high temperature (Cheng *et al*., 2011).

Figure

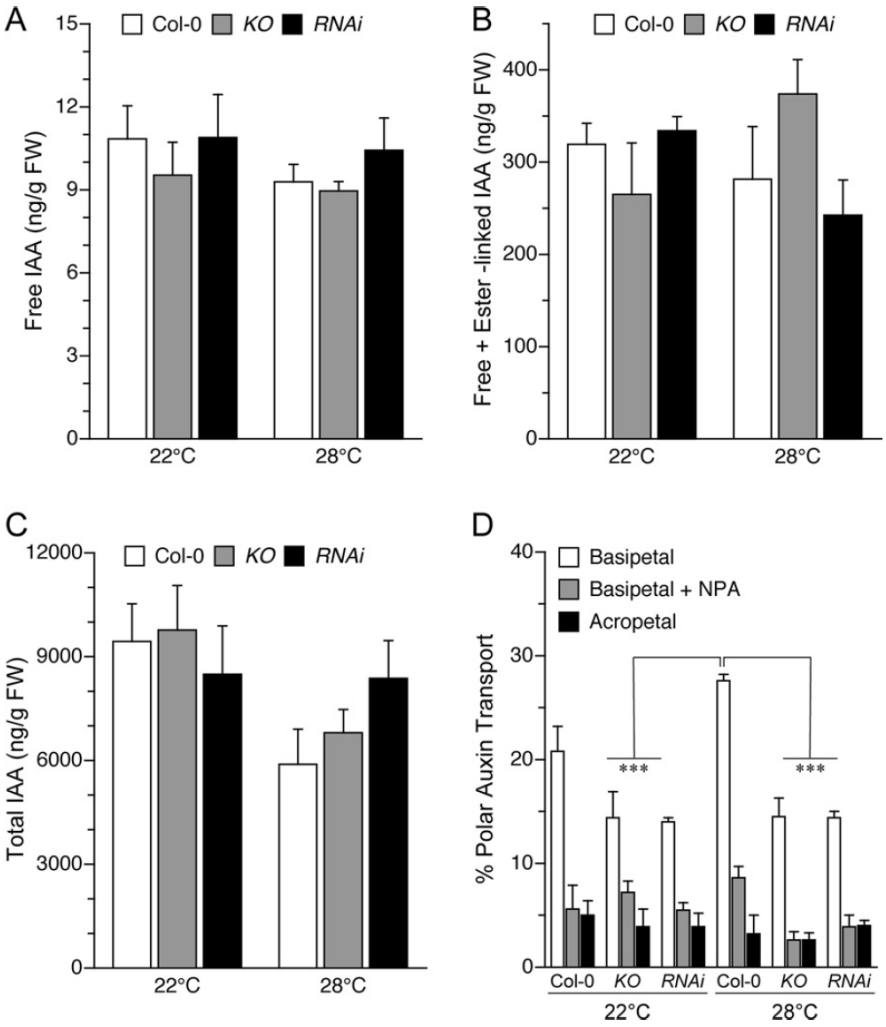

Figure A--4. Basipetal polar auxin transport but not auxin content was reduced in *atgrx 17* KO and RNAi seedlings grown at elevated temperature. (A)-(C) The level of free IAA **(A)**, free + ester-linked IAA **(B)**, and total IAA **(C)** were not significantly changed in *atgrxs 17* KO and RNAi seedlings at either 22 or 28 ºC. **(D)** Reduction of polar auxin transport in atgrxs17 KO and RNAi seedlings at 28 ºC. Wild type, *atgrxs 17*KO, and RNAi seeds were germinated and grown vertically on one-half strength MS medium at 22 or 28 ºC in darkness for 4 days and transferred to continuous cool white fluorescent light (80 µmol m^{-2} s^{-1}) for 2 days. Polar auxin transport was measured. Data are expressed as dpm in the receiver block plus the basal half of the hypocotyl as a % of total dpm in the hypocotyl and the receiver block (Basipetal). Controls were run with 10 µM NPA added in the receiver blocks (Basipetal + NPA), or an inverted orientation of the hypocotyl section (Acropetal). Error bars indicate standard error (n=9) (two-way ANOVA, ***, $p<0.001$). FW, fresh weight.

D.

Unifoliata-Afila Interactions in Pea Leaf Morphogenesis

Darleen A. DeMason[§], Venkateswari Chetty, Lana S. Barkawi, Xing Liu, and Jerry D. Cohen

§ Corresponding author; Botany and Plant Sciences, University of California, Riverside, California, USA

Manuscript in preparation

Abstract

Processes of leaf morphogenesis provide the basis for the great diversity of leaf form among higher plants. The common garden pea provides a developmental model system for understanding how gene and hormone interactions provide a large array of mutant leaf phenotypes. We compared the range of leaf phenotypes on *afila* (*af*) and *unifoliata* (*uni*) double mutants, measured auxin levels in shoot tips of a range of mutants, crossed the *DR5::GUS* reporter into a range of leaf mutants and used qRT-PCR of four auxin-regulated genes to understand the role of auxin in *AF* and *UNI* gene function and interaction. The *af/uni* double mutants have intermediate levels of leaf complexity between *af* and *uni* single mutants. The two mutants of *UNI* (*uni-tac* and *uni*) differ in the auxin content of their shoot tips, auxin perception, and auxin transport. Auxin content of the shoot tips of the *af* mutants is higher than that of wild type. The *af* mutants have higher levels of auxin responsive genes and the *uni* mutants have lower expression compared to wild type. *AF* and *UNI* have an antagonistic relationship. *AF* spreads into the leaf tip in the absence of *UNI,* and *UNI* expression spreads into the pinna primordia in the absence of *AF*. The mechanism may be modulation of auxin mediated by one or both genes.

IAA Transport in Pea Petioles

WT and *uni-tac* from the set of near-isogenic lines as well as two genotypes, *AF/AF UNI* (*WT2*) and *AF/AF uni* (*uni*), derived from the W6 15302 line were used for analysis. Plants were grown in flats in a growth chamber until leaf 12 was expanding. The centermost 6-mm region of the petioles from the 12th leaf of each plant was placed right side up (basipetal transport and NPA treatment) or upside down (acropetal transport) between two agar blocks: donor and receiver, as described previously (Liu et al, 2011; Chapter 3). Transport was allowed to occur with donor blocks down in a chamber with high humidity for 3 hours at room temperature, after which each petiole section was dissected at the center, and each piece, as well as, the receiving block was extracted individually in scintillation cocktail (Econo-Safe^{TM}) overnight. The radioactivity in each sample was determined by liquid scintillation counting (LS 6500, Beckman, Brea, CA) for 10 min or until the error was < 2%, whichever came first. Nine replicates were used for the basipetal transport measurements, four for NPA and for acropetal transport for each genotype. Statistical analysis was done with Microsoft Excel. Significance was defined at the 0.05% level.

As shown in Figure A-5, the transport of auxin in petioles of *uni-tac* plants was significantly higher than in the wild-type control plants, while auxin transport in petioles of *uni* plants was significantly lower than in the wild-type control plants. The level of auxin transport correlated well with the level of free IAA in shoot tips of the pea plants: *uni-tac* had more free IAA per shoot tip, and *uni* had less free IAA per shoot tip, compared with their corresponding wild-type plants ($P<0.005$; DeMason *et al*., 2011, unpublished data). These results support the hypothesis that IAA increases its own efflux from cells, possibly by promoting the plasma membrane localization of PIN proteins (Paciorek *et al*., 2005).

Figure

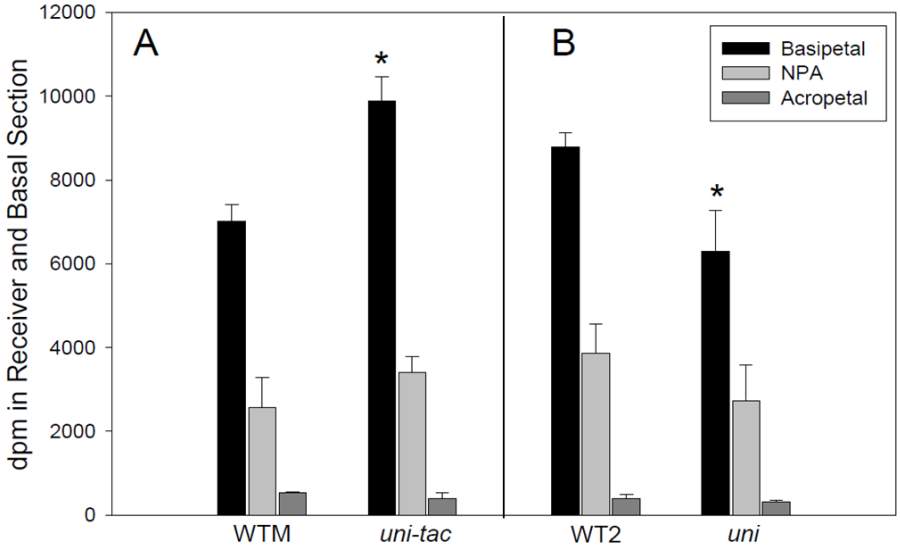

Figure A--5. Polar auxin transport in petioles of expanding leaves for *uni-tac* compared to its control (WTM) and uni and its control (WT2). Mean basipetal (nine replicates), basipetal + NPA (four replicates) and acropetal (four replicates) auxin transport and standard errors in petioles of expanding leaves for *uni-tac* compared to its control (WTM) and *uni* and its control (WT2). The asterisk (*) indicates a statistically significant difference relative to wild-type as determined by student's *t* test ($P<0.05$).

E.

The Endoplasmic Reticulum Localized PIN8 Modulates Cell and Plant Development by Regulating Intracellular Auxin Homeostasis

Cristina Dal Bosco, Alexander Dovzhenko, Xing Liu, Nina Woerner, Tatiana Rensch, Margitta Eismann, Stefan Eimer, Jan Hegermann, Ivan Paponov, Benedetto Ruperti, Alisher Touraev, Jerry D. Cohen, Klaus Palme[§]

§ Corresponding author; Insitute of Biology II, Molecular Plant Physiology, Faculty of Biology, Albert-Ludwigs University Freiburg, Freiburg, Germany

1. Poster abstract published in *22nd International Conference on Arabidopsis Research*; Madison, Wisconsin, June 22-25, 2011 (Abstract Number: 386)

2. *Manuscript* in preparation

Abstract

The plant hormone auxin is a mobile signal which effects nuclear transcription by regulating the stability of AUX/IAA repressor proteins. Auxin is polarly transported from cell to cell by auxin efflux proteins of the PIN family, but it is not clear how auxin levels are regulated within cells and how auxin access to the nucleus is controlled. The Arabidopsis genome contains eight PIN genes, encoding proteins with a similar membrane topology. While five of them are typically targeted polarly to plasma membranes, the smallest members of the family, PIN5 and PIN8, seem to be located not at the plasma membrane, but at internal membranes. Here we demonstrate by electron-microscopic analysis that PIN8 which is specifically expressed in pollen resides in the endoplasmic reticulum membrane and that it remains internally localized during pollen tube growth. Dominant mutants were generated by overexpressing functional PIN8 and its role in control of auxin homeostasis was tested in transgenic Arabidopsis and tobacco plants. Plants with elevated PIN8 levels showed strong auxin related phenotypes with reduced overall size, hyponastic leaves and longer vegetative growth periods. The severity of phenotypes depended on protein levels, suggesting a rate-limiting activity of

PIN8. Phenotypes were correlated with elevated levels of free IAA and ester-conjugated IAA. Activation of the auxin-regulated synthetic DR5 promoter was strongly repressed in seedlings with elevated PIN8 levels when exposed to externally applied 1-NAA. Thus our data show a novel function of endoplasmic reticulum-localized PIN8 in controlling auxin thresholds in nucleus, thereby regulating auxin-dependent transcriptional activity.

Quantification of Free and Conjugated IAA in Tobacco Tissues

Tobacco leaf tissue, cotyledons and pollen grains from plants grown on soil, and roots from seedlings grown on plates were collected, weighted and immediately frozen in liquid nitrogen. Each type of frozen tissue was homogenized using a Mixer Mill (MM 300; Qiagen, Valencia, CA), with a 3 mm tungsten carbide bead in 300 µl homogenization buffer (35% of 0.2 M imidazole, 65% isopropanol, pH 7) containing known amount of [$^{13}C_6$]IAA as an internal standard. After 1 hr on ice, 150 µl of the homogenate was purified through two sequential solid phase extraction columns and analyzed by GC-SIM-MS as previously described (Barkawi *et al*., 2010). The level of free IAA was quantified by isotope dilution analysis based on the [$^{13}C_6$]IAA internal standard.

For the rest of the homogenate, 100 µl was hydrolyzed in 1 N NaOH (1 hr, room temperature) for measurement of free plus ester-linked IAA, and 50 µl was hydrolyzed in 7 N NaOH (3 hours, 100 ºC under nitrogen gas) for measurement of total IAA (Bialek and Cohen, 1989). After hydrolysis, the pH of the homogenate was adjusted to 2.7, and was desalted by passing through a C18 SPE column (100 mg; Varian), washed with 3 × 0.6 ml water, eluted with 3 × 0.3 ml methanol, evaporated to dryness, and dissolved in 150 µl homogenization buffer. The purification of IAA released from the conjugates was subsequently the same as used for the purification of free IAA. The samples were analyzed using GC-SIM-MS, and the levels of free plus ester-linked IAA and total IAA were determined by isotope dilution analysis based on the [$^{13}C_6$]IAA internal standard.

As shown in Figure A-6A, tobacco plants overexpressing Arabidopsis PIN8 contained significantly more free and ester-linked IAA, compared with the wild-type

plants. This effect was stronger in fully developed leaves compared with cotyledons. However, the level of free IAA in PIN8OX tobacco roots was significantly lower than in the wild-type roots (Figure A-6B). These results suggest that changes in the activity of ER-localized PIN8 lead to changes in both IAA levels and IAA metabolism, which is likely a consequence of altered intracellular distribution of IAA. Also, this effect was different in shoots and roots, suggesting that the regulation of IAA metabolism differs in different tissue and/or cell types. In addition, Figure A-6C illustrates the different composition of IAA pools in different tobacco tissues. In cotyledons, the level of free IAA was 1.2 ng/g, which represented 1.4% of the total IAA (free + ester-linked + amide-linked IAA) pool; in anthers, the level of free IAA was 45 ng/g, which represented 2.2% of the total IAA pool; and in pollen, the level of free IAA was 177 ng/g, which represented 11% of the total IAA pool. These results further support the hypothesis that different plant tissues differently regulate IAA metabolism.

Figures

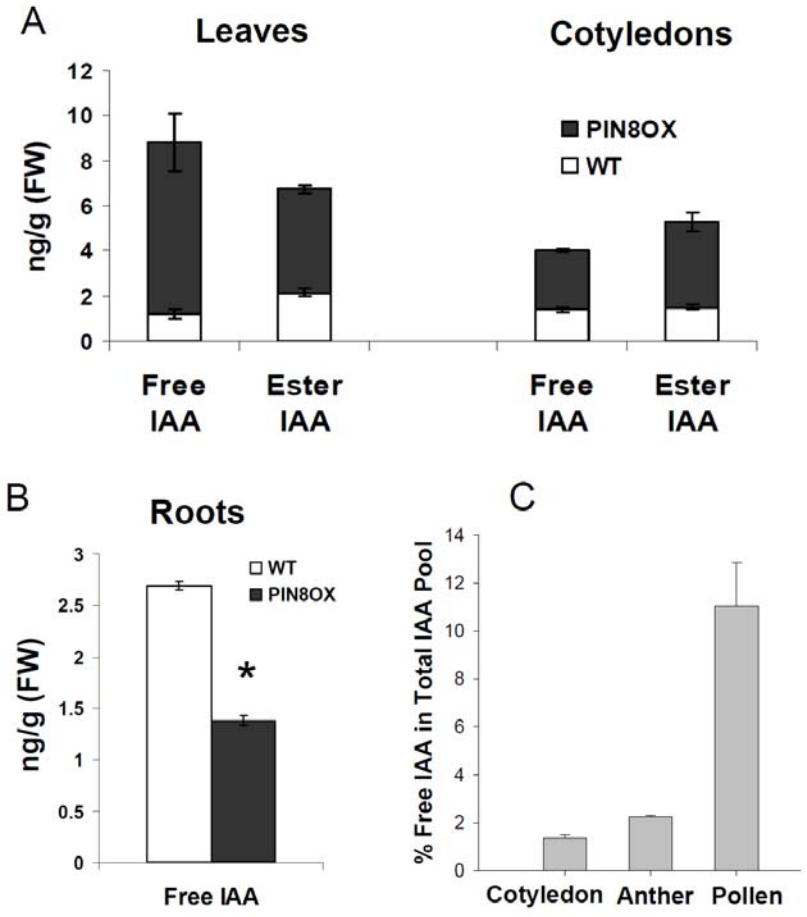

Figure A--6. Measurement of free and conjugated IAA in different tobacco tissues. Levels of IAA were changed in PIN8 overexpression (PIN8OX) plants. **(A)** Auxin quantification in leaves of four-week old plants and two-week old seedlings. **(B)** Free IAA content in root of 8-day old seedlings. **(C)** The percentage of free IAA in the total IAA pool (free + ester-linked + amide-linked IAA) in different tissues from wild type tobacco plants. Cotyledons contained 1.2 ng/g free IAA and 103 ng/g total IAA; anthers contained 45 ng/g free IAA and 2044 ng/g total IAA; pollens contained 177 ng/g free IAA and 1705 ng/g total IAA. FW, fresh weight.

F.

Role for Apyrases in Polar Auxin Transport in *Arabidopsis*

Xing Liu*, Jian Wu*, Greg Clark*, Minhui Lim, David Arnold, Gary Gardner, Stanley J. Roux[§]

* Denotes equal contribution

§ Corresponding author; Section of Molecular Cell and Developmental Biology, University of Texas, Austin, Texas, USA

1. Poster abstract published in *Plant Biology 2011, Annual Meeting of the American Society of Plant Biologists*, Minneapolis, Minnesota, August 6-10, 2011

(Poster abstract link, http://abstracts.aspb.org/pb2011/public/P20/P20041.html)

2. *Manuscript* in preparation

Abstract

Included in the recent evidence that extracellular nucleotides regulate plant growth is the discovery that exogenous ATP can block auxin transport and gravitropic growth in primary roots of Arabidopsis. Cells limit the concentration of extracellular ATP in part through the activity of ectoapyrases (ecto-nucleoside triphosphate diphosphohydrolases), and two nearly identical Arabidopsis apyrases, APY1 and APY2, appear to share this function. These findings, plus the fact that suppression of APY1 and APY2 blocks growth in Arabidopsis, suggested that the expression of these apyrases could influence auxin transport. This report tests that hypothesis. The polar movement of [^{3}H]IAA in Arabidopsis hypocotyl sections was measured after applying [^{3}H]IAA in donor blocks to the apical end of the sections. This assay revealed that basipetal auxin transport was greatly reduced in *apy2* null mutants when they were induced by estradiol to suppress the expression of *APY1* by RNAi. In these plants the basal halves of hypocotyls contained considerably lower free IAA levels when compared to wild-type plants, and there were significant morphological abnormalities in the primary root, consistent with disrupted auxin transport. When a GFP fluorescence signal encoded by a DR5:GFP construct was

measured in these mutants after apyrase suppression, their primary roots showed no signal asymmetry following gravistimulation, and both their growth and gravitropic curvature were inhibited. Chemicals that suppress apyrase activity also inhibit gravitropic curvature and, to a lesser extent, growth. Taken together these results indicate that a critical step connecting apyrase suppression to growth suppression is the inhibition of polar auxin transport.

Polar Auxin Transport in Arabidopsis Hypocotyls

Wild type and an *apy2* mutant containing an inducible RNAi construct targeting *APY1* in the Wassilewskija (Ws) ecotype were the same as previously described (Wu *et al*., 2007). Seeds were surface-sterilized and plated on MS medium containing 1% sucrose. To induce expression of the RNAi constructs, 4 μM estradiol (Sigma) was supplied in the growth medium (Wu *et al*., 2007). After 3 days in the dark at 4 °C and 12 h under cool white fluorescent lights (photosynthetically active radiation = 80 μmol m^{-2} s^{-1}), the seeds were grown at 24 °C continuously in darkness for 6 days and then exposed to continuous cool white fluorescent lights (photosynthetically active radiation = 80 μmol m^{-2} s^{-1}) for an additional 2 days. The basipetal IAA transport in hypocotyl tissues was measured as previously described (Liu *et al*., 2011, see also Chapter 3).

As shown in Figure A-7A, polar auxin transport in the *apy2* single mutant hypocotyl [RNAi (-)] was not different from the wild type control [Ws (-)]. However, when the expression of RNAi was induced by estradiol [RNAi (+)], polar auxin transport was dramatically decreased compared with the wild type control treated with estradiol [Ws(+)]. These results suggest that the activities of APY1 and APY2 are required for auxin transport in Arabidopsis hypocotyls.

Quantification of Free IAA in Arabidopsis Seedlings

The wild-type and transformed plants were grown exactly as described above. After two-days of growth under continuous white light, the apices, apical halves of hypocotyl tissues, and basal halves of the hypocotyl tissues were harvested separately,

with a minimum of 20 mg fresh weight per sample. The frozen tissue samples were homogenized using a Mixer Mill (MM 300; Qiagen, Valencia, CA), with a 3-mm tungsten carbide bead in 150 µl of homogenization buffer (35% of 0.2 M imidazole, 65% isopropanol, pH 7) containing 4 ng of [$^{13}C_6$]IAA as the internal standard. The level of free IAA was analyzed by solid phase extraction followed by GC-SIM-MS as previously described (Barkawi *et al*., 2010).

As shown in Figure A-7B, when the expression of RNAi in *apy2* mutant was induced by estradiol, a condition that led to significant reduction of auxin transport (Figure A-7A), free IAA content was significantly reduced in the basal half of hypocotyl tissues compared with the wild type control [Ws (+estradiol)]. The free IAA level was not changed in the apical half hypocotyl tissues but was increased in the apices tissues at a marginally significant level (P=0.076, n=3, student's *t* test). These results suggest that the defect in hypocotyl auxin transport resulting from disrupted apyrase activities leads to altered distribution of free IAA in plant tissues, especially a reduction of free IAA supply in the lower part of the plant.

Figures

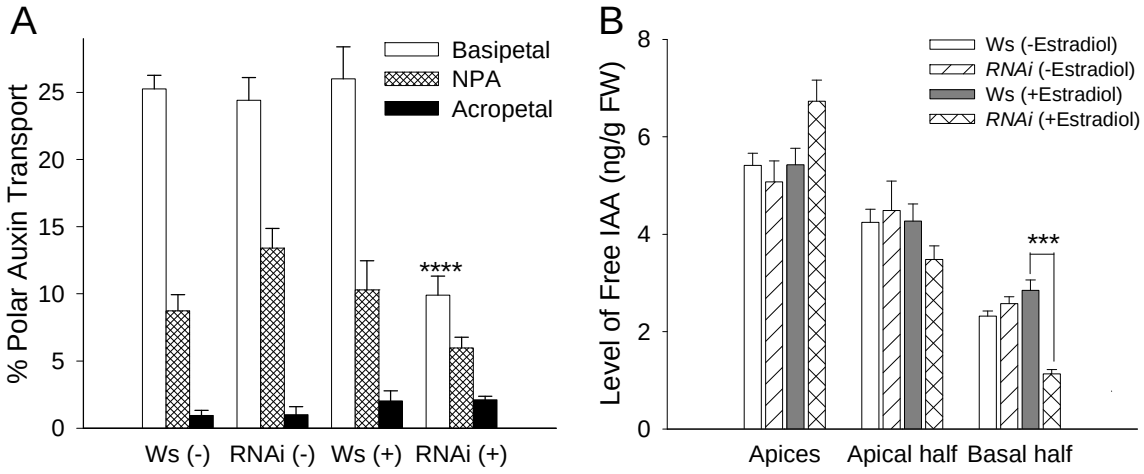

Figure A--7. Effects of reduced Arabidopsis apyrase activities on IAA transport and free IAA levels. (A) When the expression of RNAi construct targeting *APY1* was induced in *apy2* mutants by estradiol [RNAi (+)], the polar auxin transport in hypocotyl tissues was significantly reduced compared with the wild-type control treated with estradiol [Ws (+)]. The asterisk (****) indicates a significant difference ($P<0.0001$, n=10, student's *t* test,). **(B)** When the activity of both APY1 and APY2 was reduced [RNAi (+estradiol)], the level of free IAA was significantly reduced in the basal half of hypocotyl tissues and slightly increased in the apices. The asterisk (***) indicates a significant difference ($P<0.005$, n=3, student's *t* test).

Bibliography

Aloni R (2010) The induction of vascular tissues by auxin. *In* P Davies, ed, Plant Hormones, Ed 3. Springer, Dordrecht, The Netherlands, pp 485-518

Andrieux J, Demirci UB, Hannauer J, Gervais C, Goutaudier C, Miele P (2011) Spontaneous hydrolysis of sodium borohydride in harsh conditions. International Journal of Hydrogen Energy **36:** 224-233

Baldi BG, Maher BR, Cohen JD (1989) Hydrolysis of indole-3-acetic acid esters exposed to mild alkaline conditions. Plant Physiology **91:** 9-12

Baldi BG, Maher BR, Slovin JP, Cohen JD (1991) Stable isotope labeling *in vivo* of D- and L- tryptophan pools in *Lemna gibba* and the low incorporation of label into indole-3-acetic acid. Plant Physiology **95:** 1203-1208

Bandurski RS, Schulze A, Cohen JD (1977) Photo-regulation of the ratio of ester to free indole-3-acetic acid. Biochemical and Biophysical Research Communications **79:** 1219-1223

Baraldi R, Bertazza G, Bregoli AM, Fasolo F, Rotondi A, Predieri S, Serafinifracassini D, Slovin JP, Cohen JD (1995) Auxins and polyamines in relation to differential *in vitro* root induction on microcuttings of two pear cultivars. Journal of Plant Growth Regulation **14:** 49-59

Barkawi LS, Cohen JD (2010) A method for concurrent diazomethane synthesis and substrate methylation in a 96-sample format. Nature Protocols **5:** 1619-1626

Barkawi LS, Tam YY, Tillman JA, Normanly J, Cohen JD (2010) A high-throughput method for the quantitative analysis of auxins. Nature Protocols **5:** 1609-1618

Barkawi LS, Tam YY, Tillman JA, Pederson B, Calio J, Al-Amier H, Emerick M, Normanly J, Cohen JD (2008) A high-throughput method for the quantitative analysis of indole-3-acetic acid and other auxins from plant tissue. Analytical Biochemistry **372:** 177-188

Barker-Bridgers M, Ribnicky DM, Cohen JD, Jones AM (1998) Red light-regulated growth: changes in the abundance of indoleacetic acid in the maize (*Zea mays* L.) mesocotyl. Planta **204:** 207-211

Bayer EM, Smith RS, Mandel T, Nakayama N, Sauer M, Prusinkiewicz P, Kuhlemeier C (2009) Integration of transport-based models for phyllotaxis and midvein formation. Genes & Development **23:** 373-384

Behringer FJ, Davies PJ (1992) Indole-3-acetic acid levels after phytochrome-mediated changes in the stem elongation rate of dark-and light-grown Pisum seedlings. Planta **188:** 85-92

Bhalerao RP, Eklof J, Ljung K, Marchant A, Bennett M, Sandberg G (2002) Shoot-derived auxin is essential for early lateral root emergence in Arabidopsis seedlings. Plant Journal **29:** 325-332

Bialek K, Cohen JD (1989) Quantitation of indoleacetic acid conjugates in bean seeds by direct tissue hydrolysis. Plant Physiology **90:** 398-400

Bialek K, Cohen JD (1992) Amide-linked indoleacetic acid conjugates may control levels of indoleacetic acid in germinating seedlings of *Phaseolus vulgaris*. Plant Physiology **100:** 2002-2007

Briggs WR, Olney MA (2001) Photoreceptors in plant photomorphogenesis to date. Five phytochromes, two cryptochromes, one phototropin, and one superchrome. Plant Physiology **125:** 85-88

Casal JJ, Sanchez RA, Botto JF (1998) Modes of action of phytochromes. Journal of Experimental Botany **49:** 127-138

Chen WP, Yang XY, Hegeman AD, Gray WM, Cohen JD (2010) Microscale analysis of amino acids using gas chromatography-mass spectrometry after methyl chloroformate derivatization. Journal of Chromatography B-Analytical Technologies in the Biomedical and Life Sciences **878:** 2199-2208

Chisnell JR, Bandurski RS (1988) Translocation of radiolabeled indole-3-acetic acid and indole-3-acetyl-*myo*-inositol from kernel to shoot of *Zea mays* L. Plant Physiology **86:** 79-84

Christopher D (2003) Photosensory pathways regulating chloroplast gene expression. *In* M Abdel-Mottaleb, H Nalwa, eds, Handbook of Photochemistry and Photobiology, Vol 4. American Scientific Publishers, Valencia, CA, pp 249-268

Clark G, Wu J, Liu X, Pham T, Cervantes A, Cohen J, Gardner G, Rowx S (2011) Role for ectoapyrases in gravitropic responses and polar auxin transport in Arabidopsis *In* Plant Biology 2011, Annual Meeting of the American Society of Plant Biologists, Minneapolis, Minnesota

Cohen JD (1984) Convenient apparatus for the generation of small amounts of diazomethane. Journal of Chromatography **303:** 193-196

Cohen JD, Baldi BG, Slovin JP (1986) $^{13}C_6$-[Benzene ring]-indole-3-acetic acid - a new internal standard for quantitative mass-spectral analysis of indole-3-acetic-acid in plants. Plant Physiology **80:** 14-19

Cohen JD, Schulze A (1981) Double-standard isotope dilution assay. I. Quantitative assay of indole-3-acetic acid. Analytical Biochemistry **112:** 249-257

Cooney TP, Nonhebel HM (1991) Biosynthesis of indole-3-acetic-acid in tomato shoots: Measurement, mass-spectral identification and incorporation of ^2H from ^2H_2O into indole-3-acetic acid, D- and L-tryptophan, indole-3-pyruvate and tryptamine. Planta **184:** 368-376

Cordonnier MM, Pratt LH (1982) Immunopurification and initial characterization of dicotyledonous phytochrome. Plant Physiology **69:** 360-365

Dal Bosco C, Dovzhenko A, Woerner N, Liu X, Resch T, Hegermann J, Eismann M, Touraev A, Heberle-Bors E, Paponov I, Ruperti B, Cohen J, Palme K (2011) ER-localized PIN8 modulates cell and plant development by regulating intracellular auxin homeostasis. *In* 22nd International Conference on Arabidopsis Research, Madison, Wisconsin

Darwin CR, Darwin F (1881) The power of movement in plants. Appleton, New York

Davies NW, Smith JA, Molesworth PP, Ross JJ (2010) Hydrogen/deuterium exchange on aromatic rings during atmospheric pressure chemical ionization mass spectrometry. Rapid Communications in Mass Spectrometry **24:** 1105-1110

DeMason DA, Chetty V, Barkawi LS, Liu X, Cohen J (2011) *Unifoliata-Afila* interactions in pea leaf morphogenesis. Manuscript in preparation

Ding ZJ, Galvan-Ampudia CS, Demarsy E, Langowski L, Kleine-Vehn J, Fan YW, Morita MT, Tasaka M, Fankhauser C, Offringa R, Friml J (2011) Light-mediated polarization of the PIN3 auxin transporter for the phototropic response in Arabidopsis. Nature Cell Biology **13:** 447-U222

Epstein E, Ackerman A (1993) Transport and metabolism of indole-3-butyric acid in cuttings of *Leucadendron discolor*. Plant Growth Regulation **12:** 17-22

Epstein E, Cohen JD, Bandurski RS (1980) Concentration and metabolic turnover of indoles in germinating kernels of *Zea mays* L. . Plant Physiology **65:** 415-421

Epstein E, Cohen JD, Slovin JP (2002) The biosynthetic pathway for indole-3-acetic acid changes during tomato fruit development. Plant Growth Regulation **38:** 16-21

Epstein E, Sagee O (1992) Effect of ethylene treatment on transport and metabolism of indole-3-butyric acid in citrus leaf midribs. Plant Growth Regulation **11:** 357-362

Epstein E, Zilkah S, Faingersh G, Rotebaum A (1993) Transport and metabolism of indole-3-butyric acid in easy- and difficult-to-root cuttings of sweet cherry (*Prunus avium* L.). Acta Horticulturae **329:** 292-295

Gardner G, Lin CT, Tobin EM, Loehrer H, Brinkman D (2009) Photobiological properties of the inhibition of etiolated Arabidopsis seedling growth by ultraviolet-B irradiation. Plant Cell and Environment **32:** 1573-1583

Gardner G, Sanborn JR (1989) Aryl-substituted α-aminooxycarboxylic acids-A new class of auxin transport inhibitors. Plant Physiology **90:** 291-295

Gibson RA, Schneider EA, Wightman F (1972) Biosynthesis and metabolism of Indol-3yl-acetic acid. Journal of Experimental Botany **23:** 381-399

Goldsmith MHM (1982) A saturable site responsible for polar transport of indole-3-acetic acid in sections of maize coleoptiles. Planta **155:** 68-75

Gottwald JR, Krysan PJ, Young JC, Evert RF, Sussman MR (2000) Genetic evidence for the in planta role of phloem-specific plasma membrane sucrose transporters. Proceedings of the National Academy of Sciences of the United States of America **97:** 13979-13984

Gray WM, Ostin A, Sandberg G, Romano CP, Estelle M (1998) High temperature promotes auxin-mediated hypocotyl elongation in Arabidopsis. Proceedings of the National Academy of Sciences of the United States of America **95:** 7197-7202

Grieneisen VA, Xu J, Maree AFM, Hogeweg P, Scheres B (2007) Auxin transport is sufficient to generate a maximum and gradient guiding root growth. Nature **449:** 1008-1013

Hoecker U, Toledo-Ortiz G, Bender J, Quail PH (2004) The photomorphogenesis-related mutant *red1* is defective in *CYP83B1*, a red light-induced gene encoding a cytochrome P450 required for normal auxin homeostasis. Planta **219:** 195-200

Hoenicke K, Simat TJ, Steinhart H, Kohler HJ, Schwab A (2001) Determination of free and conjugated indole-3-acetic acid, tryptophan, and tryptophan metabolites in grape must and wine. Journal of Agricultural and Food Chemistry **49:** 5494-5501

Howe GT, Gardner G, Hackett WP, Furnier GR (1996) Phytochrome control of short-day-induced bud set in black cottonwood. Physiologia Plantarum **97:** 95-103

Iino M (1982) Action of red light on indole-3-acetic acid status and growth in coleoptiles of etiolated maize seedlings. Planta **156:** 21-32

Iino M (1982) Inhibitory action of red light on the growth of the maize mesocotyl: evaluation of the auxin hypothesis. Planta **156:** 388-395

Ikeda Y, Men SZ, Fischer U, Stepanova AN, Alonso JM, Ljung K, Grebe M (2009) Local auxin biosynthesis modulates gradient-directed planar polarity in *Arabidopsis*. Nature Cell Biology **11:** 731-738

Ilić N, Normanly J, Cohen JD (1996) Quantification of free plus conjugated indoleacetic acid in arabidopsis requires correction for the nonenzymatic conversion of indolic nitriles. Plant Physiology **111:** 781-788

Jensen PJ, Hangarter RP, Estelle M (1998) Auxin transport is required for hypocotyl elongation in light-grown but not dark-grown Arabidopsis. Plant Physiology **116:** 455-462

Jones AM, Cochran DS, Lamerson PM, Evans ML, Cohen JD (1991) Red light-regulated growth: I. Changes in the abundance of indoleacetic acid and a 22-Kilodalton auxin-binding protein in the Maize mesocotyl. Plant Physiology **97:** 352-358

Jones SE, DeMeo JS, Davies NW, Noonan SE, Ross JJ (2005) Stems of the Arabidopsis *pin1-1* mutant are not deficient in free indole-3-acetic acid. Planta **222:** 530-534

Kai K, Horita J, Wakasa K, Miyagawa H (2007) Three oxidative metabolites of indole-3-acetic acid from *Arabidopsis thaliana*. Phytochemistry **68:** 1651-1663

Keuskamp DH, Pollmann S, Voesenek LACJ, Peeters AJM, Pierik R (2010) Auxin transport through PIN-FORMED 3 (PIN3) controls shade avoidance and fitness during competition. Proceedings of the National Academy of Sciences of the United States of America **107:** 22740-22744

Koshiba T, Kamiya Y, Iino M (1995) Biosynthesis of indole-3-acetic acid from L-tryptophan in coleoptile tips of maize (*Zea mays* L). Plant and Cell Physiology **36:** 1503-1510

Kowalczyk M, Sandberg G (2001) Quantitative analysis of indole-3-acetic acid metabolites in Arabidopsis. Plant Physiology **127:** 1845-1853

Kraepiel Y, Miginiac E (1997) Photomorphogenesis and phytohormones. Plant Cell and Environment **20:** 807-812

Laxmi A, Pan JW, Morsy M, Chen RJ (2008) Light plays an essential role in intracellular distribution of auxin efflux carrier PIN2 in *Arabidopsis thaliana*. Plos One **3**

Lewis DR, Muday GK (2009) Measurement of auxin transport in *Arabidopsis thaliana*. Nat Protoc **4:** 437-451

Li Y, Wu YH, Hagen G, Guilfoyle T (1999) Expression of the auxin-inducible GH3 Promoter GUS fusion gene as a useful molecular marker for auxin physiology. Plant and Cell Physiology **40:** 675-682

Liu JH, Reid DM (1992) Adventitious rooting in hypocotyls of sunflower (*Helianthus annuus*) seedlings. IV. The role of changes in endogenous free and conjugated indole-3-acetic acid Physiologia Plantarum **86:** 285-292

Liu X, Barkawi LS, Gardner G, Cohen JD (2012) Transport of indole-3-butyric acid and indole-3-acetic acid in *Arabidopsis thaliana* hypocotyls using stable isotope labeling. Plant Physiology

Liu X, Cohen JD, Gardner G (2011) Low-fluence red light increases the transport and biosynthesis of auxin. Plant Physiology **157:** 891-904

Ljung K, Bhalerao RP, Sandberg G (2001) Sites and homeostatic control of auxin biosynthesis in Arabidopsis during vegetative growth. Plant Journal **28:** 465-474

Ljung K, Hull AK, Celenza J, Yamada M, Estelle M, Nonmanly J, Sandberg G (2005) Sites and regulation of auxin biosynthesis in Arabidopsis roots. Plant Cell **17:** 1090-1104

Ljung K, Ostin A, Lioussanne L, Sandberg G (2001) Developmental regulation of indole-3-acetic acid turnover in Scots pine seedlings. Plant Physiology **125:** 464-475

Long C, Iino M (2001) Light-dependent osmoregulation in pea stem protoplasts. Photoreceptors, tissue specificity, ion relationships, and physiological implications. Plant Physiology **125:** 1854-1869

Ludwig-Müller J (2000) Indole-3-butyric acid in plant growth and development. Plant Growth Regulation **32:** 219-230

Ludwig-Müller J (2007) Indole-3-butyric acid synthesis in ecotypes and mutants of *Arabidopsis thaliana* under different growth conditions. Journal of Plant Physiology **164:** 47-59

Ludwig-Müller J, Epstein E (1993) Indole-3-butyric acid in *Arabidopsis thaliana*. II. In vivo metabolism. Plant Growth Regulation **13:** 189-195

Ludwig-Müller J, Hilgenberg W, Epstein E (1995) The *in vitro* biosynthesis of indole-3-butyric acid in maize. Phytochemistry **40:** 61-68

Ludwig-Müller J, Raisig A, Hilgenberg W (1995) Uptake and transport of indole-3-butyric acid in *Arabidopsis thaliana*: comparison with other natural and synthetic auxins. Journal of Plant Physiology **147:** 351-354

Ludwig-Müller J, Sass S, Sutter EG, Wodner M, Epstein E (1993) Indole-3-butyric acid in *Arabidopsis thaliana*. I. Identification and quantification. Plant Growth Regulation **13:** 179-187

Magnus V, Bandurski RS, Schulze A (1980) Synthesis of 4,5,6,7 and 2,4,5,6,7 deuterium-labeled indole-3-acetic acid for use in mass spectrometric assays. Plant Physiology **66:** 775-781

Marx M, Djerassi C (1968) Mass spectrometry in structural and stereochemical problems. CXLIX. The question of ring expansion in the fragmentation of ^{13}C-labeled nitrogen heterocycles. journal of the American Chemical Society **90:** 678-681

Mashiguchi K, Tanaka K, Sakai T, Sugawara S, Kawaide H, Natsume M, Hanada A, Yaeno T, Shirasu K, Yao H, McSteen P, Zhao Y, Hayashi K, Kamiya Y, Kasahara H (2011) The main auxin biosynthesis pathway in Arabidopsis. Proceedings of the National Academy of Sciences of the United States of America **108:** 18512-18517

Mattsson J, Sung ZR, Berleth T (1999) Responses of plant vascular systems to auxin transport inhibition. Development **126:** 2979-2991

Michalczuk L, Cooke TJ, Cohen JD (1992) Auxin levels at different stages of carrot somatic embryogenesis. Phytochemistry **31:** 1097-1103

Miller AN, Walsh CS, Cohen JD (1987) Measurement of indole-3-acetic acid in peach fruits (*Prunus Persica* L. Batsch cv Redhaven) during development. Plant Physiology **84:** 491-494

Mravec J, Skůpa P, Bailly A, Hoyerová K, Krecek P, Bielach A, Petrásek J, Zhang J, Gaykova V, Stierhof YD, Dobrev PI, Schwarzerová K, Rolcík J, Seifertová

D, Luschnig C, Benková E, Zazímalová E, Geisler M, Friml J (2009) Subcellular homeostasis of phytohormone auxin is mediated by the ER-localized PIN5 transporter. Nature **459:** 1136-U1127

Nagashima A, Uehara Y, Sakai T (2008) The ABC subfamily B auxin transporter AtABCB19 is involved in the inhibitory effects of N-1-Naphthyphthalamic acid on the phototropic and gravitropic responses of Arabidopsis hypocotyls. Plant and Cell Physiology **49:** 1250-1255

Neff MM, Fankhauser C, Chory J (2000) Light: an indicator of time and place. Genes & Development **14:** 257-271

Negi S, Sukumar P, Liu X, Cohen JD, Muday GK (2010) Genetic dissection of the role of ethylene in regulating auxin-dependent lateral and adventitious root formation in tomato. Plant Journal **61:** 3-15

Nishimura T, Mori Y, Furukawa T, Kadota A, Koshiba T (2006) Red light causes a reduction in IAA levels at the apical tip by inhibiting de novo biosynthesis from tryptophan in maize coleoptiles. Planta **224:** 1427-1435

Normanly J, Cohen JD, Fink GR (1993) *Arabidopsis thaliana* auxotrophs reveal a tryptophan-independent biosynthetic pathway for indole-3-acetic acid. Proceedings of the National Academy of Sciences of the United States of America **90:** 10355-10359

Normanly J, Slovin J, Cohen J (2005) Auxin biosynthesis and metabolism. *In* P Davies, ed, Plant Hormones: Biosynthesis, Signal Transduction, Action! Kluwer Academic Publishers, Dordrecht, The Netherlands, pp 36-62

Nowacki J, Bandurski RS (1980) *Myo*-inositol esters of indole-3-acetic acid as seed auxin precursors of *Zea mays* L. Plant Physiology **65:** 422-427

Okada K, Ueda J, Komaki MK, Bell CJ, Shimura Y (1991) Requirement of the auxin polar transport system in early stages of Arabidopsis floral bud formation. Plant Cell **3:** 677-684

Ostin A, Kowalyczk M, Bhalerao RP, Sandberg G (1998) Metabolism of indole-3-acetic acid in Arabidopsis. Plant Physiology **118:** 285-296

Paciorek T, Zazímalová E, Ruthardt N, Petrásek J, Stierhof YD, Kleine-Vehn J, Morris DA, Emans N, Jürgens G, Geldner N, Friml J (2005) Auxin inhibits endocytosis and promotes its own efflux from cells. Nature **435:** 1251-1256

Peer WA, Blakeslee JJ, Yang HB, Murphy AS (2011) Seven things we think we know about auxin transport. Molecular Plant **4:** 487-504

Petrásek J, Friml J (2009) Auxin transport routes in plant development. Development **136:** 2675-2688

Phillips KA, Skirpan AL, Liu X, Christensen A, Slewinski TL, Hudson C, Barazesh S, Cohen JD, Malcomber S, McSteen P (2011) *vanishing tassel2* encodes a grass-specific tryptophan aminotransferase required for vegetative and reproductive development in maize. Plant Cell **23:** 550-566

Pratt LH, Briggs WR (1966) Photochemical and nonphotochemical reactions of phytochrome *in vivo*. Plant Physiology **41:** 467-474

Rapparini F, Tam YY, Cohen JD, Slovin JP (2002) Indole-3-acetic acid metabolism in *Lemna gibba* undergoes dynamic changes in response to growth temperature. Plant Physiology **128:** 1410-1416

Rashotte AM, Poupart J, Waddell CS, Muday GK (2003) Transport of the two natural auxins, indole-3-butyric acid and indole-3-acetic acid, in Arabidopsis. Plant Physiology **133:** 761-772

Reed RC, Brady SR, Muday GK (1998) Inhibition of auxin movement from the shoot into the root inhibits lateral root development in arabidopsis. Plant Physiology **118:** 1369-1378

Ribnicky DM, Cooke TJ, Cohen JD (1998) A microtechnique for the analysis of free and conjugated indole-3-acetic acid in milligram amounts of plant tissue using a benchtop gas chromatograph mass spectrometer. Planta **204:** 1-7

Ribnicky DM, Ilić N, Cohen JD, Cooke TJ (1996) The effects of exogenous auxins on endogenous indole-3-acetic acid metabolism (the implications for carrot somatic embryogenesis). Plant Physiology **112:** 549-558

Ruzicka K, Strader LC, Bailly A, Yang HB, Blakeslee J, Langowski L, Nejedla E, Fujita H, Itoh H, Syono K, Hejatko J, Gray WM, Martinoia E, Geisler M, Bartel B, Murphy AS, Friml J (2010) Arabidopsis PIS1 encodes the ABCG37 transporter of auxinic compounds including the auxin precursor indole-3-butyric acid. Proceedings of the National Academy of Sciences of the United States of America **107:** 10749-10753

Salisbury FJ, Hall A, Grierson CS, Halliday KJ (2007) Phytochrome coordinates Arabidopsis shoot and root development. Plant Journal **50:** 429-438

Sanchezbravo J, Ortuno A, Acosta M, Sabater F (1988) *In vivo* metabolism of labeled indole-3-acetic acid during polar transport in etiolated hypocotyls of *Lupinus albus*: Relationship with growth. Plant Growth Regulation **7:** 271-288

Seidel C, Walz A, Park S, Cohen JD, Ludwig-Muller J (2006) Indole-3-acetic acid protein conjugates: novel players in auxin homeostasis. Plant Biology **8:** 340-345

Shen YP, Zhou ZZ, Feng SH, Li JG, Tan-Wilson A, Qu LJ, Wang HY, Deng XW (2009) Phytochrome A mediates rapid red light-induced phosphorylation of Arabidopsis FAR-RED ELONGATED HYPOCOTYL1 in a low fluence response. Plant Cell **21:** 494-506

Shibasaki K, Uemura M, Tsurumi S, Rahman A (2009) Auxin response in Arabidopsis under cold stress: underlying molecular mechanisms. Plant Cell **21:** 3823-3838

Shinkle JR, Kadakia R, Jones AM (1998) Dim-red-light-induced increase in polar auxin transport in cucumber seedlings. Plant Physiology **116:** 1505-1513

Shinomura T, Nagatani A, Hanzawa H, Kubota M, Watanabe M, Furuya M (1996) Action spectra for phytochrome A- and B-specific photoinduction of seed germination in *Arabidopsis thaliana*. Proceedings of the National Academy of Sciences of the United States of America **93:** 8129-8133

Sitbon F, Edlund A, Gardestrom P, Olsson O, Sandberg G (1993) Compartmentation of indole-3-acetic acid metabolism in protoplasts isolated from leaves of wild-type and IAA-overproducing transgenic tobacco plants. Planta **191:** 274-279

Slovin JP, Bandurski RS, Cohen JD (1999) Auxin. *In* P Hooykaas, M Hall M, K Libbenga, eds, Biochemistry and Molecular Biology of Plant Hormones. Elsevier, Amsterdam, pp 115-140

Srivastava AC, Ganesan S, Ismail IO, Ayre BG (2008) Functional characterization of the Arabidopsis AtSUC2 sucrose/H^+ symporter by tissue-specific complementation reveals an essential role in phloem loading but not in long-distance transport. Plant Physiology **148:** 200-211

Staswick PE, Serban B, Rowe M, Tiryaki I, Maldonado MT, Maldonado MC, Suza W (2005) Characterization of an Arabidopsis enzyme family that conjugates amino acids to indole-3-acetic acid. Plant Cell **17:** 616-627

Steindler C, Matteucci A, Sessa G, Weimar T, Ohgishi M, Aoyama T, Morelli G, Ruberti I (1999) Shade avoidance responses are mediated by the ATHB-2 HD-Zip protein, a negative regulator of gene expression. Development **126:** 4235-4245

Stepanova AN, Yun J, Robles LM, Novak O, He W, Guo H, Ljung K, Alonso JM (2011) The *Arabidopsis* YUCCA1 flavin monooxygenase functions in the indole-3-pyruvic acid branch of auxin biosynthesis. Plant Cell **23:** 3961-3973

Stowe-Evans EL, Luesse DR, Liscum E (2001) The enhancement of phototropin-induced phototropic curvature in Arabidopsis occurs via a photoreversible phytochrome A-dependent modulation of auxin responsiveness. Plant Physiology **126:** 826-834

Strader LC, Bartel B (2011) Transport and metabolism of the endogenous auxin precursor indole-3-butyric acid. Molecular Plant **4:** 477-486

Strader LC, Culler AH, Cohen JD, Bartel B (2010) Conversion of endogenous indole-3-butyric acid to indole-3-acetic acid drives cell expansion in Arabidopsis seedlings. Plant Physiology **153:** 1577-1586

Strader LC, Wheeler DL, Christensen SE, Berens JC, Cohen JD, Rampey RA, Bartel B (2011) Multiple facets of Arabidopsis seedling development require indole-3-butyric acid-derived auxin. Plant Cell **23:** 984-999

Sudi J (1966) Increases in the capacity of pea tissue to form acyl-aspartic acids specifically induced by auxins. New Phytologist **65:** 9-21

Sugawara S, Hishiyama S, Jikumaru Y, Hanada A, Nishimura T, Koshiba T, Zhao Y, Kamiya Y, Kasahara H (2009) Biochemical analyses of indole-3-acetaldoxime-dependent auxin biosynthesis in Arabidopsis. Proceedings of the National Academy of Sciences of the United States of America **106:** 5430-5435

Sutter EG, Cohen JD (1992) Measurement of indolebutyric acid in plant tissues by isotope dilution gas chromatography-mass spectrometry analysis. Plant Physiology **99:** 1719-1722

Swarup K, Benková E, Swarup R, Casimiro I, Péret B, Yang Y, Parry G, Nielsen E, De Smet I, Vanneste S, Levesque MP, Carrier D, James N, Calvo V, Ljung K, Kramer E, Roberts R, Graham N, Marillonnet S, Patel K, Jones JDG, Taylor CG, Schachtman DP, May S, Sandberg G, Benfey P, Friml J, Kerr I, Beeckman T, Laplaze L, Bennett MJ (2008) The auxin influx carrier LAX3 promotes lateral root emergence. Nature Cell Biology **10:** 946-954

Symons GM, Reid JB (2003) Hormone levels and response during de-etiolation in pea. Planta **216:** 422-431

Sztein AE, Ilić N, Cohen JD, Cooke TJ (2002) Indole-3-acetic acid biosynthesis in isolated axes from germinating bean seeds: The effect of wounding on the biosynthetic pathway. Plant Growth Regulation **36:** 201-207

Taiz L, Zeiger E (2006) Plant Physiology, Ed 4th. Sinauer Associates, Inc. , Sunderland, USA

Tam YY, Epstein E, Normanly J (2000) Characterization of auxin conjugates in arabidopsis. Low steady-state levels of indole-9-acetyl-aspartate indole-3-acetyl-glutamate, and indole-3-acetyl-glucose. Plant Physiology **123:** 589-595

Tam YY, Normanly J (1998) Determination of indole-3-pyruvic acid levels in *Arabidopsis thaliana* by gas chromatography selected ion monitoring mass spectrometry. Journal of Chromatography A **800:** 101-108

Tan X, Calderon-Villalobos LIA, Sharon M, Zheng CX, Robinson CV, Estelle M, Zheng N (2007) Mechanism of auxin perception by the TIR1 ubiquitin ligase. Nature **446:** 640-645

Tao Y, Ferrer JL, Ljung K, Pojer F, Hong FX, Long JA, Li L, Moreno JE, Bowman ME, Ivans LJ, Cheng YF, Lim J, Zhao YD, Ballare CL, Sandberg G, Noel JP, Chory J (2008) Rapid synthesis of auxin via a new tryptophan-dependent pathway is required for shade avoidance in plants. Cell **133:** 164-176

Thomson K-S, Hertel R, Müller S, Tavares JE (1973) 1-N-naphthylphthalamic acid and 2,3,5-triiodobenzoic acid. Planta **109:** 337-352

Tian H, Baxter IR, Lahner B, Reinders A, Salt DE, Ward JM (2010) Arabidopsis NPCC6/NaKR1 is a phloem mobile metal binding protein necessary for phloem function and root meristem maintenance. Plant Cell **22:** 3963-3979

Tognetti VB, Van Aken O, Morreel K, Vandenbroucke K, de Cotte BV, De Clercq I, Chiwocha S, Fenske R, Prinsen E, Boerjan W, Genty B, Stubbs KA, Inze D, Van Breusegem F (2010) Perturbation of indole-3-butyric acid homeostasis by the UDP-glucosyltransferase *UGT74E2* modulates Arabidopsis architecture and water stress tolerance. Plant Cell **22:** 2660-2679

Tuominen H, Ostin A, Sandberg G, Sundberg B (1994) A novel metabolic pathway for indole-3-acetic acid in apical shoots of *Populus tremula* (L.) x *Populus tremuloides* (Michx.). Plant Physiology **106:** 1511-1520

Van Tuinen A, Kerckhoffs L, Nagatani A, Kendrick RE, Koornneef M (1995) A temporarily red light-insensitive mutant of tomato lacks a light-stable, B-like phytochrome. Plant Physiology **108:** 939-947

van Tuinen A, Kerckhoffs LH, Nagatani A, Kendrick RE, Koornneef M (1995) Far-red light-insensitive, phytochrome A-deficient mutants of tomato. Mol Gen Genet **246:** 133-141

Venis MA (1972) Auxin-induced conjugation systems in peas. Plant Physiology **49:** 24-27

Vogel G (2006) Plant science - Auxin begins to give up its secrets. Science **313:** 1230-1231

Weller JL, Perrotta G, Schreuder ME, van Tuinen A, Koornneef M, Giuliano G, Kendrick RE (2001) Genetic dissection of blue-light sensing in tomato using mutants deficient in cryptochrome 1 and phytochromes A, B1 and B2. Plant Journal **25:** 427-440

Went F, White R (1938) Experiments of the transport of auxin. Botanical Gazette **100:** 465-484

Went FW, Thimann KV (1937) Phytohormones. The Macmillan Company, New York

Wilkinson JQ, Lanahan MB, Yen HC, Giovannoni JJ, Klee HJ (1995) An ethylene-inducible component of signal-transduction encoded by *never-ripe*. Science **270:** 1807-1809

Won C, Shen X, Mashiguchi K, Zheng Z, Dai X, Cheng Y, Kasahara H, Kamiya Y, Chory J, Zhao Y (2011) Conversion of tryptophan to indole-3-acetic acid by TRYPTOPHAN AMINOTRANSFERASES OF ARABIDOPSIS and YUCCAs in Arabidopsis. Proceedings of the National Academy of Sciences of the United States of America **108:** 18518-18523

Woodward AW, Bartel B (2005) Auxin: regulation, action, and interaction. Ann Bot **95:** 707-735

Wright AD, Sampson MB, Neuffer MG, Michalczuk L, Slovin JP, Cohen JD (1991) Indole-3-acetic acid biosynthesis in the mutant maize *orange pericarp*, a tryptophan auxotroph. Science **254:** 998-1000

Wu J, Steinebrunner I, Sun Y, Butterfield T, Torres J, Arnold D, Gonzalez A, Jacob F, Reichler S, Roux SJ (2007) Apyrases (nucleoside triphosphate-diphosphohydrolases) play a key role in growth control in Arabidopsis. Plant Physiology **144:** 961-975

Yang T, Davies PJ (1999) Promotion of stem elongation by indole-3-butyric acid in intact plants of *Pisum sativum* L. Plant Growth Regulation **27:** 157-160

Yang YD, Hammes UZ, Taylor CG, Schachtman DP, Nielsen E (2006) High-affinity auxin transport by the AUX1 influx carrier protein. Current Biology **16:** 1123-1127

Zelena E (2000) The effect of light on IAA metabolism in different parts of maize seedlings in correlation with their growth. Plant Growth Regulation **32:** 239-243

Zelena E (2000) The effect of light on metabolism of IAA in maize seedlings. Plant Growth Regulation **30:** 23-29

Zeng JX, Wang QM, Lin JZ, Deng KQ, Zhao XY, Tang DY, Liu X (2010) Arabidopsis cryptochrome-1 restrains lateral roots growth by inhibiting auxin transport. Journal of Plant Physiology **167:** 670-673

Zhao YD (2010) Auxin biosynthesis and its role in plant development. Annual Review of Plant Biology **61:** 49-64